

**Hardware in the Loop Simulation of a Heavy Truck Braking System and Vehicle
Control System Design**

THESIS

Presented in Partial Fulfillment of the Requirements for the Degree Master of Science in
the Graduate School of The Ohio State University

By

Ryan Michael Ashby

Graduate Program in Mechanical Engineering

The Ohio State University

2013

Master's Examination Committee:

Dennis Guenther, Advisor, Gary Heydinger, Advisor

Copyright by
Ryan Michael Ashby
2013

Abstract

The purpose of this thesis is to evaluate the findings brought forth from a research project conducted at The Ohio State University Center for Automotive Research. The objective of the research was to accurately model a 6x4 tractor-trailer rig using TruckSim and simulate severe braking and handling maneuvers with hardware in the loop and software in the loop simulations. For the hardware in the loop simulation (HIL), the tractor model was integrated with a 4s4m anti-lock braking system (ABS) and straight line braking tests were conducted. In addition to this, CAN messages were transmitted and received with the electronic control unit utilized by the ABS system. For the software in the loop simulation (SIL), anti-lock braking (ABS) and roll stability control (RSC) algorithms were developed using Simulink and tested with the TruckSim model. By properly simulating the tractor-trailer rig using HIL and SIL simulations, severe maneuvers could be performed and the rig's response characteristics could be evaluated within a lab environment.

The first step in creating the HIL and SIL simulations was to develop a model of a 6x4 tractor using TruckSim. In order to accomplish this, over 100 vehicle parameters were acquired from a real production tractor and entered into TruckSim. Similarly, parameters from a production trailer were acquired and entered as well. By entering these parameters into TruckSim, the dynamic behavior of the actual tractor-trailer could be simulated within a computer environment. The tractor-trailer model was then subjected to simple handling maneuvers without the aid of any vehicle stability controls

and its performance was compared against experimental data from the tractor manufacturer. This was done in order to validate the accuracy of the TruckSim model.

After the tractor-trailer model was validated, the HIL simulation was developed. Essentially, the HIL simulation integrates actual braking hardware with the computer based tractor model. For this project, the hardware consisted of a 4s4m ABS braking system with six brake chambers, four modulators, a treadle and an electronic control unit (ECU). A dSPACE simulator was used as the “interface” between the TruckSim computer model and the hardware.

With the hardware working and communicating with TruckSim, braking maneuvers were carried out. The performance of the model was then compared against experimental data from the tractor manufacturer in which the ABS controller was activated. Tests were conducted on low μ , high μ , jump μ and split μ surfaces in both a laden condition and unladen condition. Overall, the HIL simulator was able to accurately emulate the performance of the actual test vehicle with deviations in stopping time and distances typically being under 10 percent.

As tests were being conducted with the HIL simulation, work began on the SIL simulation process. Within the SIL simulation, ABS and RSC control algorithms were developed using MATLAB Simulink and ran in conjunction with the TruckSim model. These algorithms were based on a 4s4m braking scheme since the tractor being modeled utilizes 4s4m controllers. The ABS algorithm was designed to measure wheel deceleration from the TruckSim vehicle model. In the event that a predefined deceleration threshold was exceeded, the controller was designed to apply a dump, hold or build pressure command to the simulated brake modulators. The RSC controller was

designed to mitigate vehicle rollover by automatically applying brakes whenever a certain lateral acceleration threshold was exceeded.

Upon completion, the ABS and RSC control strategies were evaluated by placing the model through a series of maneuvers. The braking and handling performance of the model was then compared against experimental data from the tractor manufacturer in which the ABS and RSC controllers were activated. Various maneuvers were conducted such as a double lane change, J turn, follow cone path, high dynamic steer input and a constant radius test. Overall, the SIL simulation was able to emulate the performance of the actual test vehicle.

Dedication

To my family who has always been there to support my decisions and my education.

Acknowledgments

I would like to thank my advising professors, Dr. Dennis Guenther and Dr. Gary Heydinger who entrusted me to work with them on this project. I would also like to thank the heavy truck manufacturer we worked in partnership with. They provided us with much real world knowledge and proved to be an invaluable resource.

Vita

August 1988Born in Columbus, Ohio

June 2010 to September 2010Mechanical Engineering Intern, Swagelok
Valves and Fittings

June 2011B.S. Mechanical Engineering, The Ohio
State University

June 2011 to September 2011Mechanical Engineering Intern, Commercial
Controls Inc.

April 2012Graduate Research Assistant, Center for
Automotive Research, The Ohio State
University

Fields of Study

Major Field: Mechanical Engineering

Table of Contents

Abstract	ii
Dedication	v
Acknowledgments.....	vi
Vita.....	vii
List of Tables	xiii
List of Figures	xv
Chapter 1: Introduction	1
1.1 Motivation	1
1.2 A Note to the Reader	2
1.3 Research Objectives	3
1.4 Thesis Intent	4
Chapter 2: Background Information	5
2.1 Introduction to Vehicle Dynamics	5
2.2 Anti-lock Braking System (ABS)	10
2.3 Electronic Stability Control (ESC).....	12
2.3.1 Components of Electronic Stability Control	12
2.3.2 Roll Stability Control (RSC)	13

2.3.3 Yaw Stability Control (YSC)	16
2.4 Controller Area Network (CAN) Communication.....	18
2.4.1 Introduction to the SAE J1939 Protocol.....	18
2.4.2 Network Topology.....	20
2.4.3 Message Frames	22
2.4.4 PGNs and SPNs.....	24
2.4.5 Physical Signal Values and Raw Signal Values.....	26
2.4.6 Broadcast and Peer-to-Peer Messages	28
2.4.7 Multi-packet Messages	29
Chapter 3: Tractor-Trailer Modeling.....	32
3.1 Introduction to TruckSim.....	32
3.2 General Tractor Specifications.....	33
3.3 Tractor Modeling.....	34
3.3.1 Sprung Mass Modeling.....	34
3.3.2 Suspension Modeling	36
3.3.3 Unsprung Mass Modeling	39
3.3.4 Tire Modeling.....	41
3.3.5 Brake System Modeling	43
3.4 Trailer Modeling	46
3.4.1 High C.G. Trailer.....	50

3.4.2 Low C.G. Trailer	52
3.5 Validation of Tractor-Trailer Model	55
3.5.1 Double Lane Change Maneuver	57
3.6 The TruckSim S-Function	60
Chapter 4: Hardware in the Loop Simulation	63
4.1 HIL Simulation Concept	63
4.1.1 Anti-lock Braking System Hardware	64
4.1.2 Placing the Braking Hardware in the Loop	68
4.2 HIL Hardware Configuration	72
4.2.1 dSPACE Midsize Simulator	72
4.2.2 Wheel Speed Sensor Simulation.....	75
4.2.3 Brake Chamber Rigs.....	80
4.2.4 Brake Chamber Pressure Sensing.....	88
4.2.5 Anti-lock Braking System ECU and Electrical Connections	90
4.3 HIL Simulation Software	93
4.3.1 Simulink, TruckSim and RTI Block Set.....	93
4.3.2 Creating the J1939 Messages	102
4.3.3 Building the Simulink Model for the dSPACE Real Time Processor	108
4.3.4 Running the Simulation with ControlDesk	109
Chapter 5: Validation of Hardware in the Loop Simulation.....	115

5.1 HIL Braking Tests and Validation	115
5.1.1 Braking Test Procedures.....	116
5.1.2 Simulating Road Friction Characteristics.....	117
5.1.3 Stationary Brake Chamber Pressure Test	122
5.1.4 Braking Tests	124
5.2 Overall Results for HIL Simulation	162
Chapter 6: Software in the Loop Simulation	166
6.1 SIL Simulation Concept	166
6.2 Anti-lock Brake Controller	169
6.2.1 Anti-lock Brake Controller Design.....	170
6.2.2 Validation of Anti-lock Brake Controller.....	173
6.3 Vehicle Mass Estimator	178
6.3.1 Mass Estimator Design.....	178
6.3.2 Validation of Mass Estimator	180
6.4 Roll Stability Controller	181
6.4.1 Roll Stability Controller Design.....	181
6.4.2 Validation of Roll Stability Controller	186
Chapter 7: Summary and Recommendations.....	193
7.1 Summary	193
7.2 Recommendations	197

References..... 199

List of Tables

Table 2.1: SAE J1939 Core Standards.....	20
Table 2.2: CAN Bus Voltages.....	22
Table 2.3: BAM Message.....	31
Table 3.1: Solo Tractor Static Loading.....	33
Table 3.2: Tractor Sprung Mass Parameters.....	35
Table 3.3: Tractor Suspension Parameters.....	39
Table 3.4: Tractor Unsprung Mass Parameters.....	40
Table 3.5: High C.G. Trailer Sprung Mass Parameters.....	51
Table 3.6: High C.G. Trailer Unsprung Mass Parameters.....	52
Table 3.7: High C.G. Trailer Suspension Parameters.....	52
Table 3.8: Low C.G. Trailer Sprung Mass Parameters.....	54
Table 3.9: Low C.G. Trailer Unsprung Mass Parameters.....	55
Table 3.10: Low C.G. Trailer Suspension Parameters.....	55
Table 4.1: HTM Brake Chamber Deflection Test.....	84
Table 4.2: RTI Blocks.....	94
Table 5.1: Calculating Friction for the HIL Simulation.....	121
Table 5.2: Test Configuration for HIL Validation.....	121
Table 5.3: Brake Chamber Pressure Rise Times.....	124
Table 5.4: HIL Test 1 Validation Metrics.....	130
Table 5.5: HIL Test 2 Validation Metrics.....	135

Table 5.6: HIL Test 3 Validation Metrics.....	139
Table 5.7: HIL Test 4 Validation Metrics.....	143
Table 5.8: HIL Test 5 Validation Metrics.....	147
Table 5.9: HIL Test 6 Validation Metrics.....	152
Table 5.10: HIL Test 7 Validation Metrics.....	157
Table 5.11: HIL Test 8 Validation Metrics.....	161
Table 6.1: SIL ABS Logic.....	171
Table 6.2: Test Configuration for SIL ABS Validation.....	174
Table 6.3: Test Results for SIL Mass Estimator.....	180
Table 6.4: Test Configuration for SIL RSC Validation.....	187

List of Figures

Figure 2.1: SAE Vehicle Coordinate System.....	5
Figure 2.2: Braking Coefficient versus Wheel Slip, Courtesy of [3].....	7
Figure 2.3: Lateral Force versus Slip Angle, Courtesy of [3].....	8
Figure 2.4: Vehicle Cornering Forces.....	9
Figure 2.5: Wheel Speed Under ABS Control, Courtesy of [3].....	11
Figure 2.6: Rollover Forces.....	14
Figure 2.7: Lateral Acceleration Threshold versus Payload.....	16
Figure 2.8: Under Steer and Over Steer, Courtesy of [4].....	17
Figure 2.9: CAN Bus Wiring.....	21
Figure 2.10: Extended CAN Message Frame.....	24
Figure 2.11: The EBC1 Message, Courtesy of [7].....	26
Figure 2.12: Analysis of EBC1 Message.....	29
Figure 3.1: TruckSim Vehicle Coordinate System.....	33
Figure 3.2: TruckSim Tractor Sprung Mass.....	35
Figure 3.3: TruckSim Tractor Suspension.....	36
Figure 3.4: TruckSim Tractor Spring Rate.....	38
Figure 3.5: TruckSim Tractor Shock Absorber Damping.....	38
Figure 3.6: TruckSim Tractor Suspension.....	40
Figure 3.7: TruckSim Tires.....	42
Figure 3.8: TruckSim Tires Longitudinal Force.....	42

Figure 3.9: TruckSim Tires Lateral Force.....	43
Figure 3.10: TruckSim Disc Brakes.....	44
Figure 3.11: Simulink Drum Brake Model.....	45
Figure 3.12: Drum Brake Torque versus Pressure at Varying Wheel Speed.....	46
Figure 3.13: TruckSim Trailer.....	48
Figure 3.14: TruckSim Trailer Sprung Mass.....	48
Figure 3.15: TruckSim Trailer Unsprung Mass.....	49
Figure 3.16: TruckSim Trailer Suspension.....	49
Figure 3.17: High C.G. Trailer Photo.....	50
Figure 3.18: TruckSim High C.G. Tractor-Trailer Model.....	51
Figure 3.19: Low C.G. Trailer Photo.....	53
Figure 3.20: TruckSim Low C.G. Tractor-Trailer Model.....	54
Figure 3.21: Solo Tractor Double Lane Change.....	58
Figure 3.22: High C.G. Tractor-Trailer Double Lane Change.....	59
Figure 3.23: Low C.G. Tractor-Trailer Double Lane Change.....	60
Figure 3.24: TruckSim S-Function.....	61
Figure 3.25: TruckSim S-Function Import and Export Variables.....	62
Figure 4.1: HIL Layout.....	64
Figure 4.2: Pneumatic Braking System with ABS, Courtesy of [11]	66
Figure 4.3: ABS Modulator, Courtesy of [2]	67
Figure 4.4: ABS Modulator Solenoids, Courtesy of [2]	67
Figure 4.5: HIL Signal Diagram.....	71
Figure 4.6: dSPACE Midsize Simulator.....	74

Figure 4.7: dSPACE Link board, Courtesy of [12]	75
Figure 4.8: VRS Wheel Speed Sensor, Courtesy of [13]	76
Figure 4.9: Wheel Speed Signal Generator.....	78
Figure 4.10: dSPACE Wheel Speed Generator Circuit.....	80
Figure 4.11: Drum Brake Components, Courtesy of [2]	81
Figure 4.12: Drum Brake Deflection Test.....	84
Figure 4.13: Brake Chamber Rig.....	87
Figure 4.14: Emulating Drum Brake Stiffness.....	88
Figure 4.15: Brake Chamber Pressure Sensing.....	90
Figure 4.16: dSPACE and ABS ECU Wiring Schematic.....	92
Figure 4.17: HIL Simulator Photo.....	93
Figure 4.18: HIL Simulink Model Top Layer.....	96
Figure 4.19: HIL Simulink Model Software Hardware Interface.....	97
Figure 4.20: HIL Simulink Model ECU Interface.....	99
Figure 4.21: HIL Simulink Model J1939 Messaging.....	102
Figure 4.22: Vector DBC File Editor.....	105
Figure 4.23: HIL Simulink Model TX Messages.....	107
Figure 4.24: Running the HIL Simulation from ControlDesk.....	112
Figure 4.25: Running the HIL Simulation from TruckSim.....	113
Figure 4.26: Viewing CAN Communications from ControlDesk.....	114
Figure 5.1: TruckSim Tire Efficiency.....	120
Figure 5.2: HIL Step Input Pressure Test.....	123
Figure 5.3: HIL Test 1 Front Left Pressure and Wheel Speed.....	127

Figure 5.4: HIL Test 1 Back Left Pressure and Wheel Speed.....	128
Figure 5.5: HIL Test 1 Stopping Performance.....	129
Figure 5.6: HIL Test 2 Front Left Pressure and Wheel Speed.....	133
Figure 5.7: HIL Test 2 Back Left Pressure and Wheel Speed.....	134
Figure 5.8: HIL Test 2 Stopping Performance.....	135
Figure 5.9: HIL Test 3 Front Left Pressure and Wheel Speed.....	137
Figure 5.10: HIL Test 3 Back Left Pressure and Wheel Speed.....	138
Figure 5.11 HIL Test 3 Stopping Performance.....	139
Figure 5.12: HIL Test 4 Front Left Pressure and Wheel Speed.....	141
Figure 5.13: HIL Test 4 Back Left Pressure and Wheel Speed.....	142
Figure 5.14: HIL Test 4 Stopping Performance.....	143
Figure 5.15: HIL Test 5 Front Left Pressure and Wheel Speed.....	145
Figure 5.16: HIL Test 5 Back Left Pressure and Wheel Speed.....	146
Figure 5.17: HIL Test 5 Stopping Performance.....	147
Figure 5.18: HIL Test 6 Front Left Pressure and Wheel Speed.....	149
Figure 5.19: HIL Test 6 Back Left Pressure and Wheel Speed.....	150
Figure 5.20: HIL Test 6 Wheel Slip Ratio.....	151
Figure 5.21: HIL Test 6 Stopping Performance.....	152
Figure 5.22: HIL Test 7 Front Left Pressure and Wheel Speed.....	154
Figure 5.23: HIL Test 7 Back Left Pressure and Wheel Speed.....	155
Figure 5.24: HIL Test 7 Wheel Slip Ratio.....	156
Figure 5.25: HIL Test 7 Stopping Performance.....	157
Figure 5.26: HIL Test 8 Front Left Pressure and Wheel Speed.....	159

Figure 5.27: HIL Test 8 Back Left Pressure and Wheel Speed.....	160
Figure 5.28: HIL Test 8 Stopping Performance.....	161
Figure 5.29: HIL ABS Modulation Time Differences.....	163
Figure 5.30: HIL Average Pressure Differences.....	164
Figure 5.31: HIL Stopping Performance Differences.....	165
Figure 6.1: SIL Layout.....	168
Figure 6.2: SIL Simulink Model Top Layer.....	169
Figure 6.3: Analyzing ABS Control.....	171
Figure 6.4: SIL Simulink Model for ABS.....	172
Figure 6.5: SIL ABS Test 1 Front Left Pressure and Wheel Speed.....	176
Figure 6.6: SIL ABS Test 1 Back Left Pressure and Wheel Speed.....	177
Figure 6.7: SIL ABS Test 1 Stopping Performance.....	178
Figure 6.8: SIL RSC Working Principal.....	182
Figure 6.9: SIL Simulink Model for RSC Inner Layer.....	185
Figure 6.10: SIL RSC Test 1 Pressure.....	189
Figure 6.11: SIL RSC Test 1 Vehicle Behavior.....	190
Figure 6.12: SIL RSC Test 1 Engine and Brake Control.....	191
Figure 6.13: SIL RSC TruckSim Animation During Severe Turn.....	192

Chapter 1: Introduction

1.1 Motivation

As economies expand and populations grow so will the need for transportation of goods and the demand for large cargo vehicles. Although many goods are transported via air, sea or train, perhaps the most common means for transporting goods in the U.S. is through commercial road vehicles such as tractor-trailers. With over 46,000 miles of interstate highway system, 116,000 miles of non-interstate highways and nearly 3.9 million miles of other roads [1], today's tractor-trailers have plenty of infrastructure to deliver goods to all corners of the continental United States. With millions of tractor-trailers traveling on U.S. roads each day, carrying important and sometimes dangerous cargo, it is important that we continually work to improve the safety of these vehicles.

Over the years there have been many mandates put forth by the U.S. government as well as governments around the world in an effort to improve safety within the industry. Mandates such as the Federal Motor Vehicle Standard No. 121 developed by the U.S. Department of Transportation lays down requirements for all air brake vehicles to implement anti-lock brakes and reduce stopping distances amongst other things. Although many vehicle manufactures readily comply with these requirements, the manufactures must also take it upon themselves to go beyond what is required by the government and improve vehicle performance to an extent that is truly satisfactory.

The goal of this research was to improve research and development methodologies within the trucking industry by working in partnership with a heavy truck manufacturer and studying dynamic controls through HIL and SIL simulation. These simulation techniques have great potential for increasing the efficiency in which new vehicle hardware and control systems are developed and can ultimately lead to the production of safer vehicles.

Whenever new control algorithms, brake hardware or essentially any new vehicle component is developed, it must be tested. Typically this is done with real world testing on a proving ground. Real world testing can be time consuming, costly and dangerous since a test driver is needed along with a test vehicle. When conducting severe maneuvers, the vehicle can potentially be damaged and the driver can be injured. Due to these shortcomings, HIL and SIL simulation techniques are becoming more and more popular. With HIL and SIL simulation, an array of tests can be conducted over and over again at low cost and without the need for large test crews or test facilities.

1.2 A Note to the Reader

This project was conducted in participation with a popular heavy truck manufacturer who was interested in acquiring knowledge on the HIL and SIL simulation processes. The manufacturer chose a specific tractor design to study in the HIL and SIL simulations and supplied detailed vehicle parameter data so an accurate vehicle model could be developed. In addition to this, the manufacturer supplied braking hardware from the actual production tractor so it could be used in the HIL simulation. Throughout

this thesis, the manufacturer will be referenced simply as the heavy truck manufacturer or HTM.

1.3 Research Objectives

In total there were three key objectives behind this research. The first objective was to successfully develop a computer model of a tractor-trailer rig. For this project, a 6x4 tractor from the heavy truck manufacturer (HTM) was modeled. In addition to this, a high center of gravity trailer and a low center of gravity trailer were both modeled and each was paired with the tractor. Both of these rigs were validated using real world experimental data.

The second objective behind this research was to develop a hardware in the loop (HIL) simulation and evaluate the capability of the HIL process to accurately simulate the tractor performance under braking maneuvers. This was accomplished by integrating the tractor model with MATLAB Simulink and utilizing actual braking hardware for the simulation. A dSPACE Midsize was used as the interface to facilitate interaction between the vehicle model, which operates in the computer realm, and the brake hardware, which operates in the physical realm. For this project, a braking system equipped with ABS was chosen. Upon completing the HIL simulation, the model was ran through several braking maneuvers in order to compare the simulated vehicle performance to the performance of the real tractor.

The third objective behind this research was to develop a software in the loop (SIL) simulation and evaluate the capability of the SIL process to accurately simulate tractor-trailer performance under braking and handling maneuvers. This was

accomplished by integrating the tractor-trailer model into MATLAB Simulink and developing anti-lock braking (ABS) and roll stability control (RSC) algorithms from the ground up. Upon completing the ABS and RSC algorithms, the model was ran through several braking and handling maneuvers in order to compare the simulated vehicle performance to the performance of the real tractor-trailer.

1.4 Thesis Intent

In the following chapters of this thesis, the efforts taken to create a working HIL and SIL simulation will be discussed. Upon review of this work, the reader should have a strong understanding of the vehicle simulation process. This thesis is intended to convey information for those looking to develop HIL and SIL simulations in the future as well as discuss the validity of these simulation techniques. In particular, the HIL simulation process will be emphasized here. For more information on the TruckSim modeling software and the SIL simulation processes, please refer to the corresponding work published for this project. The work is entitled "Development of a Heavy Truck Vehicle Dynamics Model using TruckSim and Model Based Design of ABS and ESC Controllers in Simulink" [2] and was authored by fellow researcher Shreesha Rao.

Chapter 2: Background Information

2.1 Introduction to Vehicle Dynamics

In order to understand the functionality of the vehicle controllers implemented in this project, it is important that the reader have an understanding of basic vehicle dynamic principles. First, a vehicle coordinate system must be defined in order to properly understand the six types of vehicular motions (longitudinal, lateral, vertical, roll, pitch and yaw). For this chapter, the SAE vehicle axis system will be referenced and it is given in Figure 2.1. As seen in the figure, the origins of the vehicle's axes are taken from the center of gravity (C.G.) of the vehicle. The x-axis runs forward longitudinally, the y-axis runs to the right laterally and the z-axis runs down vertically. In addition to this, the roll, pitch and yaw motions are rotations about the x, y, and z axes respectively.

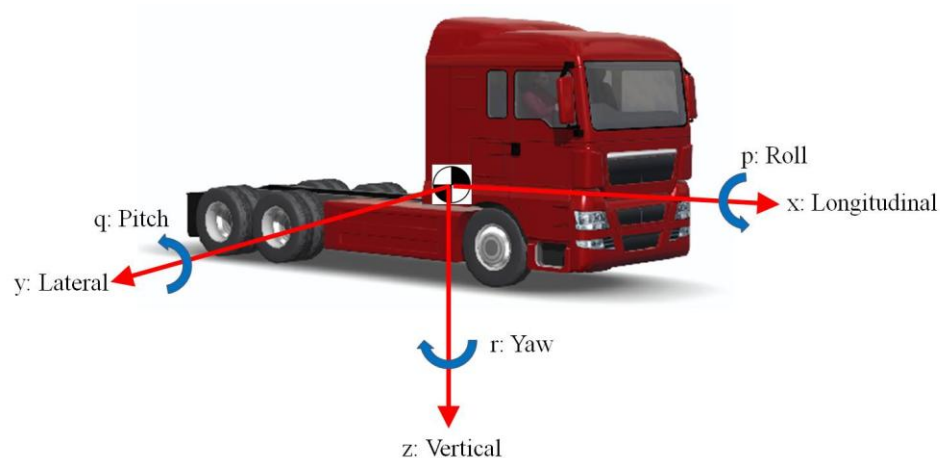


Figure 2.1: SAE Vehicle Coordinate System

It is also important to understand that in order for any type of road vehicle, whether it be a tractor-trailer or passenger car, to undergo a longitudinal acceleration maneuver, i.e. straight-line braking, or a lateral acceleration maneuver, i.e. cornering, the tires must generate force by means of friction between the tire-road contact interface. The amount of force the tires are capable of generating depends on many things such as the tire loading, the tire slip, the tread type, the inflation pressure, the road conditions and much more.

For a more general and simplified understanding of how a tire generates force, it is common to use the calculation given in Equation 2.1. In this equation, the force generated by the tire in the longitudinal direction (F_x) is equal to the coefficient of friction (μ) multiplied by the vertical force acting on the tire (W). It is also important to understand that the coefficient of friction (μ) is not a constant value. Its value depends greatly on the tire slip ratio (s) given in Equation 2.2. In this equation the slip ratio is a unit less value equal to the vehicle's velocity (V), minus the effective tire radius (r), multiplied by the rotational speed of the tire (ω), all divided by the vehicle's velocity.

$$F_x = \mu \cdot W \quad \text{Equation 2.1, Courtesy of [3]}$$

$$s = \frac{V - \omega r}{V} \quad \text{Equation 2.2, Courtesy of [3]}$$

Upon referring to Figure 2.2 we can see the coefficient of friction (μ), otherwise known as the braking coefficient, is greatly dependent on the slip ratio. According to the figure, the coefficient of friction is zero when the slip ratio is equal to zero. As the slip

ratio increases to around 20%, the coefficient of friction rises to its peak value of around 0.7 (this is for the 30 mph and dry scenario). As the slip ratio further increases, the coefficient of friction begins to fall. It should be noted that the numerical values in this figure are by no means universal or exact. The coefficient of friction versus slip ratio plot will vary on a case-to-case basis.

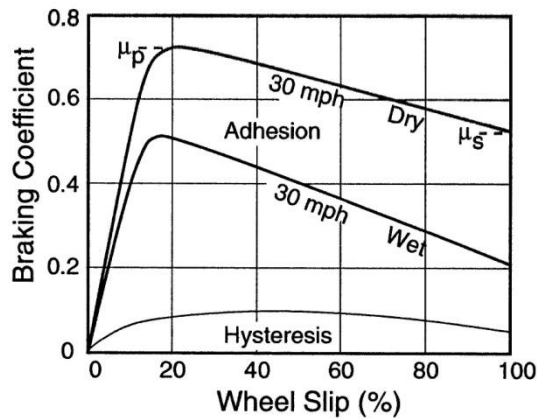


Figure 2.2: Braking Coefficient versus Wheel Slip, Courtesy of [3]

Just as Equation 2.1 is used to calculate tire force in the longitudinal direction during braking, Equation 2.3 is used to calculate the tire force in the lateral direction which is needed to overcome centripetal acceleration during cornering. As seen in the equation, the lateral force generated by the tire (F_y) is equal to the slip angle of the tire (α) multiplied by the cornering stiffness (C_α). The lateral force (F_y) is also known as cornering force and it always acts perpendicular to the tire as demonstrated in Figure 2.3. The slip angle of the tire (α) is equal to the angle between the tire heading and the

instantaneous velocity, i.e. direction of travel, of the tire. The slip angle is shown in Figure 2.3 as well.

In order to calculate the cornering force for a given slip angle, the cornering stiffness (C_α) must be known. Figure 2.3 demonstrates how the cornering stiffness is equal to the slope of the F_y versus α curve. As seen in the figure, the cornering stiffness begins to decrease as the slip angle becomes large. It should be noted that the values in this plot are meant to be used as an example and in reality the cornering force will vary with vertical tire loading and other vehicle parameters.

$$F_y = C_\alpha \cdot \alpha$$

Equation 2.3, Courtesy of [3]

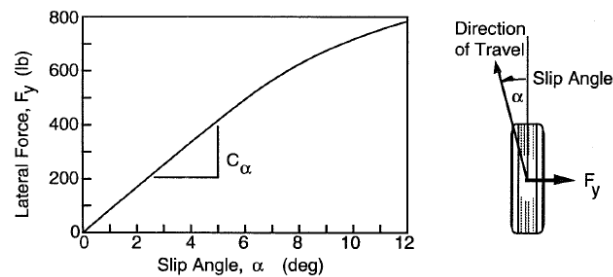


Figure 2.3: Lateral Force versus Slip Angle, Courtesy of [3]

The ability for a vehicle to accelerate, decelerate, turn left or turn right is limited by the amount of friction generated by the tire-road contact interface. In order for the vehicle to accelerate or decelerate, there must be some slip ratio (s) and some longitudinal force (F_x). Likewise, in order for the vehicle to maintain a turn, there must

be some slip angle (α) and some cornering force (F_y). Figure 2.4 illustrates a free body diagram of a simplified four wheel vehicle in which the longitudinal and lateral forces at each wheel are taken into account. This figure assumes the vehicle is making a small right hand turn (δ_l and $\delta_r \approx 0$) while braking. The vehicle's C.G. is some distance (b) from the front wheels, some distance (c) from the rear wheels and centered at one half the track width ($t/2$). We can see from the figure and Equation 2.4 that a moment about the z-axis at the C.G. is produced. This is known as a yaw moment.

$$M_{C.G.z} = (F_{y_{fl}} + F_{y_{fr}})b - (F_{y_{rl}} + F_{y_{rr}})c + (F_{x_{fr}} + F_{x_{rr}})\frac{t}{2} - (F_{x_{fl}} + F_{x_{rl}})\frac{t}{2} \quad \text{Equation 2.4}$$

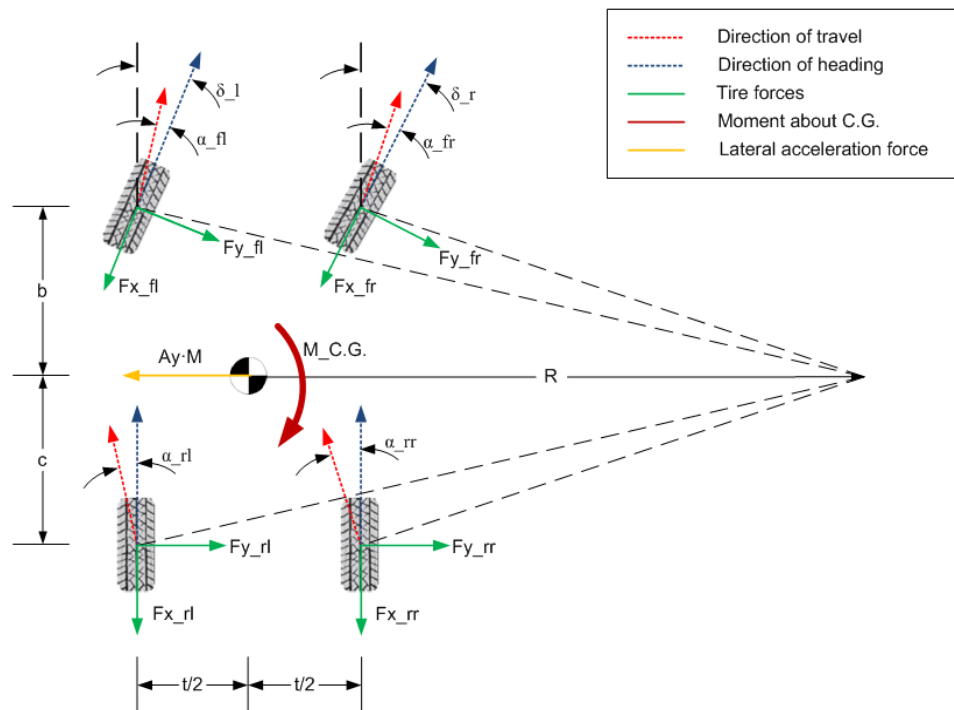


Figure 2.4: Vehicle Cornering Forces

2.2 Anti-lock Braking System (ABS)

In order to achieve maximum braking performance it is important to generate a large longitudinal force (F_x). In order to generate a large longitudinal force it is necessary to achieve a large coefficient of friction value (μ). In order to achieve a large coefficient of friction, the slip ratio must be kept around 20%; this value will vary depending on the application. Anti-lock brakes operate on this principal. The ABS in a vehicle strategically attempts to keep the slip ratio near an optimal value. It does this by releasing the brakes when the slip ratio becomes too large, i.e. when the wheels begin to lock-up. Likewise, the ABS will re-apply the brakes when the slip ratio becomes too small, i.e. when the wheels recover from the lock-up and begin to spin near the vehicle's speed. This anti-lock braking behavior is demonstrated in Figure 2.5. In this figure, the vehicle speed is plotted with respect to time along with four different wheel speeds. Upon examining the behavior of the right front wheel (RF), we can see that the wheel speed steadily decreases throughout region one, under this region the slip ratio has not yet surpassed its optimal value. As continue on to region two, the wheel speed rapidly drops. From this we can conclude that wheel lock-up is about to occur and the slip ratio has just past its optimal value for generating friction. Finally, we can see that the wheel speed begins to rise again at region three. Under this region, the ABS has released the brakes and is allowing the wheel speed to rise again. This is done in order to bring the slip ratio back to its optimal value of around 20%.

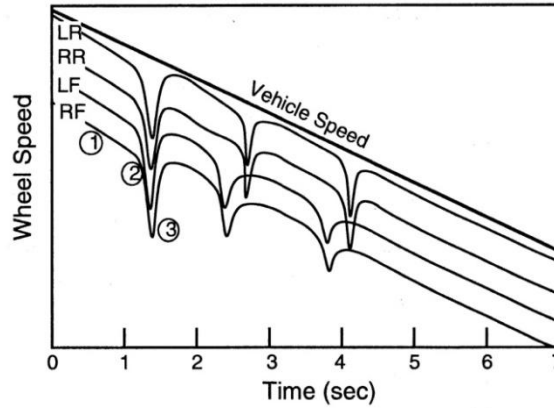


Figure 2.5: Wheel Speed Under ABS Control, Courtesy of [3]

In principal ABS is fairly simple, however, in practice many different algorithms are used to maximize the performance of the system depending on the application. The exact slip ratio at which the vehicle's ABS will release and re-apply the brakes all depends on the individuals who designed the system. In fact, some systems do not even observe wheel slip. As a substitute to this, the deceleration of the wheel is measured. In these systems, the ABS will release and re-apply the brakes in accordance with pre-defined deceleration set points. These ABS controllers may take into account what the current wheel deceleration is as well as what it was just milliseconds previously. All of this is done in an attempt to keep the wheel slip ratio at an optimal value where the greatest coefficient of friction will be generated. It should be understood that although many variations of anti-lock control exist, all ABS algorithms operate on similar principles.

2.3 Electronic Stability Control (ESC)

2.3.1 Components of Electronic Stability Control

As a road vehicle undergoes steering maneuvers, a lateral acceleration is produced upon the mass of the vehicle. For a steady-state cornering maneuver, the amount of lateral acceleration produced (A_y) is given by Equation 2.5 where V is the longitudinal velocity of the vehicle and R is the turning radius. As seen in the equation, an increase in velocity and/or decrease in the turning radius will produce an increase in lateral acceleration. This increase can have two prominent effects on the motion of the vehicle. If A_y is large enough, the vehicle will begin to lean significantly, i.e. roll, and eventually the inner wheels will lift off the road and the vehicle will roll onto its side. Likewise, if A_y is large enough and the amount of cornering force produced from the front wheels ($F_{y_{front}}$) is not balanced with the amount of cornering force produced by the rear wheels ($F_{y_{rear}}$), a yawing moment will be produced about the center of gravity of the vehicle. This will cause the vehicle to rotate too much or not enough as it takes the turn.

$$A_y = \frac{V^2}{R} \quad \text{Equation 2.5}$$

In order to prevent severe roll from occurring, tractor-trailer manufacturers implement a roll stability control system (RSC). Likewise, in order to prevent severe yaw from occurring, a yaw stability control system (YSC) is implemented. Together these two systems are usually referred to as electronic stability control (ESC) or electronic stability program (ESP). The basic operation of RSC and YSC will be discussed in the following sections

2.3.2 Roll Stability Control (RSC)

As a vehicle makes a cornering maneuver, a rolling moment is produced about the centerline of the outer wheels. This moment results from a lateral acceleration force acting upon the vehicles center of gravity. This behavior is illustrated in Figure 2.6 in which a perfectly rigid tractor-trailer with a perfectly centered mass is making a left hand turn. Upon referring to the figure we can see that the lateral force acting on the center of gravity is equal to the mass of the vehicle times the lateral acceleration. This force produces a tipping moment (clockwise) about the outer wheels. This moment is equal to the vehicle mass times the lateral acceleration times the height of the center of gravity. The vertical load on the inner wheels (F_{zi}) also produces a tipping moment equal to F_{zi} times the track width (t). In addition to this, gravity produces a counter tipping moment equal to the acceleration of gravity times the mass of the vehicle times one half of the track width. By solving for the equal net moment at the outer wheels, the load on the inner wheels can be determined for a given lateral acceleration. This calculation is given in Equation 2.6. If we modify this equation so that the load on the inner wheels (F_{zi}) is zero, as would occur during the onset of rollover, we can determine how many g's are needed to roll the vehicle over. This calculation is done in Equation 2.7. As seen from the equation, an increase in the height of the center of gravity of the vehicle (h) will cause a decrease in the number of g's the vehicle can withstand in a turn without rolling over. This lateral acceleration limit is known as the rollover threshold.

$$\frac{A_y}{g} = \frac{\frac{t}{2} \frac{F_{zi}}{M \cdot g} \cdot t}{h}$$

Equation 2.6, Courtesy of [3]

$$\frac{A_y}{g} = g_{threshold} = \frac{t/2}{h}$$

Equation 2.7, Courtesy of [3]

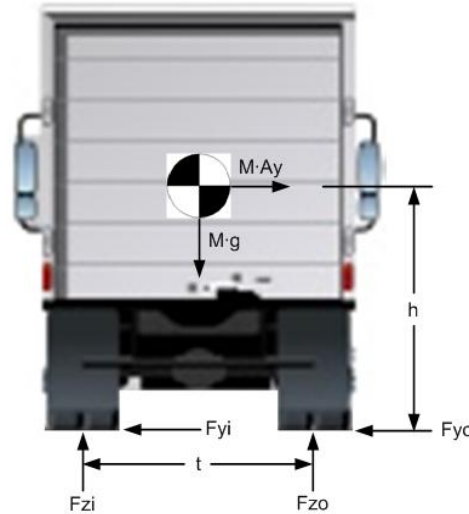


Figure 2.6: Rollover Forces

The rollover threshold must be considered when trying to design an RSC system for a tractor-trailer. Usually the rollover threshold is determined experimentally for various loads with increasing center of gravity heights. A plot is given in Figure 2.7 that shows how rollover threshold increases as load increases. This plot was taken from actual experimental data provided by the RSC ECU manufacturer. As we can see in the plot, the lateral acceleration rollover threshold decreases as the load increases. This is due to the fact that as the loading was increased on the experimental tractor-trailer rig, the center of gravity height increased as well.

In order to prevent rollover from occurring, most RSC systems incorporate a lateral acceleration sensor and a vehicle weight estimator. The RSC system is able to

detect the tractor-trailer's weight via the vehicle weight estimator; these weight estimators may rely upon active loading sensors or may estimate weight based on applied engine torque and wheel acceleration values. After the weight is estimated, an appropriate rollover threshold is decided upon for that particular weight; usually the threshold value is taken from experimental data such as that given in Figure 2.7. After the rollover threshold is determined, the RSC system will monitor the lateral acceleration using onboard accelerometers. If the vehicle's lateral acceleration approaches the rollover threshold, the brakes will automatically be applied, the vehicle's speed will be reduced, the lateral acceleration will decrease and the rollover will be prevented. Although this is the basic functionality behind RSC, there are many ways the control algorithms can be manipulated to achieve better performance.

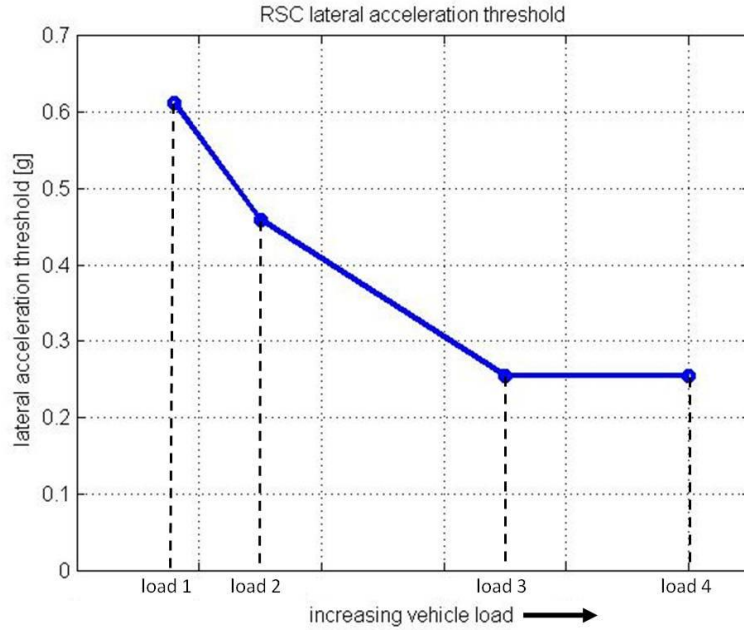


Figure 2.7: Lateral Acceleration Threshold versus Payload

2.3.3 Yaw Stability Control (YSC)

As a vehicle undergoes a cornering maneuver, a certain amount of yawing motion is needed in order to rotate the body of the vehicle as it goes around the turn. If the amount of yaw is too small, the vehicle will not be able to complete the turn and will go straight ahead instead of staying on track. This will occur if the front tires cannot generate sufficient lateral force to produce the proper yaw moment about the C.G. of the vehicle. Under this circumstance the slip angle of the front wheels would become sufficiently large in comparison to that of the rear wheels. This behavior is known as under-steer. Similarly, if the amount of yaw is too large and the slip angle of the rear wheels is sufficiently large in comparison to that of the front wheels, the vehicle will

again veer off course. This behavior is known as over-steer. An example of both of these behaviors is illustrated in Figure 2.8.

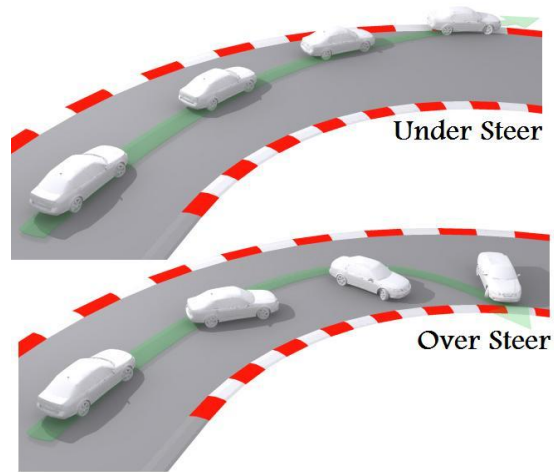


Figure 2.8: Under Steer and Over Steer, Courtesy of [4]

In order assist the vehicle in producing a proper yaw motion during a severe turn, a YSC controller is used. The YSC controller incorporates a yaw sensor, a lateral acceleration sensor and wheel speed sensors. The YSC controller is able to sense the amount of yaw the vehicle is undergoing via the yaw sensor. This is known as the “actual yaw rate” and it is measured in radians per second. The YSC controller is also able to estimate what the proper yaw rate should be given the vehicle's speed and lateral acceleration. This is known as "desired yaw rate" and it is equal to lateral acceleration (A_y) divided by the vehicle's speed (V).

The YSC control algorithm works by attempting to match the actual yaw rate value to the demanded yaw rate value. This is done by first subtracting the desired yaw rate from the actual yaw rate to produce the yaw rate error (YR_{error}). This is done in Equation 2.8. Next, the YSC controller sends differential braking commands to the wheels based on the sign and magnitude of the error. If the vehicle is making a right hand turn and the actual yaw rate is too small, then the error will be negative and the controller will send braking commands to the right side wheels in order to increase the yaw moment in the direction of the turn. Likewise, if the yaw rate is too large then the error will be positive and the controller will send braking commands to the left side wheels in order to decrease the yaw moment in the direction of the turn. Figure 2.4 shown in Section 2.1 is helpful in illustrating this behavior.

$$Y_{error} = YR_{actual} - YR_{desired} = YR_{actual} - \frac{Ay}{v} \quad \text{Equation 2.8, Courtesy of [5]}$$

2.4 Controller Area Network (CAN) Communication

2.4.1 Introduction to the SAE J1939 Protocol

Today's modern vehicles utilize many onboard computers which control different components throughout the vehicle. These controllers, also known as electronic control units (ECUs), are designed to control one or more sub-systems within the vehicle and do so in an efficient and optimal manner. For example, a vehicle's engine may have one or more controllers devoted to adjusting fuel flow and other engine variables while maximizing fuel efficiency and power. In many cases, several ECUs are connected to one another in order to exchange data such as parameters and variables which pertain to

different sub-systems. For example, an electronic engine controller (EEC) may send and receive messages with an electronic transmission controller (ETC) in order to adjust engine speed and torque while a gear change is being performed. In this particular example, the EEC and ETC are connected in a controller area network, also known as a CAN network. The EEC and ETC controllers are each considered to be "nodes" on the CAN network.

There are several different types of CAN networks used in many different applications such as passenger vehicle control, marine control, aviation control and more. In this paper we will focus on the Society of Automotive Engineers (SAE) J1939 CAN protocol. This protocol was developed by SAE in 1998 and it is an adaptation of the International Organization for Standardization (ISO) 11898 high speed CAN protocol [6]. The SAE J1939 protocol was developed with the goal of standardizing CAN network topology and communications for heavy-truck control applications. The SAE J1939 CAN standards are defined throughout several secure documents published by SAE. A list of some of the primary SAE J1939 document names and descriptions is given in Table 2.1. Out of these documents, it was determined that SAE J1939-71 [7], SAE J1939-14 [8], SAE J1939-21 [9] and SAE J1939-73 [10] were most relevant and most useful for implementing CAN communications with the braking system ECU used in this project. These documents will be furthered discussed in later sections.

<u>Document Name</u>	<u>Description</u>
J1939	Recommended Practice for a Serial Control and Communications Vehicle Network
J1939-01	Recommended Practice for Control And Communications Network for On-Highway Equipment
J1939-02	Agricultural and Forestry Off-Road Machinery Control and Communication Network
J1939-03	On Board Diagnostics Implementation Guide
J1939-05	Marine Stern Drive and Inboard Spark-Ignition Engine On-Board Diagnostics Implementation Guide
J1939-11	Physical Layer - 250k bits/s, Twisted Shielded Pair
J1939-14	Physical Layer - 500k bits/s, Twisted Shielded Pair
J1939-13	Off-Board Diagnostic Connector
J1939-15	Reduced Physical Layer, 250K bits/sec, Un-Shielded Twisted Pair (UTP)
J1939-21	Data Link Layer
J1939-31	Network Layer
J1939-71	Vehicle Application Layer
J1939-73	Application Layer - Diagnostics
J1939-74	Application - Configurable Messaging
J1939-75	Application Layer - Generator Sets and Industrial
J1939-81	Network Management
J1939-82	Compliance - Truck and Bus
J1939-84	OBD Communications Compliance Test Cases for Heavy Duty Components and Vehicles

Table 2.1: SAE J1939 Core Standards

2.4.2 Network Topology

The J1939 CAN network topology is specified by the Society of Automotive Engineers in the document entitled J1939-14 [8]. This document includes information on the wire type, connection methodology, data transfer rate and much more. Although

there are many specifications for the network topology, only a few of the key requirements will be discussed here.

When constructing a J1939 network, it is important to first take the proper steps when connecting the ECUs together. Figure 2.9 demonstrates a simple wiring schematic for a two node network. As we can see in the figure, the two CAN devices are wired together in parallel. The wires that connect the devices together are referred to as the CAN bus. The CAN bus consists of two wires; a shielded CAN High wire given in yellow and a shielded CAN Low wire given in green. These wires are twisted together with approximately one twist every 25 millimeters in order to lower electromagnetic interference; also known as crosstalk. In addition to this, the CAN High and CAN Low wires must be separated with a 120 ohm resistor at each node. Typically this resistance is already built into the ECU by the device manufacturer. It can also be noted that according to the SAE standards, the J1939 communication protocol can support a data transfer rate of either 250 kBaud or 500 kBaud. This essentially means that ECUs on a J1939 bus can communicate with one another at a rate of either 250,000 bits per second or 500,000 bits per second depending on the network settings [8].

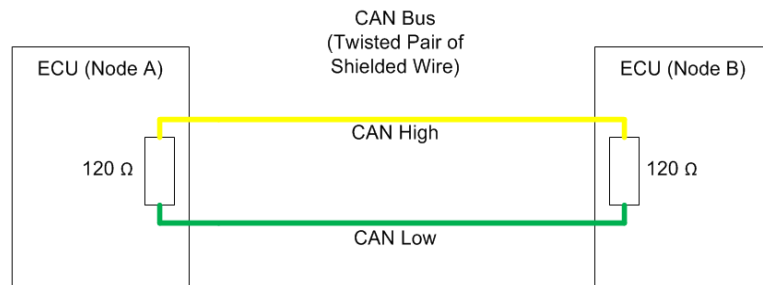


Figure 2.9: CAN Bus Wiring

2.4.3 Message Frames

At the heart of CAN communications is the message frame. In the “CAN world” all ECUs communicate with one another by sending message frames over the CAN bus. In the “physical world”, a message frame is simply an interval of time in which a node sends a series of voltage pulses over the CAN bus. These voltage pulses represent binary values in the “computer world”, i.e. one or zero, and therefore must have one of two values. This essentially means the bus can transmit either a zero, known as the dominant state, or a one, known as the recessive state. The corresponding bus voltages for each state are given in Table 2.2. [8].

Every voltage pulse a node sends across the bus is interpreted by the other nodes as a single bit of data. The network implemented in this particular project utilized a 250 kBaud transfer rate. This means each node can send voltage pulses at a rate of 250,000 times per second and therefore 250,000 bits of data can be transferred each second.

<u>BUS Value Type</u>	<u>Bus Voltage</u>	<u>Corresponding Binary Value</u>
Dominant	CAN High = 3.5 V CAN Low = 1.5 V	0
Recessive	CAN High = 2.5 V CAN Low = 2.5 V	1

Table 2.2: CAN Bus Voltages

When implementing a CAN network, it is important to understand the architecture of the message frame. Figure 2.10 illustrates all the components of the CAN 2.0B extended message frame format which is utilized in the J1939 protocol. Although the message frame consists of many components, only a few of the most significant components will be discussed here.

As shown in the figure, the arbitration field contains an 11 bit identifier component and an 18 bit identifier component. Together, these two components make up the 29 bit message identifier. Within this 29 bit identifier is a three bit priority field, a 16 bit parameter group number (PGN) field, an eight bit source address (SA) field and a remaining two bit field which will not be discussed here; it can be noted that none of these fields are illustrated in Figure 2.10. The three bit priority field value is used in bus arbitration. Essentially, arbitration is the process of handling "traffic" on a communications bus. If multiple ECUs are trying to send messages at the same time, the message with the highest priority, i.e. lowest numerical value, will win and be allowed to transmit first [9]. The 16 bit PGN field identifies the message and the signals it contains. These signals are essentially a compilation of parameters and variables which are also known as suspect parameter numbers (SPNs); the concept of PGNs and SPNs will be discussed in further detail in the proceeding sections. Finally, the eight bit source address value is used to identify which node the message is being transmitted from. Each node is assigned a unique address on the CAN network in order to distinguish it from other nodes.

Another important field to understand is the data field. This field contains eight bytes (equal to 64 bits or 16 hexadecimals) of SPN data. This 64 bit data field is perhaps

the most significant component of the message frame since it contains all the parameters and variables a particular node is transmitting. For messages which contain more than 64 bits of SPN data, a special multi-packet data transfer protocol is utilized. This protocol will be discussed in proceeding sections. Further information on the other message frame fields can be found online or in the SAE J1939-21 document [9].

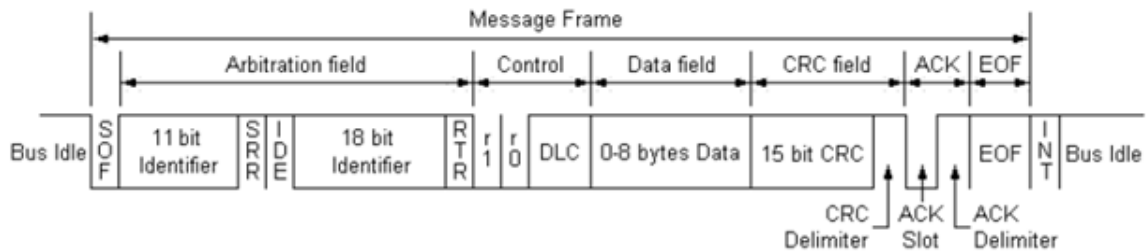


Figure 2.10: Extended CAN Message Frame

2.4.4 PGNs and SPNs

The best way to think of J1939 CAN communications is as a network of nodes which are all sending messages back and forth on a network bus. Each of these messages has a PGN. The PGN is a 16 bit long value (equal to two bytes or five decimals or four hexadecimals) given in the SAE J1939-71 [7]. Each type of PGN contains unique parameters and variables called signals or SPNs. Each SPN is assigned a unique numerical value in the SAE J1939-71 [7] document. An example of a PGN with its corresponding SPNs is given in Figure 2.11. This figure shows the electronic brake controller message (EBC1) and its SAE defined PGN of 61441 (equal to F001 in

hexadecimal). This message is transmitted by the vehicle's brake control unit and contains critical information on the brake system.

We can also see from the figure that the EBC1 message has a transmission rate of 100 milliseconds. This means the message frame is transmitted in a cyclic fashion once every 100 milliseconds. In addition to this we can see it has a data length of eight bytes meaning all eight bytes of the message data field are used. We can also see the three bit message priority field has a decimal value of six (equal to 110 in binary format). Figure 2.12 in the proceeding section better illustrates these fields and how they fit together within the 29 bit CAN identification field.

Information regarding each signal is also given in Figure 2.11. We can see there are 22 individual SPNs for this particular PGN. Each SPN has a predefined starting location within the message, as seen in the left most column, as well as a predefined bit length, as seen in the second column. For example SPN 973 is eight bits in length (equal to one byte) and starts in byte number five of the message data field; the starting location of the SPN is also referred to as the start bit.

PGN 61441		Electronic Brake Controller 1		EBC1
Used for brake control information				
Transmission Repetition Rate:	100 ms			
Data Length:	8			
Extended Data Page:	0			
Data Page:	0			
PDU Format:	240			
PDU Specific:	1	PGN Supporting Information:		
Default Priority:	6			
Parameter Group Number:	61441 (0x00F001)			
Start Position	Length	Parameter Name	SPN	
1.1	2 bits	ASR Engine Control Active	561	
1.3	2 bits	ASR Brake Control Active	562	
1.5	2 bits	Anti-Lock Braking (ABS) Active	563	
1.7	2 bits	EBS Brake Switch	1121	
2	1 byte	Brake Pedal Position	521	
3.1	2 bits	ABS Off-road Switch	575	
3.3	2 bits	ASR Off-road Switch	576	
3.5	2 bits	ASR "Hill Holder" Switch	577	
3.7	2 bits	Traction Control Override Switch	1238	
4.1	2 bits	Accelerator Interlock Switch	972	
4.3	2 bits	Engine Derate Switch	971	
4.5	2 bits	Engine Auxiliary Shutdown Switch	970	
4.7	2 bits	Remote Accelerator Enable Switch	969	
5	1 byte	Engine Retarder Selection	973	
6.1	2 bits	ABS Fully Operational	1243	
6.3	2 bits	EBS Red Warning Signal	1439	
6.5	2 bits	ABS/EBS Amber Warning Signal (Powered Vehicle)	1438	
6.7	2 bits	ATC/ASR Information Signal	1793	
7	1 byte	Source Address of Controlling Device for Brake Control	1481	
8.3	2 bits	Halt brake switch	2911	
8.5	2 bits	Trailer ABS Status	1836	
8.7	2 bits	Tractor-Mounted Trailer ABS Warning Signal	1792	

Figure 2.11: The EBC1 Message, Courtesy of [7]

2.4.5 Physical Signal Values and Raw Signal Values

When studying the working principals of CAN communications, it is important to understand the methods used to encode the SPN signals. The encoding process is responsible for converting physical signal values to raw signal values and vice versa. Essentially, a physical value represents the real world value of a variable or parameter which is being measured or calculated by a CAN ECU. For example, the EBC2 message transmits a signal referred to as the Front Axle Speed (SPN = 904). This signal gives the average front wheel speed of the vehicle based on wheel speed sensor measurements. It is transmitted from the brake controller ECU to other ECUs on the CAN bus. For this

signal, the physical value is given in units of kilometers per hour. This value represents the physical speed of the front wheels. Alternatively, the raw value would be given in bits and it represents the raw binary data which is transmitted by the brake controller on the bus. When a CAN ECU encodes a physical signal to produce a raw signal, it is essentially digitizing the value so it can be transmitted on the bus.

In order to convert a physical value to a raw value, the factor and offset of the SPN must be known. The SPN factor is a constant gain which is multiplied by the raw value. The SPN offset is a constant value which is added to the product of the raw value and factor. These values can be found in the J1939-71 [7] document which contains factor and offset information for all SPNs standardized by SAE.

An example of the signal conversion process is given in Equation 2.9. For this example, we are converting the raw signal value for SPN 904 to its corresponding physical value. For this SPN, the factor has a value of 2^{-8} and is given in units of kilometers per hour. The offset has a value of zero and is given in units of kilometers per hour as well. The raw signal value is 16 bits in length, specified by J1939-71 [7], and represents the digitization of the average front axle wheel speed. This 16 bit value is given in line two of the equation and was chosen at random just for demonstration purposes. In line three of the equation, the binary value has been converted to a decimal value as part of the encoding process. We can see here, the decimal value is equal to 12800. As we multiply by the factor and add the offset, the resulting physical signal value of 50 kilometers per hour is given; refer to line four. Essentially what this means is that the brake controller transmits a binary value of 0011001000000000 for SPN 904 on

the CAN bus in order to communicate the fact that the average front axle wheel speed is equal to 50 kilometers per hour.

$$\begin{aligned} physical &= raw \cdot factor + offset \\ &= (0011001000000000b) \cdot 2^{-8}[kmph] + 0[kmph] \\ &= (12800d) \cdot 2^{-8}[kmph] + 0[kmph] \\ &= 50[kmph] \end{aligned} \tag{Equation 2.9}$$

2.4.6 Broadcast and Peer-to-Peer Messages

Each message being transmitted on the CAN bus has what is known as source/destination mapping information associated with it. As mentioned previously, the source address is an eight bit (equal to one byte or two hexadecimals) value that represents the unique node address from which the message originated. Similarly the message will have destination information which informs all the nodes on the network which node the message is intended for; this is also known as the destination address (DA). Some messages are designed to be received by only a select number of nodes on the CAN network, these are referred to as peer-to-peer messages. Others are designed to be received by all nodes on the network; these are referred to as broadcast messages.

It is possible to determine whether a message is peer-to-peer or broadcast by examining its PGN. This is done by referring to the PDU Format field within the PGN field of the message. The PDU Format field for the EBC1 message is shown in Figure 2.12. We can see from the figure that it is eight bits in length and has a decimal value of 240. According to the SAE J1939 protocol, all messages with a PDU Format value less

than 240 are defined as peer-to-peer. All messages with a PDU Format value equal to or greater than 240 are defined as broadcast messages. Since the EBC1 message has a value of 240, it is therefore a broadcasted message. In fact the majority of J1939 messages will be broadcast messages and thus are transmitted and received by all the nodes on the network [9].

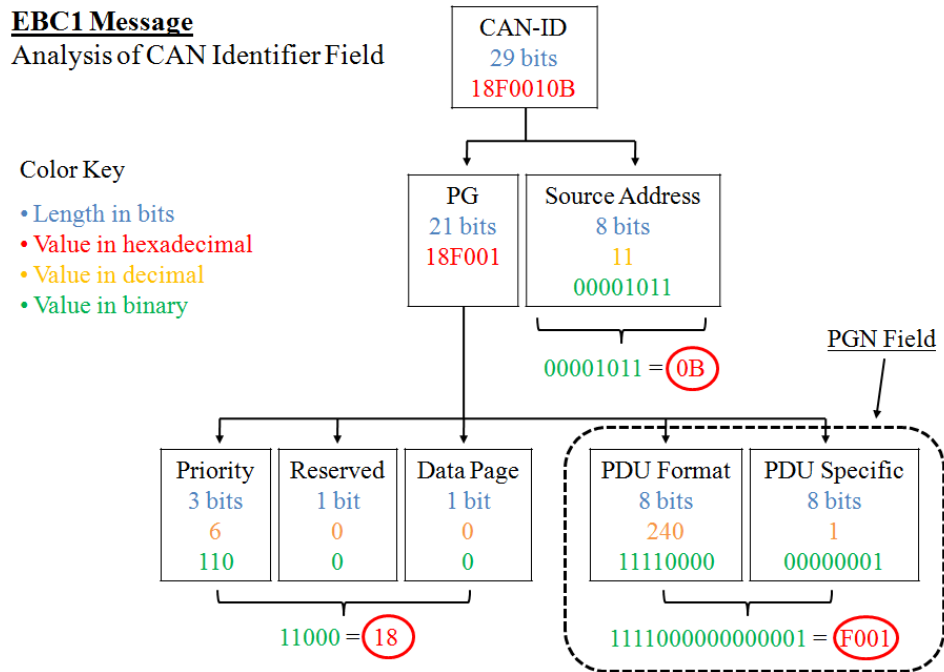


Figure 2.12: Analysis of EBC1 Message

2.4.7 Multi-packet Messages

As mentioned previously, the data field is eight bytes in length and contains all the SPN signals transmitted within a message frame. In some instances, a node may need to transmit more than eight bytes of SPN data for a particular PGN message. When this

is the case, a multi-packet message must be used. Within the J1939 protocol there are two types of multi-packet message systems that can be implemented; both are specified in the J1939-21 [9] document and are formally referred to as data transport protocols. For this project the broadcast announce message (BAM) protocol was required for multi-packet messaging. Under this scheme, the node transmitting the multi-packet message first sends a BAM message on the CAN bus. This BAM message announces to all the nodes on the network that a multi-packet message is about to be transmitted. It also contains information regarding the PGN and size of the pending message.

After the BAM message is transmitted, the node will wait for a period of 50 to 200 milliseconds before transmitting the first packet of the message. Each packet contains the actual SPN data that needs to be sent and because of this the packets are referred to as data transfers (DT). Table 2.3 presents an example of how the BAM and DT packets are sent progressively on the CAN bus. For this example the engine configuration message (CFG_E) was used; in many J1939 networks the CFG messages are multi-packets. At time t_0 the BAM message is sent. We can see from its message ID that the priority is 18, the PGN is ECFE and the source address is 00; this address of 00 is commonly used for the engine controller's source address. At time t_1 the first DT packet is sent. Similarly we can see it has a priority of 18 and a source address of 00, however, the PGN has changed to EBFE. Upon examining the data field of the first packet, we can see the first two hexadecimal characters are 01. These first two characters represent the packet number also known as the sequence number. The remaining 14 hexadecimals (equal to seven bytes) are used for the SPN data. We can see in this example that a total

of four DT packets are sent. Each data field of each packet begins with the sequence number...01...02...03...04...etc.

<u>BUS Time [ms]</u>	<u>Message Name</u>	<u>Message ID (hexadecimal)</u>	<u>Data Field (hexadecimal)</u>
t_0	CFG_E (BAM)	18ECFF00	20 1C 01 FF DD 3E EF 00
$t_1 = t_0 + (50 \text{ to } 200)$	CFG_E (DT)	18EBFF00	01 A0 05 B0 C0 45 7D 00
$t_2 = t_1 + (50 \text{ to } 200)$	CFG_E (DT)	18EBFF00	02 20 C5 66 1F E2 85 25
$t_3 = t_2 + (50 \text{ to } 200)$	CFG_E (DT)	18EBFF00	03 EF 40 4C FF FF C6 10
$t_4 = t_3 + (50 \text{ to } 200)$	CFG_E (DT)	18EBFF00	04 40 4C 00 FE 00 7C E1

Table 2.3: BAM Message

Chapter 3: Tractor-Trailer Modeling

3.1 Introduction to TruckSim

TruckSim is a vehicle dynamics modeling software developed by Mechanical Simulation. TruckSim can be used to simulate the performance of various heavy vehicle designs such as 4x2 tractors, 6x4 tractors as well as box trucks and buses. From within TruckSim, the user can build vehicle models by defining hundreds of vehicle parameters which affect the dynamic behavior of the model. In addition to this, the user can build trailers, add payloads and design various test maneuvers to subject the model to.

For this project, TruckSim was used extensively for developing the tractor-trailer model and performing validation testing. When using TruckSim for the first time, it is important to recognize that a unique vehicle coordinate system is used when defining certain parameters. An illustration of this coordinate system is given in Figure 3.1. As we can see, the origin of the coordinate system is at the front axle and at the middle of the track width. The vertical coordinate points upward, the lateral coordinate points leftward and the longitudinal coordinate points rearward.

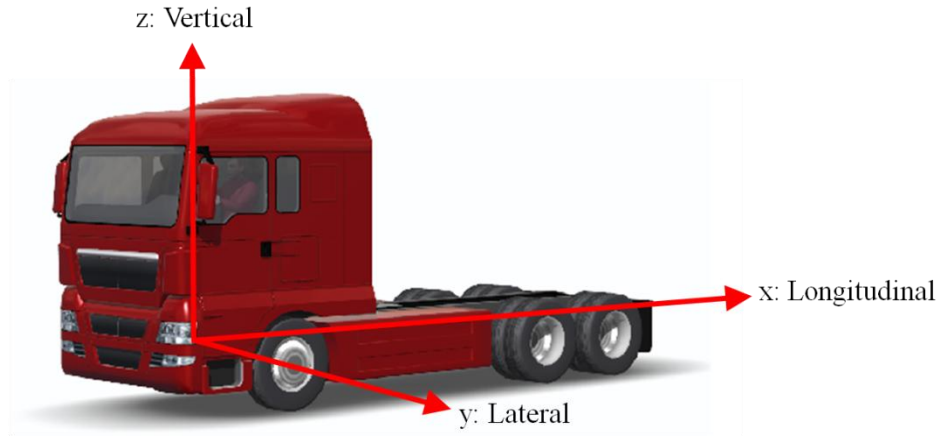


Figure 3.1: TruckSim Vehicle Coordinate System

3.2 General Tractor Specifications

The tractor modeled for this project is a 6x4 cab over engine design. It utilizes a pneumatic brake system with 8 bar maximum pressure and is available with either drum brakes or disc brakes. Power is transferred to the four drive wheels with a 16 speed transmission and transfer case. The total mass of the tractor without additional loading or trailers is 9,320 kilograms. The static loading for the front tires, middle tires and rear tires is given in Table 3.1.

<u>Vehicle Parameter</u>	<u>Front Tires</u>	<u>Middle Tires</u>	<u>Back Tires</u>	<u>Total</u>
Vertical Loading	5120 [kg]	2130 [kg]	2070 [kg]	9320 [kg]

Table 3.1: Solo Tractor Static Loading

3.3 Tractor Modeling

3.3.1 Sprung Mass Modeling

The sprung mass of the 6x4 tractor consists of the body and frame of the vehicle. These components are supported entirely by the suspension and are allowed to vibrate as a mass, spring, damper system as the vehicle travels down the road. The main parameters that characterize the sprung mass are the total mass, C.G. location, roll inertia, pitch inertia and yaw inertia. When developing the TruckSim model, it is important that accurate data be used for these parameters as they significantly influence the overall behavior of the vehicle and determine how loads transfer from wheel to wheel during dynamic maneuvers.

A screenshot of the sprung mass parameter window of TruckSim has been given in Figure 3.2. As we can see from the figure, values must be entered for inertia, C.G. location as well as the dimension of the sprung mass. All of these values were obtained from the heavy truck manufacturer and are given in Table 3.2.

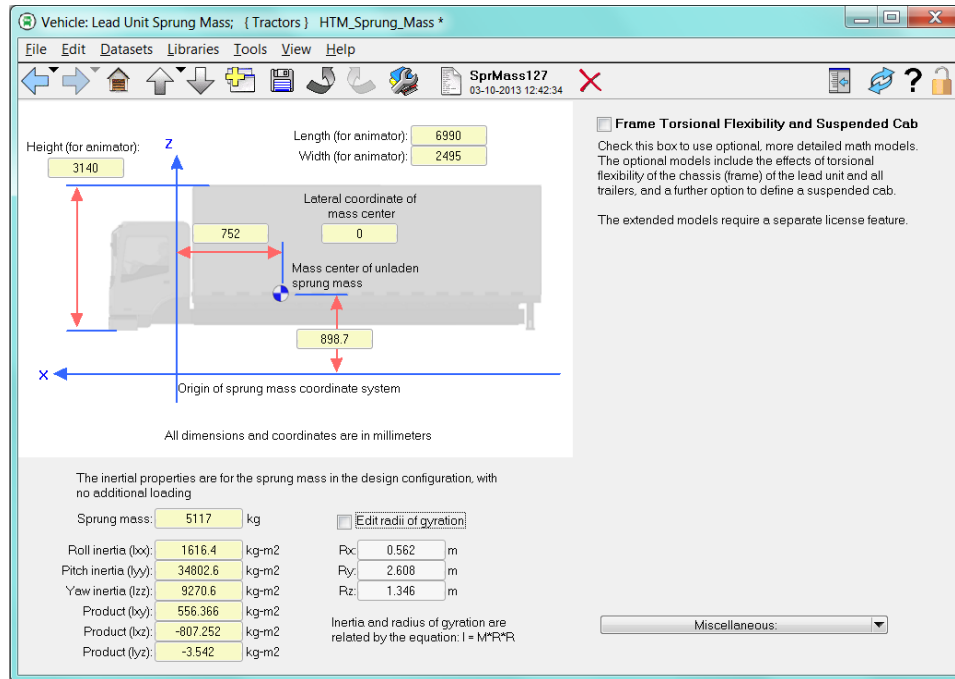


Figure 3.2: TruckSim Tractor Sprung Mass

<u>Vehicle Parameter</u>	<u>Values</u>	<u>Units</u>
Sprung Mass	5117	kg
Roll Inertia (I_{XX})	1616.4	kg-m ²
Pitch Inertia (I_{YY})	10015.3	kg-m ²
Yaw Inertia (I_{ZZ})	9275.5	kg-m ²
Horizontal Distance of the CG from the Front Axle	752	mm
Vertical Distance of the CG from the Ground Plane	898.7	mm
Lateral Distance of the CG from Vehicle Centerline	0	mm
Length of the Tractor (For Animator)	6990	mm
Width of the Tractor (For Animator)	2495	mm
Height of the Tractor (For Animator)	3140	mm

Table 3.2: Tractor Sprung Mass Parameters

3.3.2 Suspension Modeling

As mentioned previously, the tractor's sprung mass is supported by the suspension of the vehicle. In order to define the suspension characteristics of the TruckSim model, the user must enter the Suspensions window. A screenshot of this window is illustrated in Figure 3.3. As we can see from the figure, there are options to adjust the suspension spring rate, shock absorber damping coefficient and much more. For this section we will discuss just the spring rate and damping.

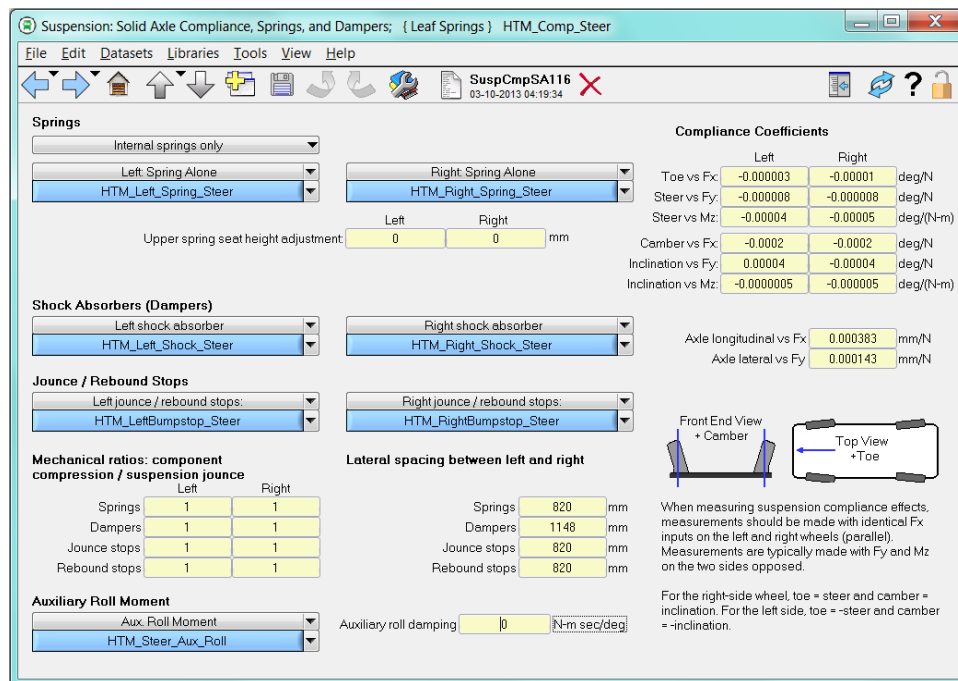


Figure 3.3: TruckSim Tractor Suspension

The 6x4 tractor utilizes a leaf spring type suspension. The stiffness of the suspension was measured by the vehicle manufacture and the resulting values were used for developing the suspension model. In order to enter these values into TruckSim, the user must enter the Suspension: Spring window, given in Figure 3.4. From here the user can specify the spring stiffness constant for the vehicle and view a spring force versus spring compression plot. As we can see from this plot, the front axle leaf springs demonstrate a linear behavior with a spring rate of $328 \frac{N}{mm}$. The spring rates for the rear axle leaf springs are $204 \frac{N}{mm}$ and are given in Table 3.3.

In addition to defining the spring rate, the user can also enter values for the shock absorber damping coefficients. The damping coefficients for this vehicle were also measured by the manufacture and were determined to be $17.004 \frac{N-sec}{mm}$ at the front axle and $9.908 \frac{N-sec}{mm}$ at the rear axles. The TruckSim window for entering the shock absorber damping coefficient is illustrated in Figure 3.5 and the overall shock absorber data is given in Table 3.3.

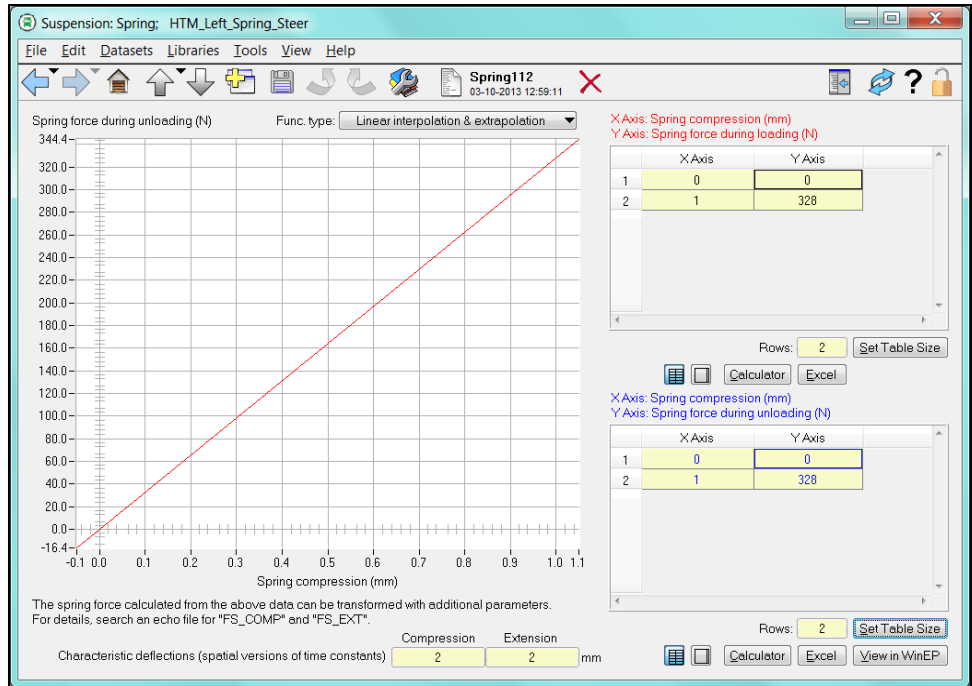


Figure 3.4: TruckSim Tractor Spring Rate

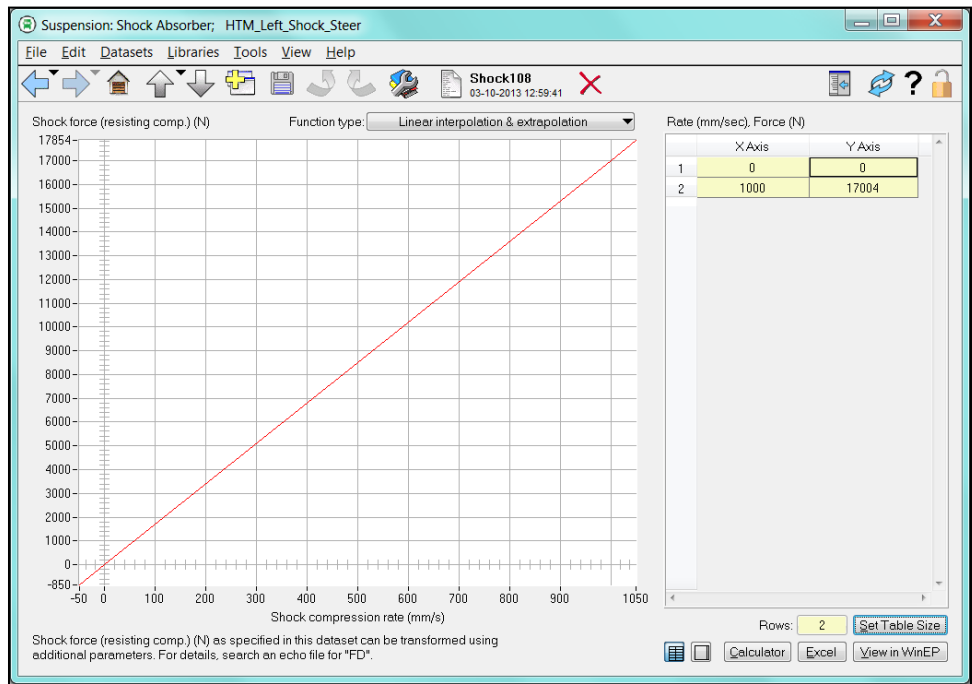


Figure 3.5: TruckSim Tractor Shock Absorber Damping

<u>Parameter</u>	<u>Steer Axle</u>	<u>Drive Axles</u>	<u>Unit</u>
Left and Right Leaf Spring Stiffness	328	204	N/mm
Left and Right Shock Absorber Damping Coefficient	17.004	9.908	N-sec/mm

Table 3.3: Tractor Suspension Parameters

3.3.3 *Unsprung Mass Modeling*

The unsprung mass of the vehicle consists mainly of the vehicle's axles and wheels. Parameters for these components can be set from the Suspension: Axle System Kinematics window within TruckSim. Figure 3.6 gives as screenshot of this window. We can see from the figure that the user can set the mass and inertia of each axle as well as the C.G. location, track width, axle height and the rotational inertia for each output shaft of the axle. Values for these parameters were obtained from the tractor manufacturer and are given in Table 3.4.

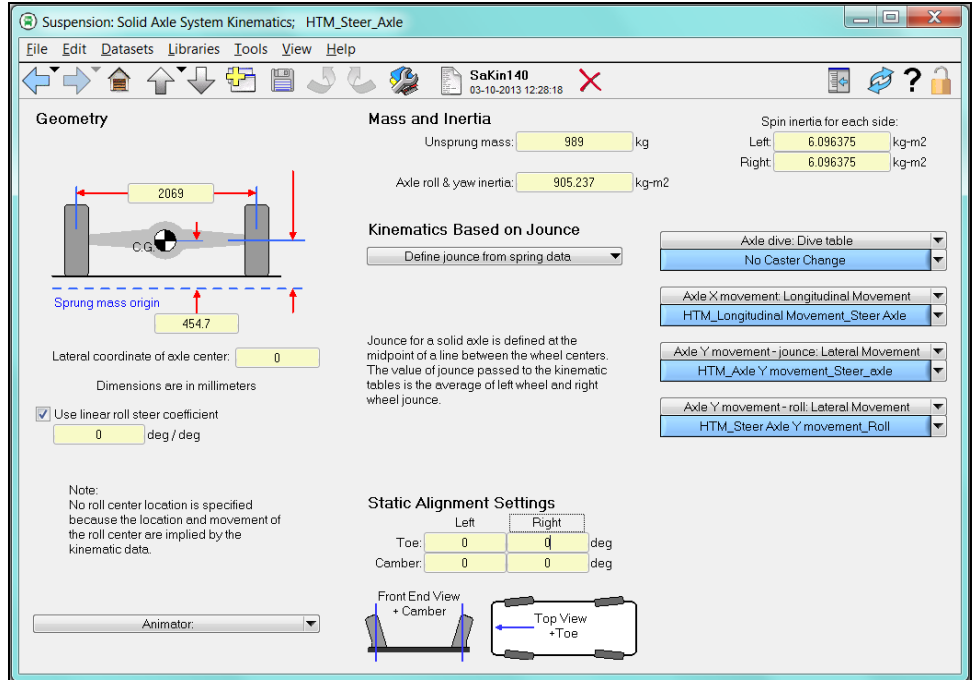


Figure 3.6: TruckSim Tractor Suspension

<u>Parameter</u>	<u>Steer Axle</u>	<u>Drive Axles</u>	<u>Unit</u>
Track Width	2069	1850	mm
C.G Location of Axle from Ground Plane	454.7	521	mm
Wheel Center from Ground Plane	514.7	514.7	mm
Lateral Coordinate of Axle Center	0	0	mm
Spin Inertia - Left Side	6.09	12.2	kg-m ²
Spin Inertia - Right Side	6.09	12.2	kg-m ²
Unsprung Mass	989	1607	kg

Table 3.4: Tractor Unsprung Mass Parameters

3.3.4 Tire Modeling

When developing any vehicle simulation, it is essential that accurate data be used for tire modeling. The tires are responsible for generating all the forces that the vehicle experiences during a maneuver. This includes vertical forces produced from gravity and vertical acceleration, lateral forces produced from cornering and longitudinal forces produced from straight line acceleration and deceleration. Fortunately, the vehicle manufacturer had access to a tire testing machine from which longitudinal and lateral performance data was obtained.

Properties for the wheels and tires of the vehicle model can be set from the Tire window within TruckSim; refer to Figure 3.7. From within this window, the user can access the longitudinal force characteristics screen which is illustrated in Figure 3.8. In this figure, data for the longitudinal tire force versus tire slip ratio is given. We can see from the plot within the figure that there are three data curves, each of which represents the tire performance at different vertical loads. It is also important to mention that the sliding friction for the tire-surface interface on which the tire was tested on must be entered. The entry field for this parameter is given at the bottom of the window and the value is equal to 0.9 in this case.

The user can also specify lateral tire force characteristics in the Tire: Lateral Force window which can be opened from the main Tire screen. This window is illustrated in Figure 3.9 and data for lateral tire force versus tire slip angle is given for three different vertical loads. The sliding friction for the tire-surface interface must also be entered within this window and the entry field is located towards the bottom just as before.

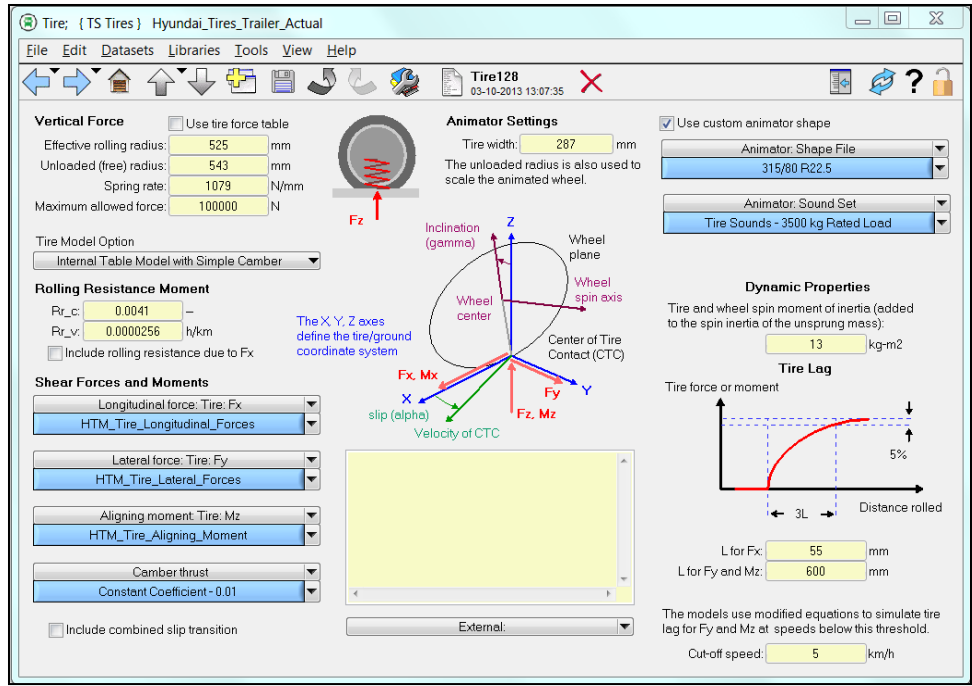


Figure 3.7: TruckSim Tires

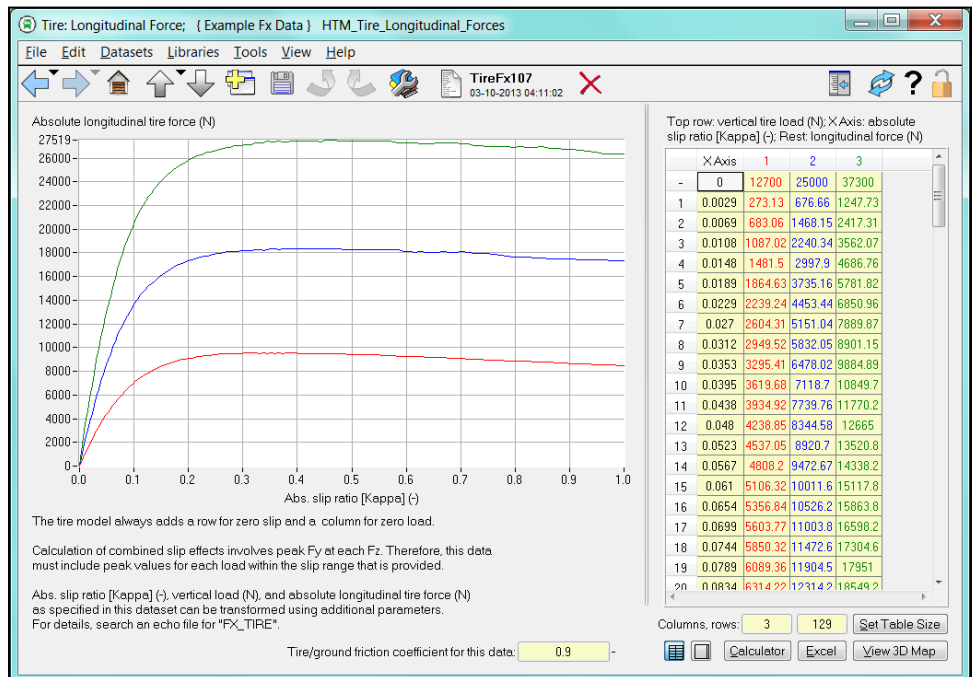


Figure 3.8: TruckSim Tires Longitudinal Force

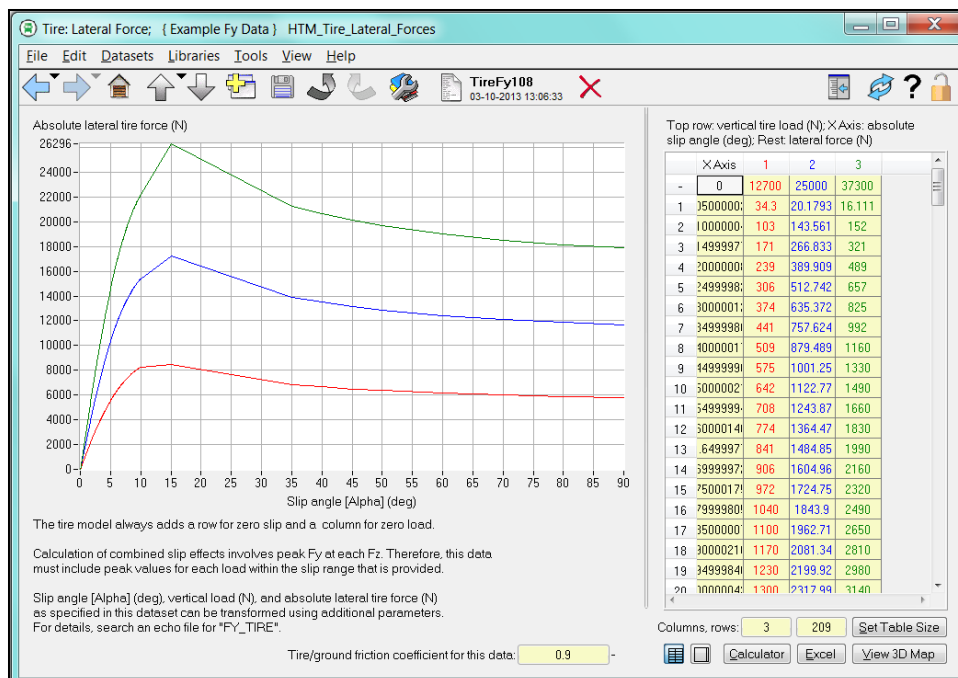


Figure 3.9: TruckSim Tires Lateral Force

3.3.5 Brake System Modeling

For this project, two tractor brake systems were modeled; a disc brake system and a drum brake system. It was necessary to model both of these configurations since some tests performed by the heavy truck manufacturer were conducted with a disc brake vehicle and others with a drum brake vehicle. For example, the tests used to validate the tractor model in this section utilize disc brakes while the tests used to validate the hardware in the loop simulator in chapter five utilize drum brakes.

When modeling the brake system for the vehicle, there are two options available to the user. One option is to enter the Brakes: Torque screen within TruckSim and enter data for brake torque versus brake chamber pressure. A screenshot of this window is given in Figure 3.10, in which a plot for brake torque versus wheel cylinder pressure, i.e.

brake chamber pressure, is given. This figure illustrates the brake torque data for the disc brake system.

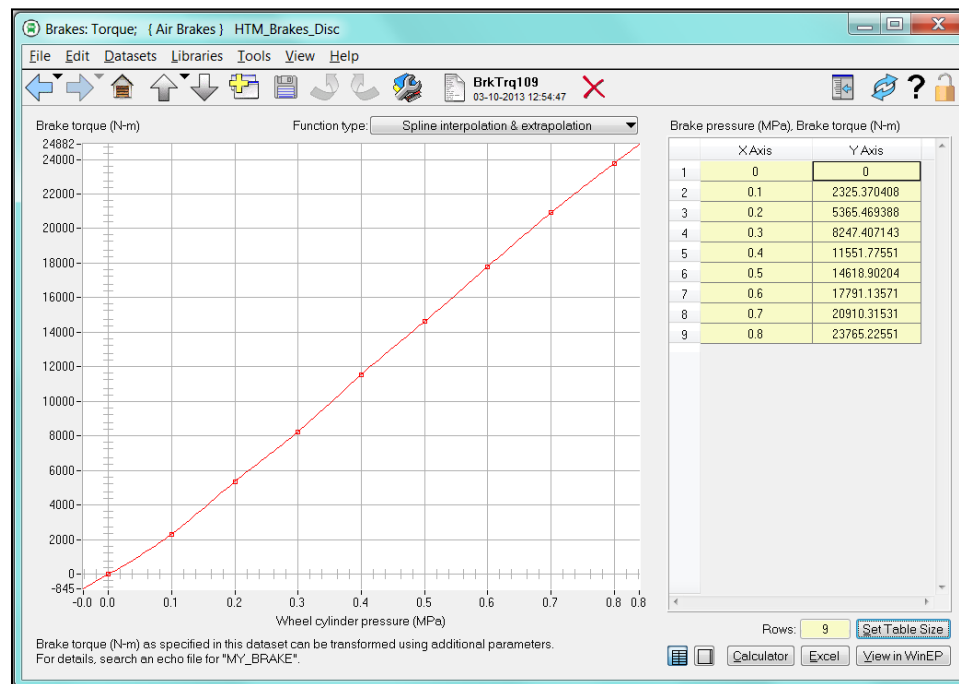


Figure 3.10: TruckSim Disc Brakes

A second option for developing a brake model is to export the TruckSim model to an S-Function which operates within Simulink. With the TruckSim model in Simulink, a brake torque model can be developed as a peripheral subsystem. In this case, the torque model was created from a Simulink lookup table in which a brake torque value is generated for a given brake chamber pressure. The resulting brake torque is then transmitted to the TruckSim S-Function to effectively decelerate the vehicle.

If we refer to Figure 3.11, a screenshot of the Simulink brake torque model is given. This particular model is used to represent the drum brake system. As we can see in the figure, the wheel speed and brake chamber pressure are inputs to the model and brake torque is the output. The box labeled DrumBrakeTorqueGenerator is the lookup table which contains torque versus pressure versus wheel speed data provided by the manufacturer. A plot of this data is given in Figure 3.12.

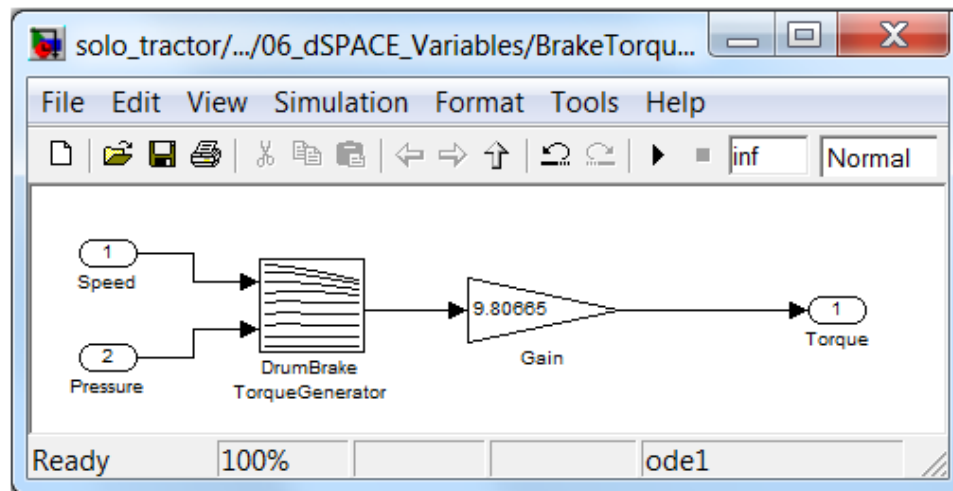


Figure 3.11: Simulink Drum Brake Model

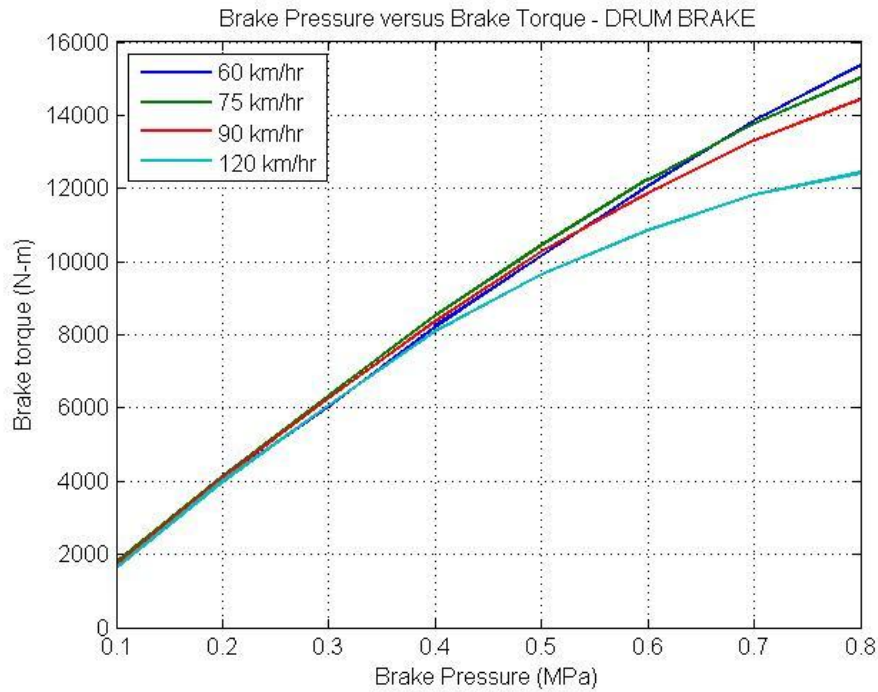


Figure 3.12: Drum Brake Torque versus Pressure at Varying Wheel Speed

3.4 Trailer Modeling

For this project, two semitrailers were modeled; a high C.G. trailer and a low C.G. trailer. Both trailer models were based off of a two axle flatbed configuration with applied loading. The models were designed in TruckSim using parameters provided by the manufacture. These parameters include sprung mass C.G. location, roll inertia, yaw inertia, pitch inertia, suspension stiffness and damping as well as trailer geometry and more. In addition to this, the mass, inertia and positioning of the payloads were accounted for.

In order to develop a two axle trailer with TruckSim, the user must enter the Trailer with 2 Axles window. A screenshot of this window is given in Figure 3.13. As

we can see from the figure, there are individual links for configuring the sprung mass, tires, suspension and brakes of the trailer. Upon selecting the sprung mass link, the Trailer Sprung Mass configuration window opens. A screenshot of this window is given in Figure 3.14. From here, the user can enter the mass, C.G., inertia and overall dimensions of the trailer. Upon selecting the suspension kinematics link in Figure 3.13, the Solid Axle System Kinematics window opens. A screenshot of this window is given in Figure 3.15. From here, the user can enter properties for the unsprung mass such as the C.G., and inertia of each trailer axle along with axle geometry. Finally, upon selecting the compliance link in Figure 3.13, the Solid Axle Compliance, Springs, and Dampers window opens. A screenshot of this window is given in Figure 3.16. From here, the user can enter the stiffness and shock absorber damping coefficients for each suspension element along with suspension geometry data.

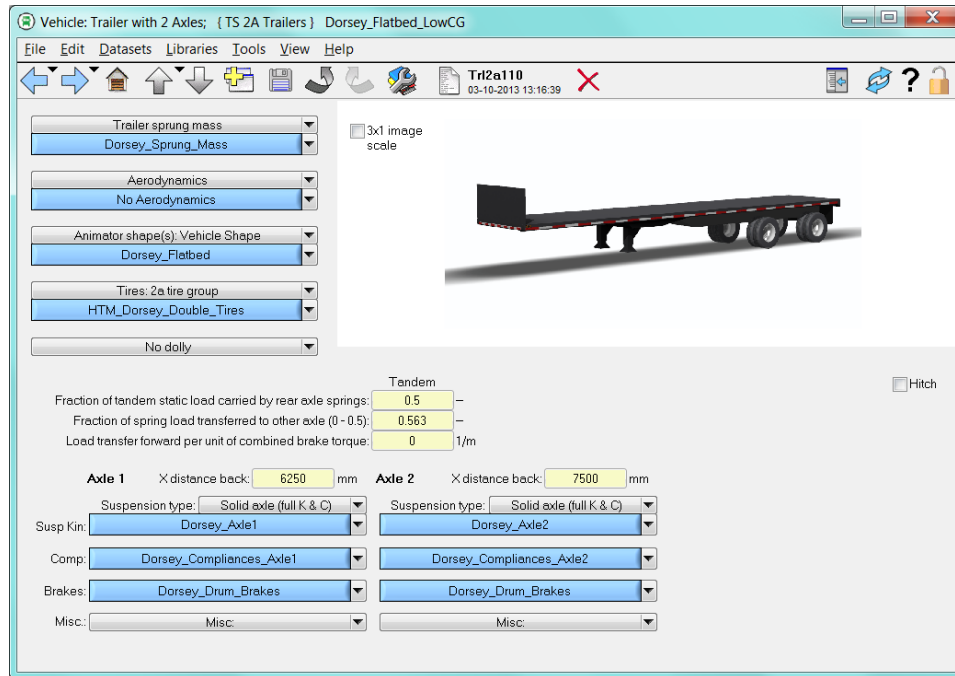


Figure 3.13: TruckSim Trailer

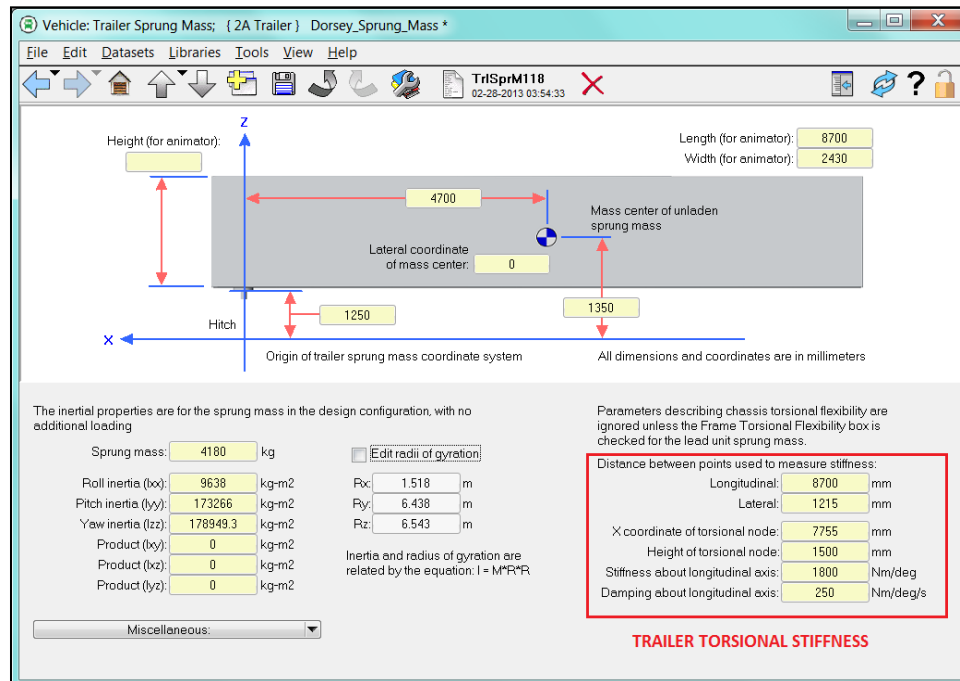


Figure 3.14: TruckSim Trailer Sprung Mass

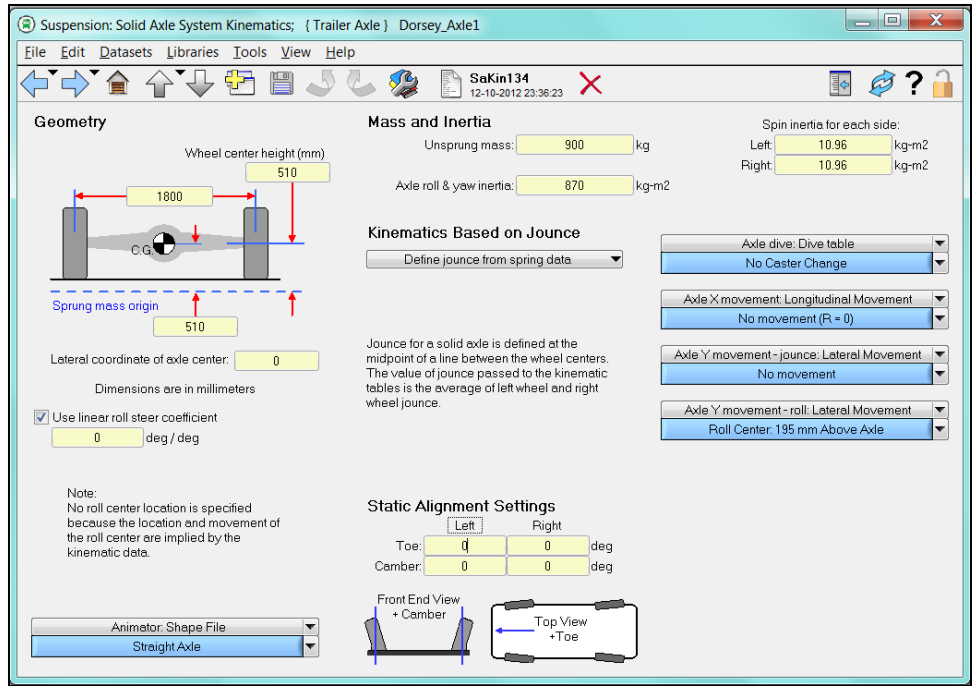


Figure 3.15: TruckSim Trailer Unsprung Mass

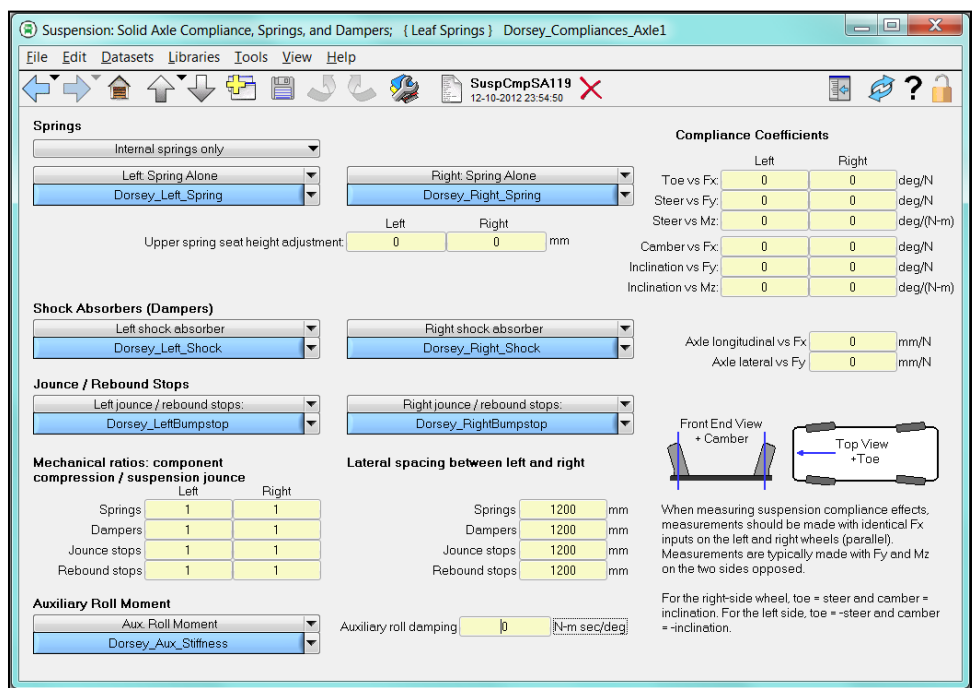


Figure 3.16: TruckSim Trailer Suspension

3.4.1 High C.G. Trailer

The high C.G. trailer consisted of a two axle flat bed with a loading frame and six, two ton concrete blocks as payload. This trailer was utilized primarily for the TruckSim tractor-trailer model validation as well as the RSC control system development for the software in the loop simulation. The total mass of this trailer with loading was 18,880 kilograms. Images of the actual trailer and the tractor-trailer model are given in Figures 3.17 and 3.18 along with parameters for the sprung mass, unsprung mass and suspension in Tables 3.5, 3.6 and 3.7 respectively.



Figure 3.17: High C.G. Trailer Photo



Figure 3.18: TruckSim High C.G. Tractor-Trailer Model

<u>Vehicle Parameter</u>	<u>Values</u>	<u>Units</u>
Sprung Mass	9480	kg
Roll Inertia (I_{XX})	18639	kg-m ²
Pitch Inertia (I_{YY})	335096	kg-m ²
Yaw Inertia (I_{ZZ})	346085	kg-m ²
Horizontal Distance of the CG from Fifth Wheel	5500	mm
Vertical Distance of The CG from the Ground Plane	1430	mm
Vertical Distance of The Hitch from the Ground Plane	1250	mm
Vertical Distance of Load Floor from the Ground	1300	mm
Lateral Distance of the CG from Vehicle Centerline	0	mm
Length of the Tractor (For Animator)	12400	mm
Width of the Tractor (For Animator)	2450	mm
Height of the Tractor (For Animator)	3500	mm

Table 3.5: High C.G. Trailer Sprung Mass Parameters

<u>Vehicle Parameter</u>	<u>Trailer Axle 1</u>	<u>Trailer Axle 2</u>	<u>Units</u>
Track Width	2000	2000	mm
CG Location of Axle from Ground Plane	510	510	mm
Wheel Center from Ground Plane	510	510	mm
Lateral Coordinate of Axle Center	0	0	mm
Spin Inertia - Left Side	12.4	12.4	kg-m ²
Spin inertia - Right side	12.4	12.4	kg-m ²
Unsprung Mass	700	700	kg
Axle Roll and Yaw inertia	890	890	kg-m ²
Linear Roll steer coefficient	0	0	deg/deg

Table 3.6: High C.G. Trailer Unsprung Mass Parameters

<u>Vehicle Parameter</u>	<u>Trailer Axle 1</u>	<u>Trailer Axle 2</u>	<u>Units</u>
Left and Right Shock Absorbers	24.27	24.27	N-sec/mm
Jounce Stop Clearance	127	127	mm
Rebound Stop Clearance	127	127	mm
Spacing Between Left and Right	Springs	1200	mm
	Dampers	1200	mm
	Jounce Stops	1200	mm
	Rebound Stops	1200	mm

Table 3.7: High C.G. Trailer Suspension Parameters

3.4.2 Low C.G. Trailer

The low C.G. trailer consisted of a two axle flat bed with a loading cage and four, two ton concrete blocks as payload. This trailer was utilized primarily for the TruckSim tractor-trailer model validation as well as the RSC control system development for the

software in the loop simulation. The total mass of this trailer with loading was 17,980 kilograms. Images of the actual trailer and the tractor-trailer model are given in Figures 3.19 and 3.20 along with parameters for the sprung mass, unsprung mass and suspension in Tables 3.8, 3.9 and 3.10 respectively.



Figure 3.19: Low C.G. Trailer Photo



Figure 3.20: TruckSim Low C.G. Tractor-Trailer Model

<u>Vehicle Parameter</u>	<u>Values</u>	<u>Units</u>
Sprung Mass	4180	kg
Roll Inertia (I_{XX})	9638	kg-m ²
Pitch Inertia (I_{YY})	173266	kg-m ²
Yaw Inertia (I_{ZZ})	178949.3	kg-m ²
Horizontal Distance of the CG from Fifth Wheel	4700	mm
Vertical Distance of the CG from the Ground Plane	1350	mm
Vertical Distance of the Hitch from The Ground Plane	1250	mm
Vertical Distance of Load Floor from the Ground	1500	mm
Lateral Distance of the CG from Vehicle Centerline	0	mm
Length of the Tractor (For Animator)	8700	mm
Width of the Tractor (For Animator)	2430	mm
Height of the Tractor (For Animator)	2180	mm

Table 3.8: Low C.G. Trailer Sprung Mass Parameters

<u>Vehicle Parameter</u>	<u>Trailer Axle 1</u>	<u>Trailer Axle 2</u>	<u>Units</u>
Track Width	1800	1800	mm
C.G Location of Axle from Ground Plane	510	510	mm
Wheel Center from Ground Plane	510	510	mm
Lateral Coordinate of Axle Center	0	0	mm
Spin Inertia - Left Side	10.96	10.96	kg-m ²
Spin Inertia - Right Side	10.96	10.96	kg-m ²
Unsprung Mass	900	900	kg
Axle Roll and Yaw Inertia	870	870	kg-m ²
Linear Roll Steer Coefficient	0	0	deg/deg

Table 3.9: Low C.G. Trailer Unsprung Mass Parameters

<u>Vehicle Parameter</u>	<u>Trailer Axle 1</u>	<u>Trailer Axle 2</u>	<u>Units</u>
Left and Right Shock Absorbers	26.4	26.4	N-sec/mm
Jounce Stop Clearance	105	105	mm
Rebound Stop Clearance	105	105	mm
Spacing Between Left and Right	Springs	1200	mm
	Dampers	1200	mm
	Jounce Stops	1200	mm
	Rebound Stops	1200	mm

Table 3.10: Low C.G. Trailer Suspension Parameters

3.5 Validation of Tractor-Trailer Model

In order to validate the performance of the high C.G. and low C.G tractor-trailer models, several cornering maneuvers were performed and the resulting simulation data was compared against real world experimental data from the manufacturer. For these

maneuvers, the vehicles were tested without the aid of any stability control systems. This was done so the basic performance characteristics of each vehicle could be observed.

The metrics for validating the TruckSim model were lateral acceleration, yaw rate, road wheel angle and velocity. In total, six different tests were conducted which consisted of:

1. A ramp steer maneuver in which the steering wheel angle is gradually increased to a maximum angle, held constant for a certain period of time and then decreased at the same rate back to zero degrees.
2. A high dynamic steer input in which the steering angle is quickly increased to a maximum value, held there for a period of time and then quickly decreased back to zero.
3. A follow-cone-path maneuver in which the vehicle navigates a predetermined path whose radius continually decreases while the vehicle's speed is held constant.
4. A constant radius maneuver in which the vehicle navigates a circular path of constant radius while the speed is gradually increased.
5. A double lane change maneuver in which the vehicle quickly shifts from one lane to another and then back again.
6. A J-turn maneuver in which the vehicle navigates a path which is shaped like the letter 'J'.

One of the most common dynamic maneuvers experienced under real world circumstances is the double lane change. For this reason, vehicle manufacturers place emphasis on abrupt lane change testing when developing new vehicles and control systems. In this section, the validation results for the double lane change maneuver will be discussed. These tests were conducted without the aid of any stability control systems.

3.5.1 Double Lane Change Maneuver

In the first double lane change maneuver the solo tractor was tested. In order to produce a double lane change identical to the one performed by the manufacturer, it was important that the steering input for the simulation match the test vehicle. This was accomplished by entering road wheel angle data from the test vehicle into TruckSim. The resulting steering behavior is given in the road wheel angle subplot of Figure 3.21. It was also important that the simulation vehicle speed match the test vehicle speed. If there are large differences here, the lateral acceleration and yaw rate values will not match. We can see from the tractor speed subplot that the speeds do match and the deviations are less than one kilometer per hour for most of the maneuver.

With steering and velocity values properly simulated, we can now observe the lateral acceleration and yaw rate behavior. As we can see in the lateral acceleration subplot of Figure 3.21, the values for both vehicles match throughout the maneuver. The simulation is able to capture the large accelerations that occur from side to side as the double lane change takes place. The yaw rate subplot demonstrates similar behavior and again, both vehicles match.

The validation data for the tractor with the high C.G. and low C.G. trailers is given in Figures 3.22 and 3.23 respectively. Again, we can see from these figures that the road wheel angle and vehicle speed for the test data and simulation data both match. Both data sets demonstrate similar lateral accelerations and yaw rates as the double lane change is performed.

Double Lane Change on Wet Asphalt
(Solo Tractor, ESC OFF, 62km/hr)

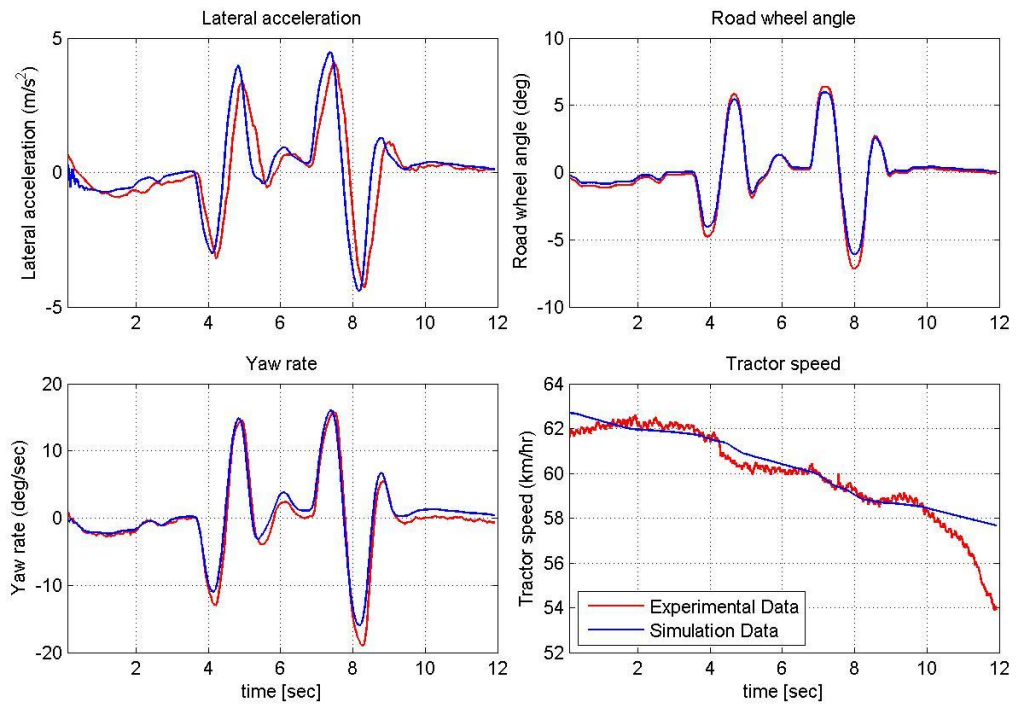


Figure 3.21: Solo Tractor Double Lane Change

Double lane change from Dry asphalt to Wet asphalt
(Tractor + High CG trailer, ESC OFF, 51km/hr)

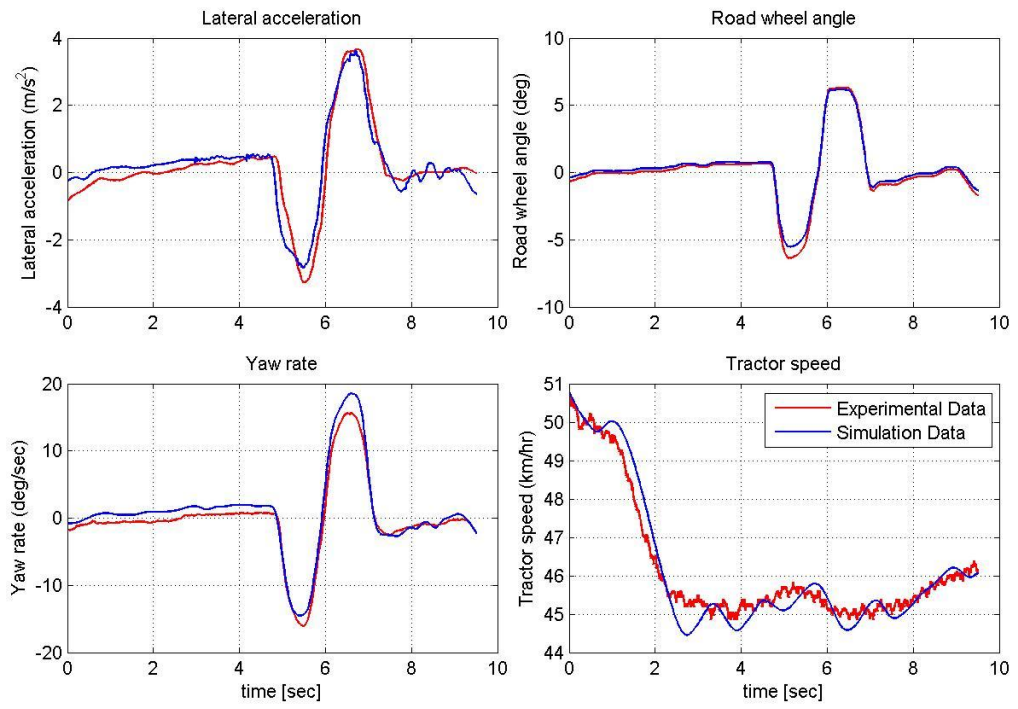


Figure 3.22: High C.G. Tractor-Trailer Double Lane Change

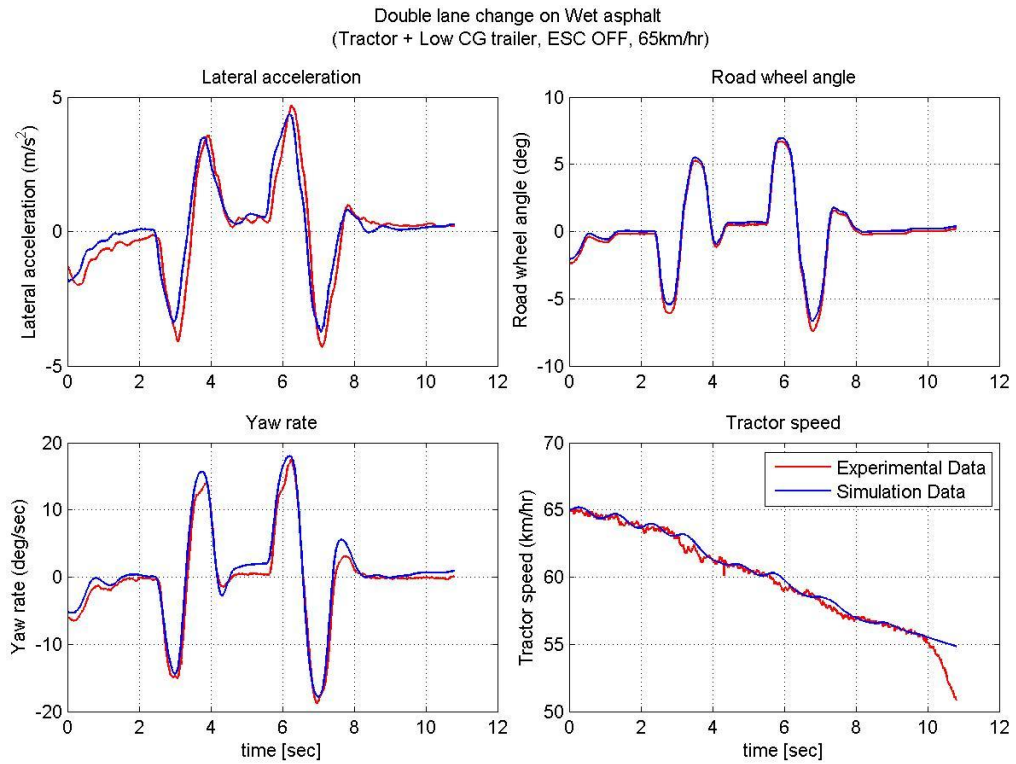


Figure 3.23: Low C.G. Tractor-Trailer Double Lane Change

3.6 The TruckSim S-Function

When developing the HIL and SIL simulations, peripheral subsystems will be created in Simulink which will interact with the TruckSim model. In order for this to be possible, the TruckSim model must be exported to Simulink as an S-Function.

Essentially, the S-Function is a representation of the entire vehicle model for use in the Simulink environment. The S-Function appears in the Simulink block set library as a square block with the TruckSim logo on the front; refer to Figure 3.24.

Within TruckSim there are options to create the S-Function as well as set the import and export variables. The import variables are signals which are fed into the

TruckSim S-Function from the Simulink environment and may include variables such as the vehicle brake pressure. The export variables are signals which are sent to the Simulink environment from the TruckSim S-Function and may include variables such as the vehicle wheel speed. Figure 3.25 gives a screenshot of the S-Function configuration window in TruckSim. In this window, the user can browse through a list of available imports and exports and choose those which are relevant.

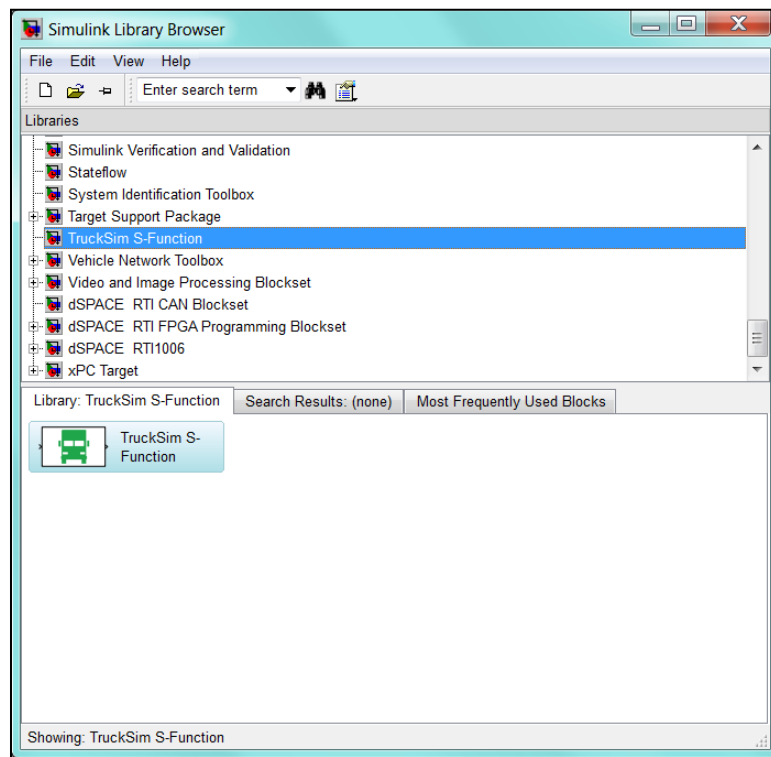


Figure 3.24: TruckSim S-Function

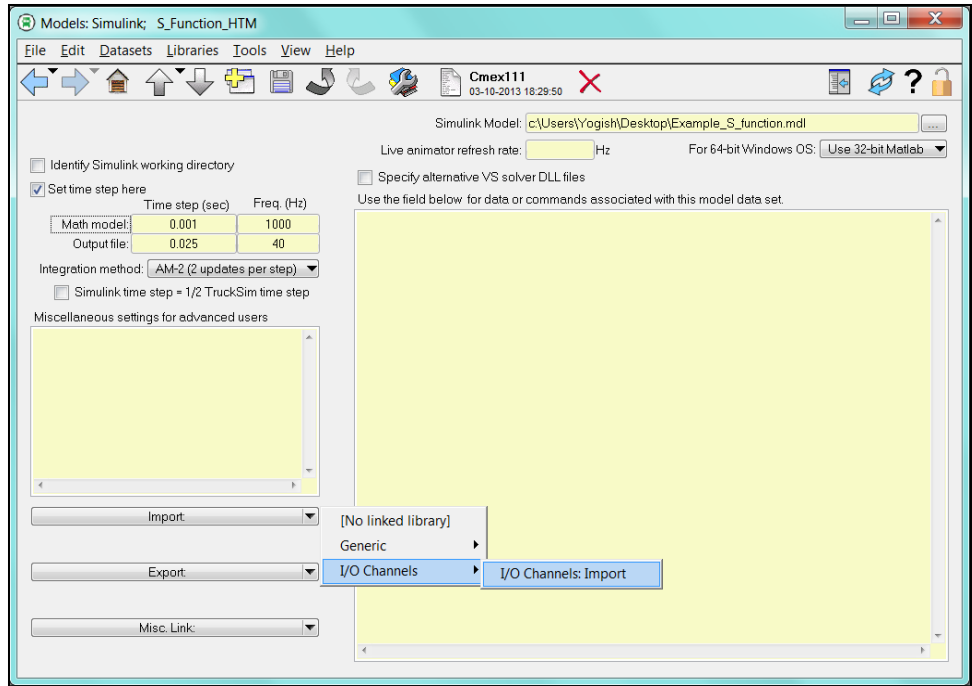


Figure 3.25: TruckSim S-Function Import and Export Variables

Chapter 4: Hardware in the Loop Simulation

4.1 HIL Simulation Concept

Within an HIL simulation, a plant model runs on a platform using a real time processor. The plant model interacts with real world hardware via an input/output signal board. With HIL simulation, the hardware can be fully exercised just as if it were being tested on the real life plant. In Figure 4.1, we can see a simplified illustration which represents the overall working principal of the HIL simulation for this project.

Essentially, the plant consists of the heavy truck model which was designed in TruckSim and integrated into MATLAB Simulink. This plant model runs on a dSPACE simulator in which the simulation is processed in real time. A host PC is used to run ControlDesk instrumentation software so the operator can observe the simulation and interact with it in real time as it runs. The simulation hardware consists of a real world ABS braking system. This hardware sends brake pressure signals to the plant model and receives wheel speed signals from the plant model via the dSPACE input/output board. In addition to this, CAN messages are transmitted back and forth between the hardware ECU and dSPACE.

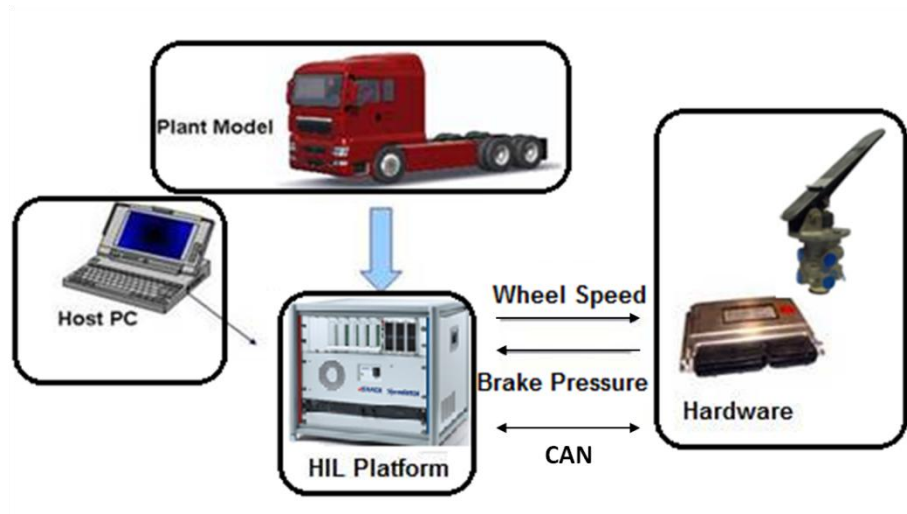


Figure 4.1: HIL Layout

Before beginning to design the layout of the HIL simulation for this project, it was important that the layout and functionality of the braking hardware being implemented was thoroughly studied. It was also important to understand exactly how the braking hardware should be integrated with the dSPACE simulator and the software components such as TruckSim and Simulink. The overall design of the HIL simulator will be discussed in the following sections.

4.1.1 Anti-lock Braking System Hardware

The braking system utilized for the HIL simulator was a traditional pneumatic ABS system with pneumatic braking control; as opposed to an electronic braking system in which an electronic brake pedal may be used along with electronic pressure relay modules to deliver pressure to the brake chambers. This system is identical to the one found on the actual HTM tractor with the exception of a few modifications which will be

discussed later. Figure 4.2 shows the layout of the ABS system as it would be found on the production tractor. As seen in the figure, the system utilizes a 4s/4m configuration which means there are four wheel speed sensors and four pressure modulators for monitoring wheel lock up and regulating braking pressure respectively. It can also be noted that the front left and front right wheels each have their own speed sensor and modulator. The middle and back wheels on each side of the vehicle must share a modulator and only the back wheels have speed sensors. This 4s/4m setup is a common configuration and it is effective in reducing the overall number of ABS components and the system cost.

We can also see from Figure 4.2 that there are multiple air reservoirs which supply air pressure directly to the brake treadle. The driver can depress this treadle in order to supply pressure to the brake chambers and stop the vehicle. The treadle is also equipped with a small exhaust port which expels air from the brake system as the driver eases off the brakes.

Between the treadle and the front ABS modulators there is a quick release valve which simply acts as an exhaust module to quickly expel air from the brake chambers when the driver releases the brakes. In addition to this there is a relay valve in the rear of the vehicle which is used to supply air to the rear four brake chambers. This relay valve is used to reduce the air transport delay experienced by the rear chambers immediately after the treadle is pressed. This delay occurs since there is a significant distance between the rear chambers and the treadle.

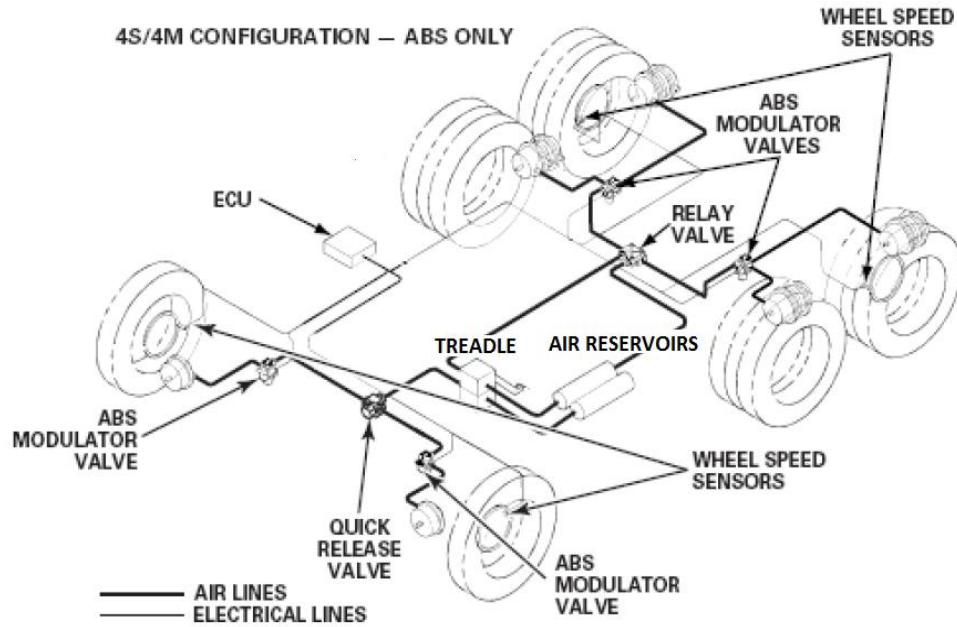


Figure 4.2: Pneumatic Braking System with ABS, Courtesy of [11]

Another important component of the ABS system is the ECU. The ECU is in charge of calculating the wheel speed based on the analogue signals generated by the wheel speed sensors. It must also determine whether or not to build pressure, hold pressure or dump pressure in the brake chambers. The ECU does this by continually monitoring the wheel deceleration. If large deceleration occurs and the ECU believes tire grip has been compromised, it will send either a dump or hold brake pressure command to the ABS modulators in order to reduce the wheel deceleration and restore tire grip. After the deceleration is stabilized, the ECU will command the modulators to proceed to build pressure.

The ABS modulators are able to dump, hold or build pressure by utilizing two solenoid valves; the inlet valve (IV) and the exhaust valve (EV). Each of these solenoid

valves are connected to the ECU on an individual control circuit. Figures 4.3 and 4.4 illustrate the design of these modulators.

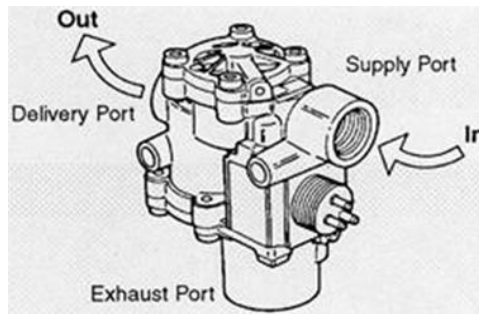


Figure 4.3: ABS Modulator, Courtesy of [2]

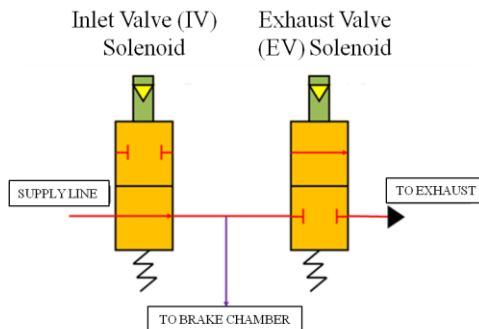


Figure 4.4: ABS Modulator Solenoids, Courtesy of [2]

In addition to calculating wheel speed and controlling the ABS modulators, the ECU is also connected to the vehicle's J1939 CAN communications bus. The ECU transmits and receives messages with other ECUs on the bus. The two most significant messages the ABS ECU transmits are the EBC1 and EBC2 messages. The EBC1 message informs all the CAN ECUs in the vehicle whether or not the ABS system is functioning properly, whether there are any warning lamps and whether or not anti-lock control is currently taking place. The EBC2 message transmits digitized wheel speed values to all the CAN ECUs to be used for additional vehicle control processes.

4.1.2 Placing the Braking Hardware in the Loop

After the basic functionality of the braking hardware was understood, a plan for integrating the hardware with the TruckSim vehicle model was developed. In this case, the simulator was designed so the TruckSim model calculates the wheel speeds of the vehicle. These wheel speeds are then transmitted to the ABS ECU which controls the brake chamber pressures with the ABS modulators when severe wheel deceleration is sensed. The pressure modulation then causes a corresponding pressure fluctuation in each of the six brake chambers. These pressure fluctuations are sensed by six separate pressure transducers and the pressure data is transmitted back to the TruckSim model and converted to brake torque. The brake torque then influences the wheel speeds of the TruckSim vehicle model. Finally, the wheel speed values are then transmitted from the TruckSim model back to the ABS ECU again. By configuring the brake hardware and TruckSim model in this fashion, a loop is created which consists of real life ABS braking

hardware and a software based vehicle dynamics computer model. This configuration is referred to as hardware in the loop.

In Figure 4.5, a signal flow diagram for the HIL simulator is given. This diagram is a visual representation of what was discussed in the previous paragraph, the only difference here is that blocks have been added which represent the dSPACE real time processor (RTP) and the dSPACE input/output (I/O) board. The dSPACE RTP can be thought of as the main processor inside the dSPACE unit that actually runs the TruckSim vehicle model, also known as the TruckSim S-Function, and corresponding Simulink model. The dSPACE RTP is unique when compared to a standard desktop processor because it is configured to run in real time. This means if the TruckSim model numerical solvers are set to solve the model at a time interval of once every millisecond in simulation time, the dSPACE processor will solve the model once every millisecond in real time. By solving the vehicle model in real time, we are able to integrate real life hardware, such as the braking system, which is designed to operate in the real time domain.

While the dSPACE processor runs the simulation software, electrical signals from the hardware, such as the brake chamber pressure transducer signals, are transmitted to the dSPACE (I/O) board and converted to computerized signals. This is accomplished through a bank of built-in analogue to digital converters (ADC). These computerized signals are then fed to the TruckSim S-Function by use of the dSPACE real time interface blocks (RTI). These RTI blocks are provided in a software toolbox that comes with the dSPACE installation disc. They can be inserted into any Simulink model in order to channel signals from the dSPACE input/output board to which ever Simulink block they

need to go to, in this case the TruckSim model S-Function. This process of channeling signals to and from the I/O board is also known as signal mapping.

We can also see from Figure 4.5 that computerized signals from the TruckSim S-Function can be mapped to the I/O board and converted to analogue electrical signals with the use of the RTI blocks. In this case the wheel speeds signals, which are generated from TruckSim, are mapped to an RTI block designed specifically for wheel speed sensor simulation; this block is referred to as a wheel speed signal generator (WSSG) block. The WSSG block along with the I/O board then convert the computerized wheel speed values to analogue electrical signals which can then be wired to the ABS ECU. The I/O board is able to generate these analogue wheel speed signals through the use of specially designed digital to analogue (DAC) converters.

In addition to receiving brake chamber pressure signals and transmitting wheel speed signals, dSPACE has the capability of transmitting and receiving J1939 messages. This is done through the use of special RTI blocks that come with the J1939 software toolbox known as the CAN J1939 Multimessage toolbox. Unfortunately this toolbox does not come standard with the dSPACE installation software and it has to be purchased separately from dSPACE. As we can see in Figure 4.5, the CAN messages flow between the ABS ECU and the Simulink model running on the RTP. This is made possible through specially designed electrical components called transceivers which are implemented as part of the I/O board.

this delay, additional pneumatic tubing was added where the valve would normally be present. We can also recall from the previous section that the HTM tractor is equipped with a relay valve to reduce transport delay from the treadle to the rear chambers which occurs due to the great distance the air must travel to reach the rear of the tractor. This valve was not utilized for this project since we were able to configure the brake hardware in such a way that the air supply line running from the treadle to the rear brake chambers was significantly shortened.

4.2 HIL Hardware Configuration

4.2.1 dSPACE Midsize Simulator

Before HIL simulations could be ran, much effort was devoted to understanding the functionality of the dSPACE unit used for this project. Many hours were spent reading through dSPACE user documents and completing tutorials that came with the dSPACE software. Although this is very time consuming, it is quite possible to become proficient in using dSPACE without attending seminars or taking classes which are offered by dSPACE.

For this particular project, the dSPACE Midsize simulator was used for running the simulations since it readily available at the Center for Automotive Research where the project was conducted. As the name implies, the Midsize is the middle of the line HIL simulator offered by dSPACE. The particular unit used for this project came equipped with four real time processors, model ds1006, and an input/output interface board, model ds2211. For this project the processing power required to run the HIL simulation was fairly minimal so only a single ds1006 processor was commissioned, however, for more

computationally intensive simulations, the additional processors can be utilized. The Midsize simulator also has a power supply unit, referred to as VBAT1, which can supply DC voltage to any external ECUs or hardware components that require power.

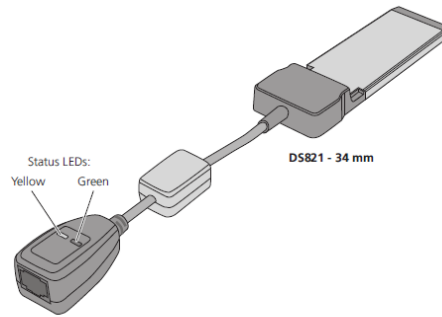
Figure 4.6 shows an image of a dSPACE Midsize simulator which is similar to the one used for this project. We can see from the figure that at the top of the unit there are three black rectangular connectors. These are referred to as HYP connectors. Each of the HYP connectors contains 90 individual contacts which are hard wired to the simulator's analogue to digital converters, digital to analogue converters, wheel speed signal generators, power supply, circuit grounds, CAN transceivers and more. We can also see from the figure that at the bottom of the unit there is a black power supply module. For this project the power supply module was set to run at 24 volts to power the ABS ECU and the brake chamber pressure transducers. It should be noted that on the face of the power supply module there are two knobs for limiting the output voltage and current. These knobs should be turned all the way clockwise so neither the voltage nor output current of the power supply are limited. The voltage for the power supply is set through the use of RTI blocks in the simulation software model. This will be discussed in proceeding sections.



Figure 4.6: dSPACE Midsize Simulator

In addition to the dSPACE unit itself, a host PC is needed for running simulations. The host PC connects directly to dSPACE and contains the model which will be loaded to the dSPACE RTP when the simulation is ran. The host PC is also able to start and stop the simulation and is in charge of running the ControlDesk instrumentation software which facilitates user interaction with the simulation as it is running.

There are various options available for connecting the host PC to the dSPACE Midsize which are discussed in the dSPACE user document entitled "Hardware Installation and Configuration Guide For DS1006 Processor Boards and I/O Boards" [12]. For this project, a laptop with a PCI Express Card slot was chosen as the host PC. In order to connect it to dSPACE, the DS821-34 mm link board was needed. This link board goes into the laptop's PCI Express Card slot at one end and connects to the Midsize via an Ethernet patch cable at the other end; Figure 4.7 illustrates the DS821-34 mm link board.



Yellow LED A lit yellow LED indicates that the connection between the host PC and the expansion box is ready for communication.
Green LED A lit green LED indicates that data is being sent or received.

Figure 4.7: dSPACE Link board, Courtesy of [12]

4.2.2 Wheel Speed Sensor Simulation

In order for the ABS ECU to determine when high levels of wheel deceleration and/or lockup are occurring, it must be able to sense the vehicle's wheel speeds. As previously illustrated in Figure 4.2, the HTM tractor comes equipped with four wheel speed sensors which measure the speed of the front left, front right, back left and back right wheels. In order to determine wheel speed, today's modern vehicles use either a Hall Effect sensor, which is an active sensor and requires a voltage power supply, or a variable reluctance sensor (VRS), which is a passive sensor and does not require a power supply. The HTM braking system used for this project comes equipped with VRS wheel speed sensors. The sensor itself consists of a permanent magnet core which is wrapped in many coils of wire, refer to Figure 4.8. The magnetic core produces magnetic flux lines around the sensor. Whenever these flux lines are disturbed by a passing metallic object, such as a toothed pole wheel which rotates with the vehicle's wheel, a voltage is induced in the coils of wire. This voltage has a sinusoidal waveform in which the frequency is

proportional to the angular velocity of the wheel and the number of teeth on the pole wheel. This sinusoidal waveform is then fed directly to the ABS ECU.

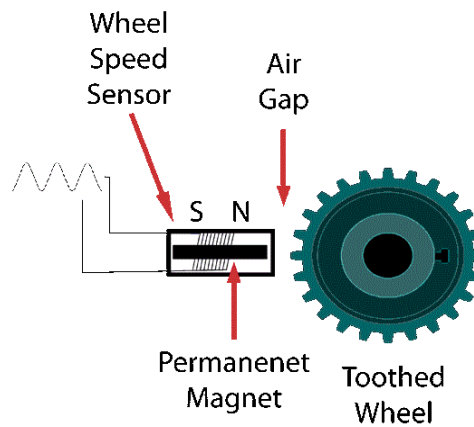


Figure 4.8: VRS Wheel Speed Sensor, Courtesy of [13]

Since the wheel speeds for the HIL simulation actually originate from the TruckSim model and not a sensor, it was important that the properties of the sinusoidal waveform, such as the frequency and amplitude, were studied so they could be properly replicated by the dSPACE wheel speed signal generators (WSSG). Fortunately, the manufacturer of the wheel speed sensors and ABS ECU were able to provide technical documents and test reports on the sensors and pole wheels. Upon analyzing this information, it was determined that the pole wheels used on the HTM tractor have 100 teeth each. It was also determined that the amplitude of the sine wave generated by the sensor is not constant but actually increases with wheel speed. When the wave frequency

reaches 100 Hz, the voltage amplitude must be equal to or greater than 191 millivolts in order to be detectable by the ABS ECU.

In order to generate the wheel speed signals, the dSPACE Midsize comes equipped with four output channels or WSSGs which are internally hardwired to the HYP connectors. The wheel speed (given in revolutions per minute), amplitude (given in volts) and number of pole wheel teeth can be configured with the WSSG RTI blocks which come with the dSPACE RTI toolbox software. The right hand window in Figure 4.9 illustrates the WSSG RTI block. As we can see, there are options within the RTI block where the number of pole wheel teeth can be set as well as signal amplitude and the wheel speed. Since the wheel speeds are variables which are calculated by TruckSim, they must come from the TruckSim S-Function within the Simulink model.

In the left hand window of Figure 4.9, we can see the four wheel speeds come from the TruckSim S-Function all muxed together via input number one which is labeled Wheel_Speeds. The input then passes through a rectangular demux bar to separate the four wheel speeds into the front left, front right, back left and back right values. Finally each demuxed wheel speed passes through a gain block equal to 5.0525. This value takes the rolling tire diameter into account and converts the wheel speeds from kilometers per hour (used by TruckSim) to revolutions per minute as required by the WSSG blocks. We can also see at the bottom of this window there is a constant block labeled WSS Amplitude. This block is used to adjust the amplitude of the sine wave for the wheel speed signal. For this model, the amplitude was set to two volts. This was done to ensure the minimum requirement of 191 millivolts was met, however, not exceeded by such an extent that the ECU may be damaged.

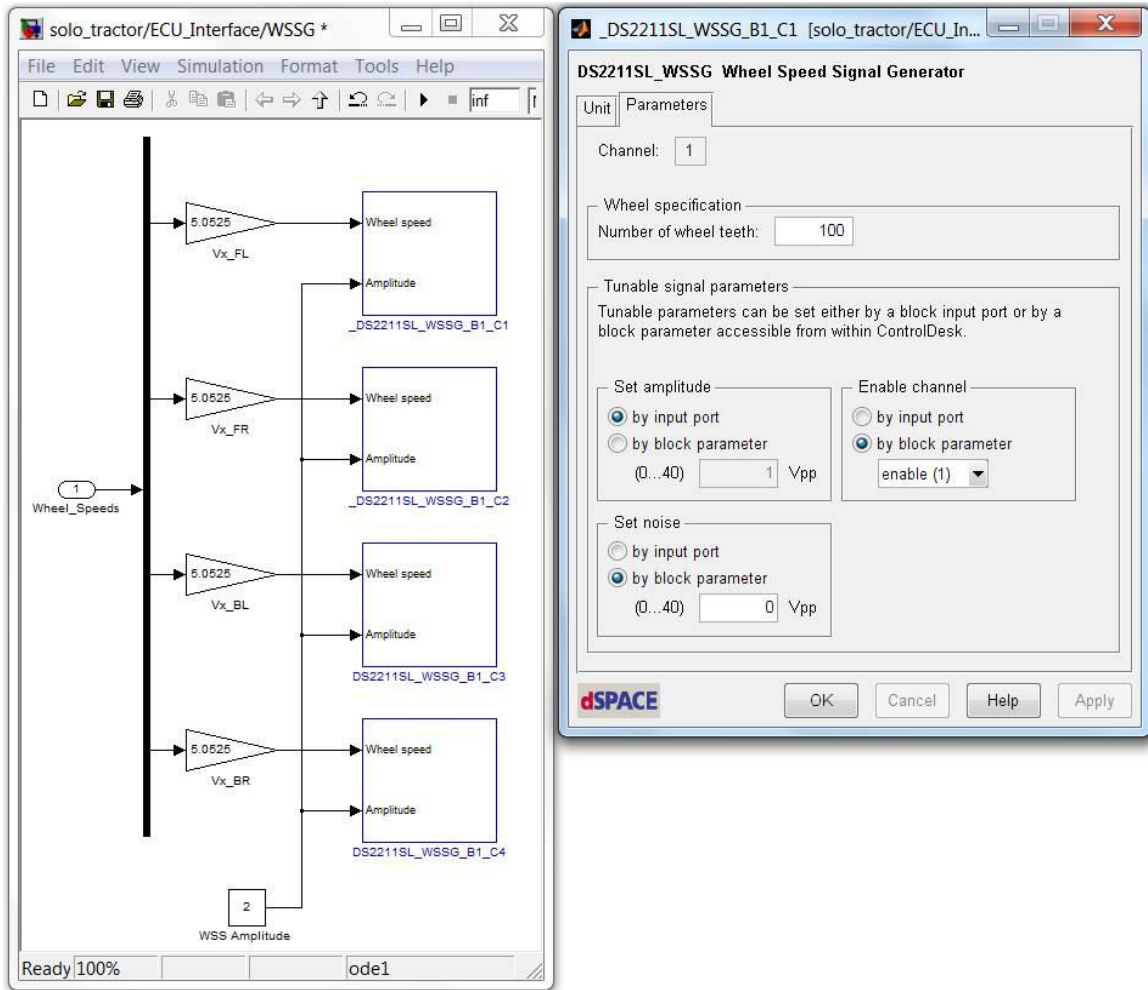


Figure 4.9: Wheel Speed Signal Generator

In addition to generating a wheel speed signal with the correct amplitude and frequency, the DC resistance, or DCR, of the sensor circuit must also be taken into account. This is important because when the wheel speed sensors are connected to the ECU on the actual vehicle, the ECU sees some resistive load across the sensor input terminals due to the inherent resistance and inductance of the sensors themselves. Replicating this load is important because the ECU sends a DC voltage through the

sensors and measures the resulting DCR in order to determine if there are any shorts or other faults with the sensor; this voltage is referred to as the offset voltage and its magnitude was measured to be roughly 800 millivolts. If the DCR of the WSSG circuitry which connects the ECU to the dSPACE I/O board is too large or too small, the ECU will recognize this discrepancy as a fault with the sensor and the ABS will not work properly. In addition to this, if there is any continuity between the WSSG circuitry and other electrical circuits that go to the ECU, the system will again recognize this as a circuitry fault. In other words, all four WSSG circuits going to the ECU must be noncontiguous or decoupled from each other as well as all other circuits and ground connections. For these reasons, it was important that the internal circuitry of the dSPACE WSSG was understood and measures were taken to replicate the DCR of the sensor circuitry found on the actual vehicle.

Figure 4.10 illustrates the manner in which the ABS ECU was connected to the dSPACE WSSG. We can see from the figure, the ECU is wired to the dSPACE WSSG outputs with a wheel speed sensor connected in series between the two. This sensor is identical to the one used on the actual test vehicle and is used here in order to replicate the correct DC resistance required by the ECU when checking for wiring faults. We can also see there is an isolation transformer within the WSSG circuitry which is housed within the dSPACE input/output board. The output side of this transformer, also known as the secondary coil, has a DC resistance of only a couple hundred ohms. In comparison to the wheel speed sensor, we can think of this resistance as being relatively insignificant and so a value of zero ohms is given in the figure. The main purpose of this transformer is to completely decouple the ECU sensor circuit from the internal circuitry of dSPACE.

Any DC offset current passed from the ECU through the secondary coil of the isolation transformer cannot propagate to the primary coil and into any internal circuitry within the input/output board. As a result, the ECU cannot tell it's connected to a signal generating device and instead it thinks it's connected to a sensor and nothing else. It should be noted that this figure shows only one wheel speed signal circuit, in actuality there are a total of four.

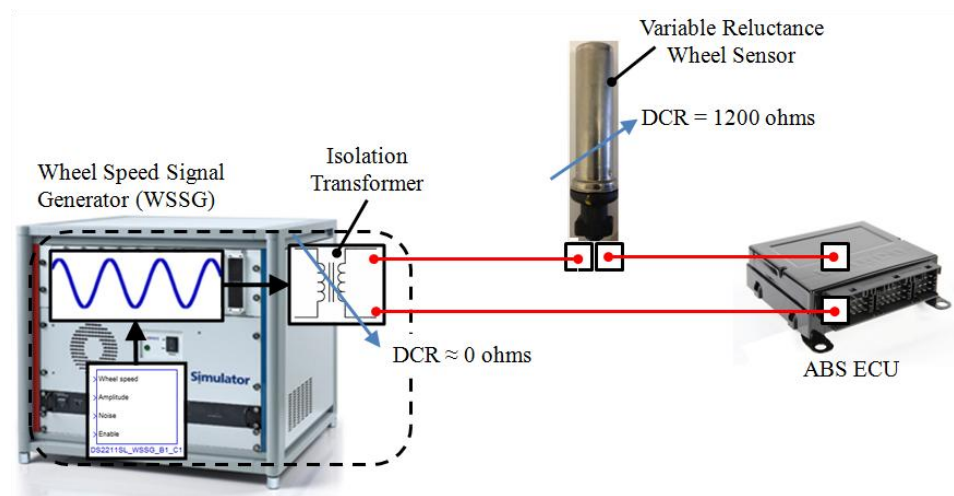


Figure 4.10: dSPACE Wheel Speed Generator Circuit

4.2.3 Brake Chamber Rigs

When implementing the brake chambers into the HIL simulation, the compliance of the drum brake assembly had to be replicated. The reasoning for this is that in the actual vehicle, the brake chamber piston comes into contact with the drum brake assembly as it is actuated. The drum brake assembly itself is not completely rigid and

therefore behaves as an ultra-stiff spring. In Figure 4.11, the main components within a typical drum brake system are illustrated. We can see from the figure that the brake chamber acts on several components including the chamber bracket, slack adjuster, camshaft, shoe/lining assembly and finally the brake drum which all have some stiffness characteristics. This stiffness produces resistance against the brake chamber piston as it is actuated and ultimately decreases the rate at which the volume within the chamber diaphragm can expand when supplied with pressure. If the brake chamber piston had no resistive load during actuation, the piston would quickly travel to its maximum stroke, the effective volume within the brake chamber would quickly rise and the pressure rise time would differ from that of the actual vehicle. For this reason a brake chamber rig was designed to replicate the compliance of the drum brakes found on the actual vehicle.

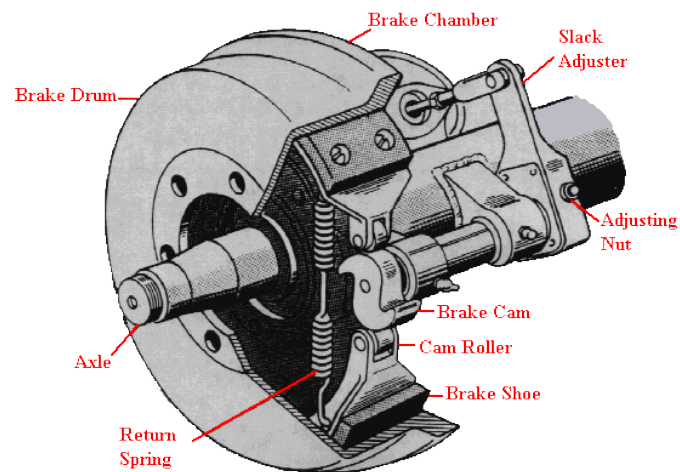


Figure 4.11: Drum Brake Components, Courtesy of [2]

In order to create a rig that could accurately replicate the compliance of the drum brake assembly, bench test data from the vehicle manufacturer was analyzed. As seen in Figure 4.12, the results from a static deflection test conducted by the manufacturer are given. In this test, the brake chamber was first installed on the actual drum brake assembly used on the vehicle. Next, air was supplied to the chamber and the pressure was slowly increased. As this was done, the stroke of the piston was measured. It should be noted that the pressure was increased slowly in order to prevent any dynamic effects from being observed.

We can see from the figure that there are three significant points along the pressure versus stroke curve. At A, the push out point is given. This is the point at which the brake chamber piston first begins to move out of its housing. The pressure at this point, also known as the push out pressure, is given in Table 4.1 and is 0.15 bar. The next significant point is B. This point represents the pressure and stroke at which the brake shoes have actually engaged the brake drum and are generating braking torque. This point occurs at a stroke of 34.5 millimeters and a pressure of 0.30 bar. Finally we can see the point of maximum stroke, point C, which occurs at 45.0 millimeters and a pressure of 7.00 bar. It should be noted that in addition to pressure and stroke, the force exerted on the piston at each point is given in Table 4.1. These forces, given in Newtons, are calculated using Equation 4.1 by multiplying the brake chamber diaphragm area, equal to $1.43 \cdot 10^{-2}$ square meters, by the chamber pressure, which must be converted from bar to Newtons per meter squared.

$$\begin{aligned}
F_p[N] &= P[bar] \cdot \frac{100,000 [N/m^2]}{1[bar]} \cdot A_{diaph} [m^2] \\
&= P[bar] \cdot \frac{100,000 [N/m^2]}{1[bar]} \cdot 1.43 \cdot 10^{-2} [m^2]
\end{aligned}
\tag{Equation 4.1}$$

When developing the brake chamber rig, the goal was to design it in such a way that the brake chamber would produce a similar pressure versus stroke curve as seen in Figure 4.12. In order to accomplish this, the stiffness characteristics of the drum brake assembly were assessed and replicated. The first assessment made was that two stiffness regimes occur as the chamber piston travels. Regime one occurs between points A and B; this will be known as the AB regime. Regime two occurs between points B and C; this will be known as the BC regime. It was known from the vehicle manufacturer that as the piston travels through the AB regime, it travels freely with little or no external resistance from the drum brake assembly. We can therefore conclude that all the stiffness that occurs in this regime is produced by an internal brake chamber spring with linear stiffness characteristics. This stiffness will be known as k_{AB} and it is calculated in Equation 4.2 by dividing change in piston force by the change in piston stroke that occurs from point A to point B. It can also be concluded that the stiffness which occurs in regime BC must be a cumulative stiffness that results from k_{AB} as well as some stiffness inherent to the drum brake assembly, denoted here as $k_{drum\ brake}$. The value of k_{BC} is determined in the same manner as k_{AB} and the calculation is given in Equation 4.3. Since k_{BC} is a cumulative stiffness, it must be equal to $k_{drum\ brake}$ plus k_{AB} . Based on this principal, the value for $k_{drum\ brake}$ is determined using Equation 4.4. The resulting

stiffness for the drum brake assembly at the engagement point is 906 Newtons per millimeter.

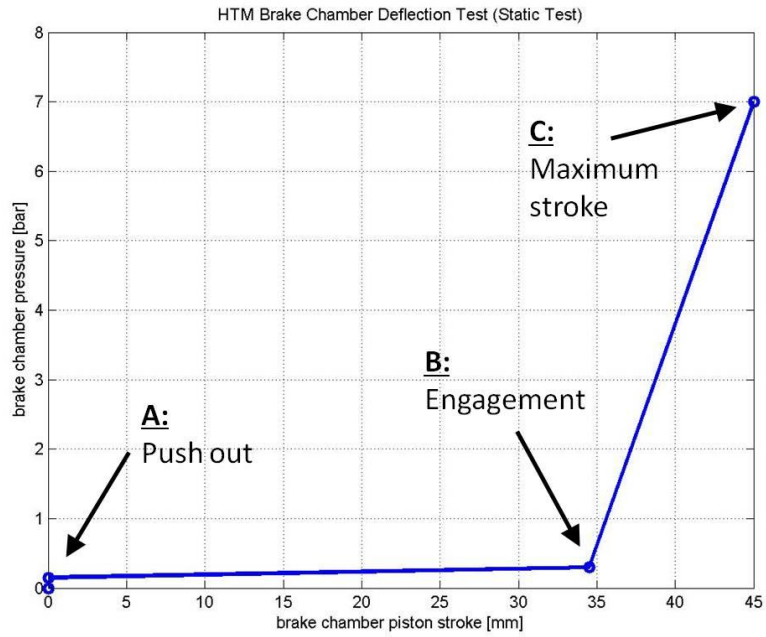


Figure 4.12: Drum Brake Deflection Test

<u>Point</u>	<u>Stroke [mm]</u>	<u>Chamber Pressure [bar]</u>	<u>Piston Force [N]</u>
A	0.0	0.15	215
B	34.5	0.30	429
C	45.0	7.00	10010

Table 4.1: HTM Brake Chamber Deflection Test

$$\begin{aligned}
k_{AB} &= \frac{\Delta force}{\Delta stroke} = \frac{(P_2[bar] - P_1[bar]) \cdot \frac{100,000 [N/m^2]}{1[bar]} \cdot A_{diaph} [m^2]}{x_2[mm] - x_1[mm]} \\
&= \frac{(0.30[bar] - 0.15[bar]) \cdot \frac{100,000 [N/m^2]}{1[bar]} \cdot 1.43 \cdot 10^{-2}[m^2]}{34.5[mm] - 0[mm]} \\
&= 6.22[N/mm]
\end{aligned}
\tag{Equation 4.2}$$

$$\begin{aligned}
k_{BC} &= \frac{\Delta force}{\Delta stroke} = \frac{(P_2[bar] - P_1[bar]) \cdot \frac{100,000 [N/m^2]}{1[bar]} \cdot A_{diaph} [m^2]}{x_2[mm] - x_1[mm]} \\
&= \frac{(7.00[bar] - 0.30[bar]) \cdot \frac{100,000 [N/m^2]}{1[bar]} \cdot 1.43 \cdot 10^{-2}[m^2]}{45.0[mm] - 34.5[mm]} \\
&= 912[N/mm]
\end{aligned}
\tag{Equation 4.3}$$

$$\begin{aligned}
k_{drum\ brake} &= k_{BC}[N/mm] - k_{AB}[N/mm] \\
&= 912.48[N/mm] - 6.22[N/mm] = 906[N/mm]
\end{aligned}
\tag{Equation 4.4}$$

Once the stiffness of the drum brake assembly was known, a material with similar stiffness properties needed to be selected for the brake chamber rig and placed at a distance equal to the engagement point; 34.5 millimeters from the piston push out point. By doing this the compliance of the entire drum brake assembly could be properly replicated.

After researching many different materials such as coil springs, cantilever springs and rubber blocks, the most cost effective and practical material to use for this

application was determined to be a tubular style viscoelastic rubber damper. These rubber dampers were chosen since they are fairly inexpensive and deflect only small distances when subjected to extremely large loads. By studying force versus deflection curves supplied by the damper manufacturer, the stiffness of various sizes of dampers could be calculated. After analyzing many different dampers, a particular model was found to have a nominal stiffness of approximately 500 to 600 Newtons per millimeter. This stiffness is roughly half the value of the required stiffness which is equal to $k_{drum\ brake}$ with a numerical value of 906 Newtons per millimeter. It was therefore determined that two of these dampers could be placed in parallel to create the desired stiffness characteristics.

Figure 4.13 shows a top view of the final brake chamber rig design. As seen in the figure, two brake chambers are integrated into each brake chamber rig. Each brake chamber piston is coupled to a cylindrical aluminum coupler which is then bolted to a rectangular aluminum slider; these components are referred to as the piston assembly. Each aluminum slider also contains two flange-mount linear bearings which allow the piston assembly to travel smoothly along two slider shafts. We can also see from Figure 4.13 that two rubber dampers are configured in parallel for each brake chamber and are placed 34.5 millimeters from the piston assembly.

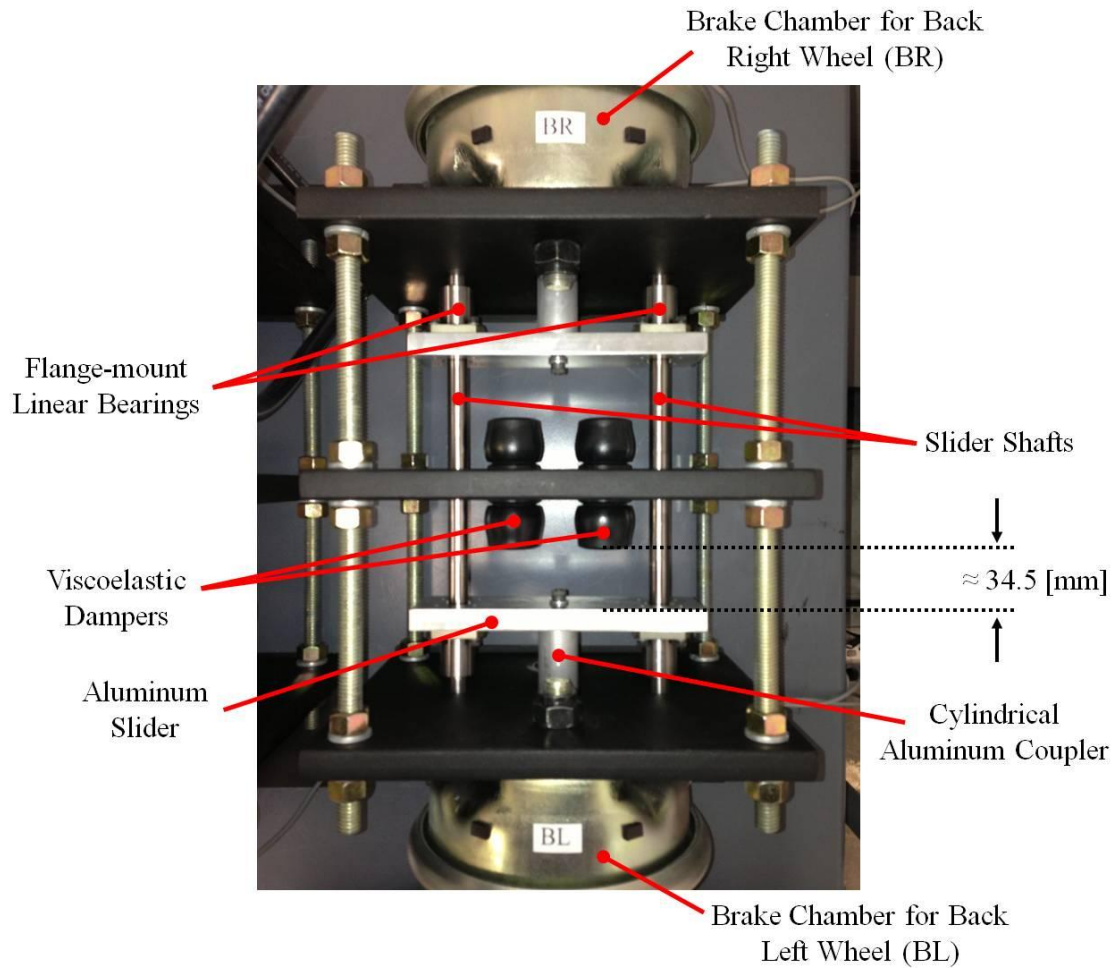


Figure 4.13: Brake Chamber Rig

In total there are three brake chamber rigs and six brake chambers. In order to validate the stiffness characteristics of these rigs, a static deflection test was conducted and the results were compared to the bench test from Figure 4.12. The test result for one of the brake chambers is plotted in Figure 4.14. We can see from the figure, the deflection performance of the brake chamber rig, represented as HIL, is very similar to the performance recorded by the heavy truck manufacturer, represented as HTM. The points of push out and engagement match nearly perfectly and the points of maximum

stroke are fairly close as well. At seven bar, the test vehicle chambers have a stroke of 45 millimeters and the HIL rig has a stroke of 42 millimeters (a difference of only -6.7 percent). It can therefore be concluded that the brake rig successfully emulates the stiffness characteristics of the drum brakes on the actual test vehicle.

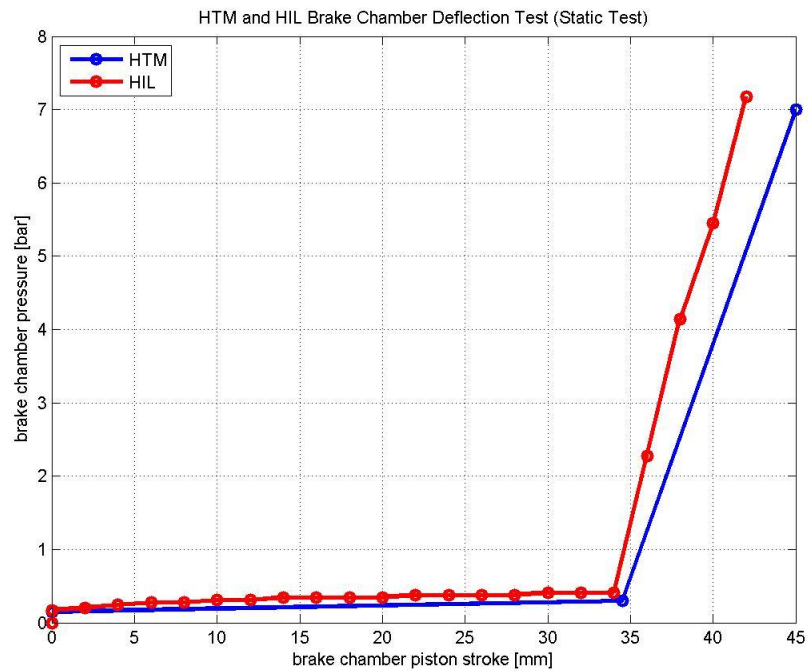


Figure 4.14: Emulating Drum Brake Stiffness

4.2.4 Brake Chamber Pressure Sensing

In order for the vehicle model to undergo braking during a simulation, the user must press the brake treadle so the brake chambers fill with pressure. The pressure in each of the six brake chambers must then be measured with pressure transducers and the

resulting pressure signal voltages must be transmitted to the dSPACE analogue to digital converters on the I/O board. These converters will then digitize the pressure signal voltages so they can be sent to the Simulink model running on the RTP. Within the Simulink model, the pressure voltages are then converted back to pressure values via a gain block and ultimately converted to brake torque values with a brake torque generator model. These brake torques are then sent to the TruckSim S-Function within Simulink to slow down the vehicle model.

When choosing transducers to measure the brake chamber pressures, several factors were taken into consideration. First, the transducer would need to be capable of measuring pressures from zero bar all the way up to eight or nine bar; this is the maximum system pressure. In addition to this, the transducers would need to be able to take rapid pressure measurements due to the fact that the chamber pressures fluctuate rapidly during ABS modulation. Finally the transducers would need to be compatible with a 24 volt power supply, known as the excitation voltage, since the dSPACE power supply would already be set to 24 volts for powering the ABS ECU.

After researching several options, the Omega PX209-200G5V transducer was chosen. This is a gauge type transducer and has an operating range of zero to 200 psi (13.8 bar). The excitation voltage is 24 volts DC and the response time is two milliseconds which is sufficiently fast for capturing any pressure fluctuations. An image of one of the Omega transducers mounted to a brake chamber is given in Figure 4.15. As seen in the figure, the transducer is mounted between the air inlet line and the brake chamber with the use of a tee fitting. It should be noted that due to the fact the transducer is mounted outside the brake chamber, there may be a small pressure delay which exists

between the actual brake chamber pressure and measured pressure, however, this delay was assumed to be relatively insignificant since the vehicle manufacturer used a similar configuration to measure brake chamber pressure on their test vehicles.

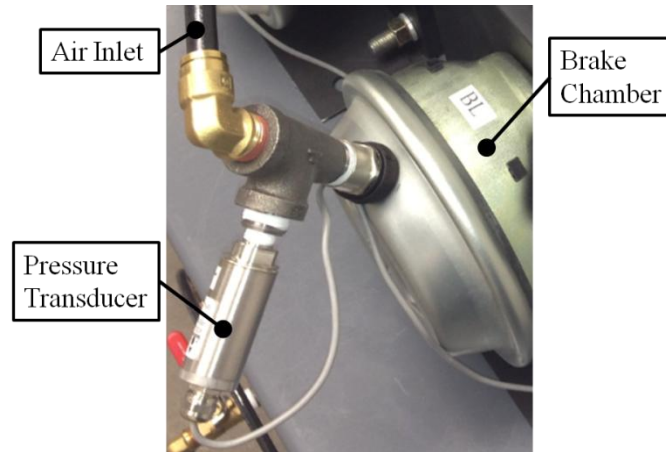


Figure 4.15: Brake Chamber Pressure Sensing

4.2.5 Anti-lock Braking System ECU and Electrical Connections

After all the hardware components were assembled and the methodology for implementing the braking system with dSPACE was determined, the electrical components of the HIL system could be connected. Figure 4.16 illustrates a wiring schematic for connecting the various hardware components. As seen in the figure, the main two electrical components are the dSPACE I/O board and the ABS ECU. In order to make electrical connections to the I/O board, the dSPACE HYP connectors are utilized. For making connections to the ECU, plastic connectors and pins are used; these were provided by the manufacturer. From the figure we can see each of the four wheel

speed signal circuits along with the J1939 bus, ignition circuit and power circuit which all run from dSPACE to the ECU. In addition to this, the ECU has several excitation lines going to the inlet valve (IV) and exhaust valve (EV) for each of the four ABS modulators. All four modulators are connected in parallel to the main system ground as well.

In order to supply power to the pressure transducers, the excitation terminals of all six transducers are wired in parallel and connected to the VBAT1 power supply terminal. The ground terminals of all six transducers are wired in parallel and connect to the main system ground. In order to read the transducer voltage signals, each one is connected to the positive terminal of an analogue to digital converter. It is important to note that the negative terminal of each ADC must be connected to the main system ground to serve as a reference voltage.

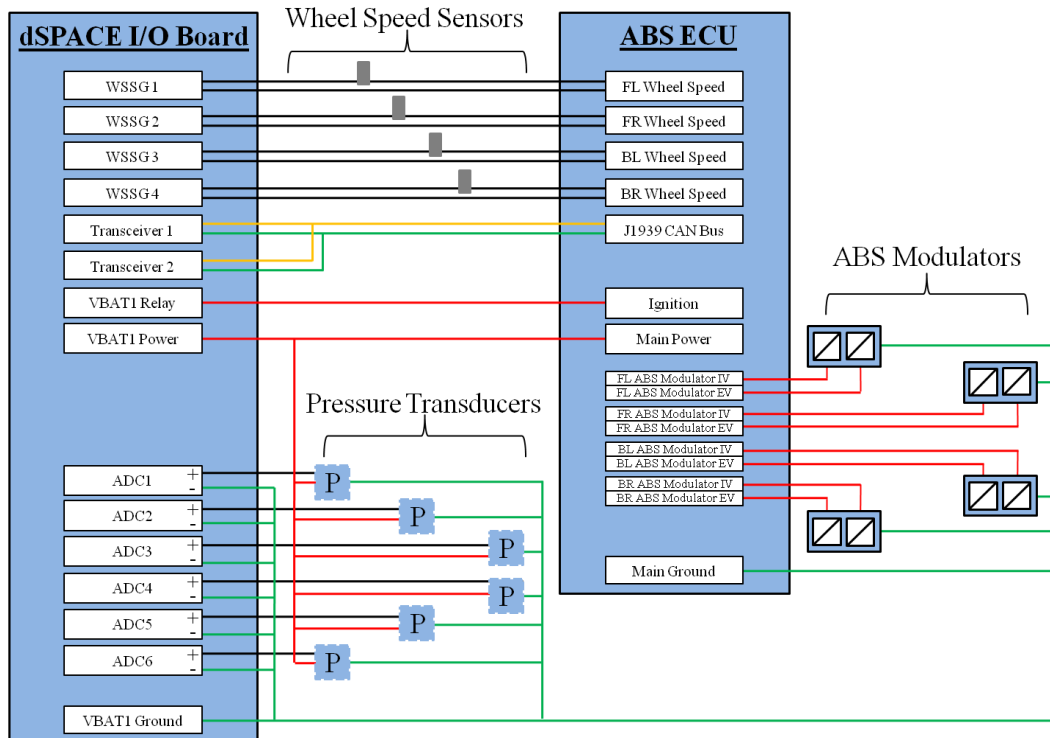


Figure 4.16: dSPACE and ABS ECU Wiring Schematic

There were additional terminals present on the ABS ECU for features such as warning lamp indication, diagnostics and anti-slip regulation (similar to acceleration traction control), however, these features were not assessed in this project and thus they are not pictured in the wiring schematic. An overall picture of the HIL simulator is given in Figure 4.17.

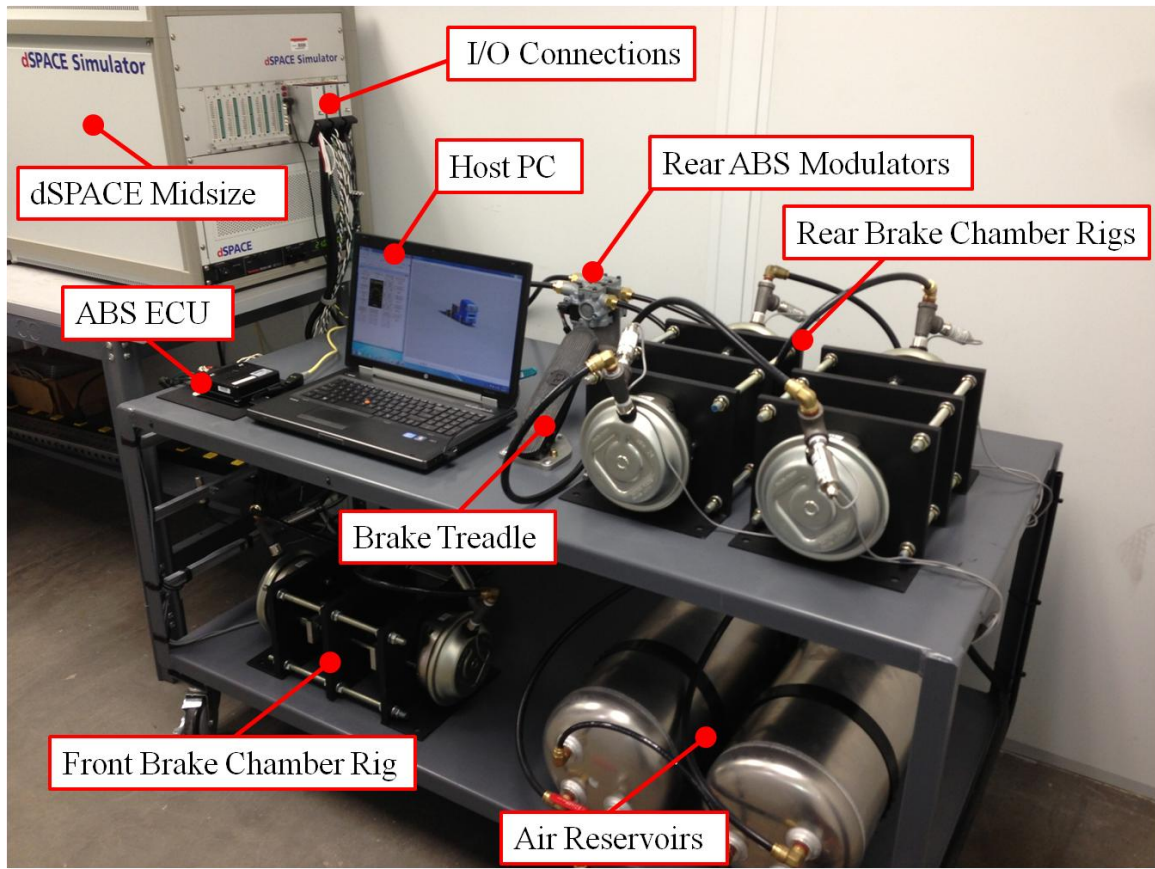


Figure 4.17: HIL Simulator Photo

4.3 HIL Simulation Software

4.3.1 Simulink, TruckSim and RTI Block Set

The hardware in the loop simulation process consists of integrating a hardware subsystem with a software subsystem. As explained in the previous sections, the heart of the hardware subsystem consists of the brake chambers, treadle, ABS modulators, and ABS ECU. On the other hand, the heart of the software subsystem is the MATLAB Simulink model which is created on the host PC and is then run on the dSPACE RTP.

In order for the Simulink model to interact with the ABS hardware, the dSPACE input/output board must be able to interpret any signals from Simulink and convert them to real world electrical signals. For example, the wheels speeds which are calculated within the Simulink/TruckSim model must be converted to real world sine wave voltages which the ABS ECU can interpret. In addition to this, the dSPACE input/output board must be able to interpret any signals from the hardware and convert them to computerized signals which can be utilized by the Simulink model. For example, the voltages produced by the brake chamber pressure transducers must be "computerized" so they can be fed into the Simulink/TruckSim model. Both of these actions can be accomplished through the use of the dSPACE real time interface (RTI) blocks. A list of the most important RTI blocks is given in Table 4.2.

<u>RTI Block Icon</u>	<u>Block Name</u>	<u>Block Description</u>
	Analogue to Digital Converter (ADC)	This RTI block is used to take analogue input signals from the dSPACE IO board and digitize them for use in the Simulink model. In this project the ADC block was utilized for measuring the pressure sensor output voltages.
	Digital to Analogue Converter (DAC)	This RTI block is used to take digital signals from the Simulink model and turn them into analogue signals for use with the hardware. In this project the DAC block was utilized for controlling the power supply output voltage found in the dSPACE Midsize simulator.
	Wheel Speed Signal Generator (WSSG)	This RTI block is used to generate a sinusoidal wheel speed signal. The two key inputs to this block are wheel speed and signal amplitude voltage. In addition to this the user must go within the parameter settings of the block to define the number of teeth on the vehicle's pole wheels. In this project four of these blocks were used to generate signals representing each of the four wheel speed sensors.
	CAN Multimessage Main Block	This RTI block is used for CAN communications. From within this block DBC files describing the CAN messages and signals can be uploaded. The user can choose which messages and signals are transmitted and received at any instant. For this project two of these blocks were used to transmit and receive SAE J1939 CAN messages with the WABCO ECU.

Table 4.2: RTI Blocks

We will now discuss the basic layout of the Simulink model. If we refer to Figure 4.18, we can see the top level of the model built for this project, in which there are three main blocks. Block number one is the TruckSim S-Function. The S-Function is a representation of the mathematical vehicle model. It is essentially a link to the vehicle equations of motion, also known as the vehicle simulation (VS) model which was developed with TruckSim. From within TruckSim, the S-Function can be configured to have imports (variables coming from the Simulink environment) and exports (variables going to the Simulink environment). As seen in the figure, the S-Function has imports coming from block number two which consist of the brake torque (N-m) of all six wheels, brake status (on or off) and transmission status (neutral or drive). When the simulation is running, the S-Function will solve the VS model in real time based on these import values.

We can also see from Figure 4.18 that the S-Function has exports which are going into block number two. In total there were nearly 100 export variables going to block two from the S-Function that consist mainly of vehicle motion variables such as wheel speed, wheel slip and vehicle C.G. speed as well as vehicle loading and road friction conditions. These export variables were chosen because they were deemed necessary for HIL functionality or because they were necessary to capture for analysis of the vehicle performance.

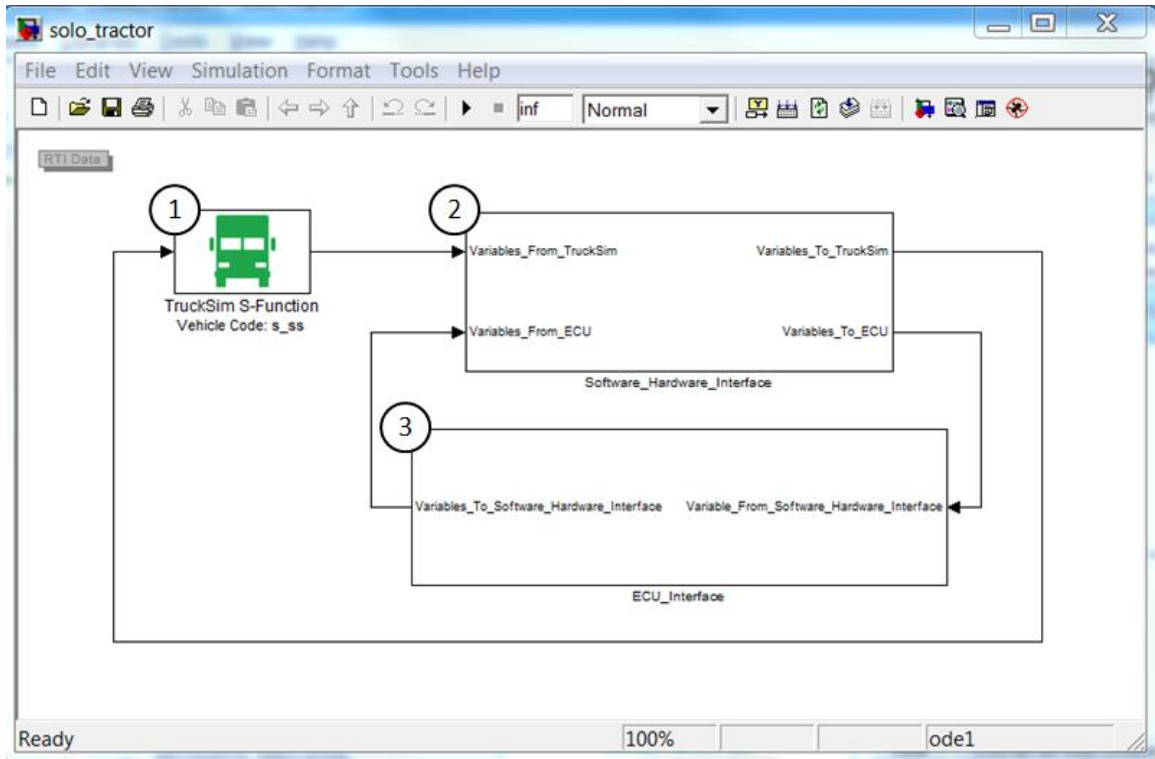


Figure 4.18: HIL Simulink Model Top Layer

Figure 4.19 illustrates the contents of block two. This block is also referred to as the `Software_Hardware_Interface` block. Within it is a block labeled `Capture_Variables` which contains all the variables present in the simulation. Going into this block are inputs such as `Variables_From_TruckSim`, which was previously discussed, as well as `dSPACE_Variables`, which consists of the measured brake chamber pressures coming from the ADC inputs on the dSPACE I/O board. There is also an input labeled `Variables_From_ECU` which consists of the EBC1 and EBC2 CAN messages coming directly from the ABS ECU. These CAN messages are read through the dSPACE CAN transceivers which are connected to the ECU via the CAN bus.

In addition to having inputs, the Capture_Variables block also has two outputs labeled Variables_To_TruckSim and Variables_To_ECU. For this simulation, the Variables_To_ECU output consists of the front left, front right, back left and back right wheel speeds in kilometers per hour. These wheel speeds are calculated via the TruckSim S-Function and then passed through this output to block number three.

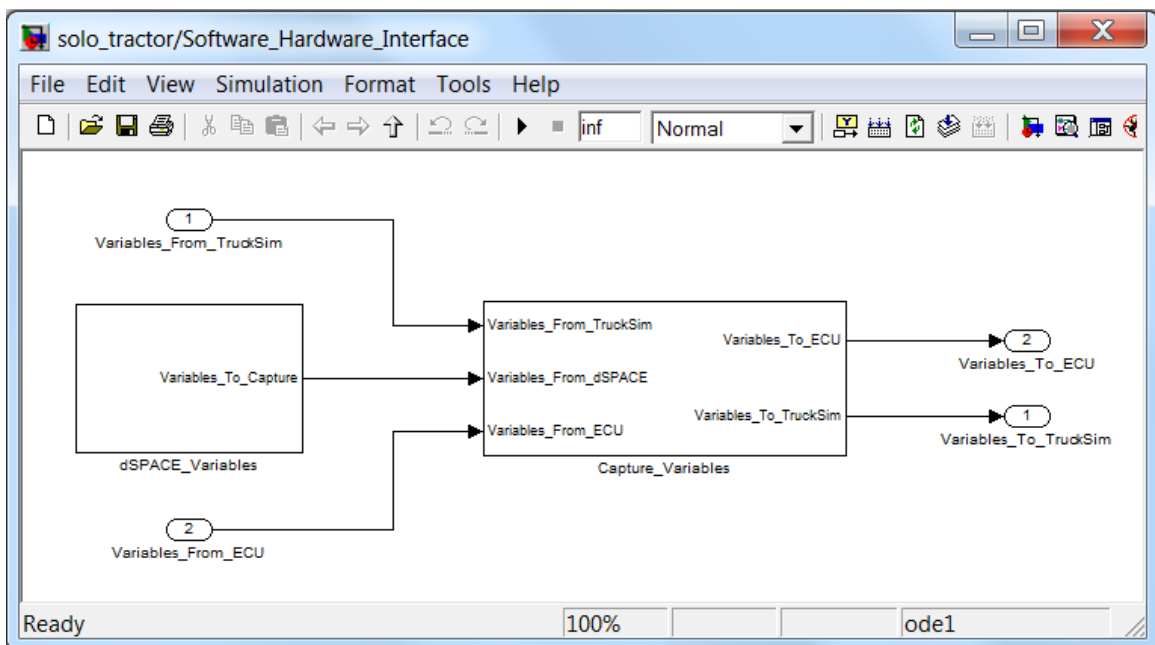


Figure 4.19: HIL Simulink Model Software Hardware Interface

The contents of block three, also referred to as the ECU_Interface block, are given in Figure 4.20. As illustrated in the figure, the Variables_To_ECU output from block two are now going into block three as Variables_From_Software_Hardware_Interface. As previously mentioned, this input

consists of the four wheel speed values calculated from TruckSim. These wheel speeds are then sent to the wheel speed signal generators which are hardwired to the ABS ECU. We can also see from the figure that there is a block labeled Power. Within this block are two important control features. First, there is an RTI block which controls the dSPACE DAC channel 12. DAC channel 12 is reserved in the dSPACE Midsize to control the voltage output of VBAT1; this is the power supply which provides power to the ECU and pressure transducers. In order to set VBAT1 to the proper voltage of 24 volts, a Simulink constant block is inserted in the model and connected directly to the DAC channel 12 RTI block. The constant block must then be set to the desired voltage output divided by the maximum achievable VBAT1 voltage. For example, the VBAT1 power supply can produce a maximum voltage of 33.8 volts and the desired voltage is 24 volts, therefore, the Simulink constant block must be set to $24/33.8$.

The second important control feature of the Power block is the vehicle ignition control. The ignition control is essentially a switchable voltage source that is hardwired to the ignition on/off terminal on the ABS ECU. In the actual HTM tractor, this ignition terminal is supplied with 24 volts when the driver starts the vehicle. In the simulation, the ignition circuit is set to come on as soon as the simulation starts and turn off one second prior to the simulation finishing; the ignition is set to turn off one second early in order spare the ECU from observing the erratic wheel speeds and decelerations that occur when the simulation instantaneously stops at the end of a run. The ignition circuit is controlled through what is referred to as a digital out (DIG OUT) RTI block which sends an activation voltage to a relay within dSPACE and ultimately supplies the VBAT1 voltage to the ECU ignition terminal.

The final block within the ECU_Interface is labeled J1939. This block contains the J1939 CAN RTI blocks that facilitate CAN communications with the ECU. For this particular model, there were no inputs being sent into the J1939 block from the rest of the Simulink model, however, there is an output line going to the Software_Hardware_Interface block which contains the EBC1 and EBC2 messages as previously mentioned. It should be noted that there are many dynamic CAN signals (variable based signals which have non-constant values) that go to the ABS ECU which could have been implemented here, however, they were not of importance for ABS functionality and thus were not implemented for this model.

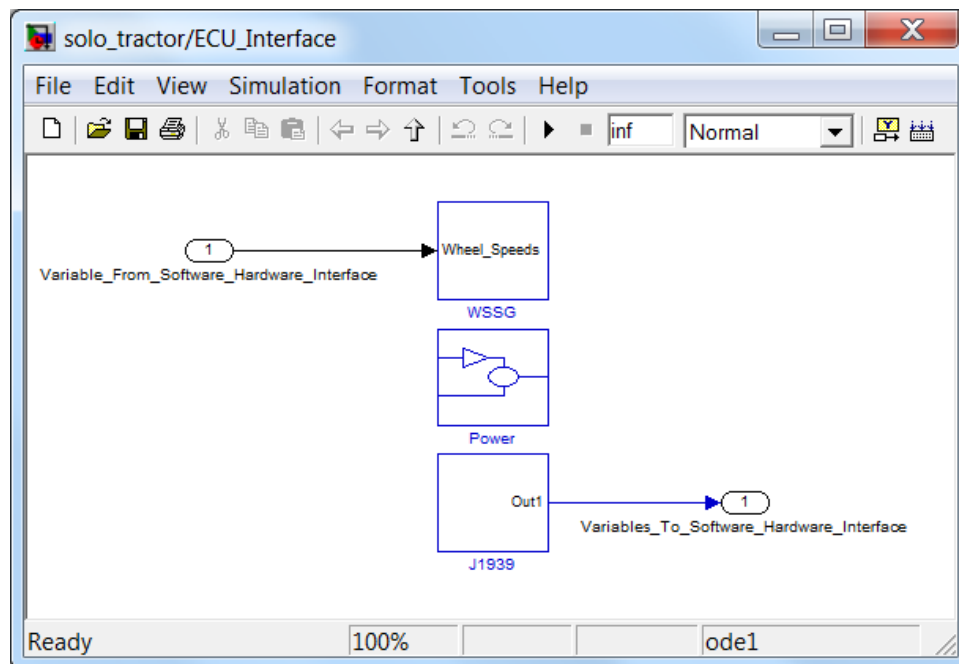


Figure 4.20: HIL Simulink Model ECU Interface

Figure 4.21 illustrates the contents of the J1939 block. Upon referring to the figure, we can see several RTI blocks which are all numbered as well as an additional window named TX MainBlock which has been opened. All of these RTI blocks come with the CAN J1939 multimessage toolbox which can be purchased from dSPACE. The toolbox contains all of the blocks needed to transmit and receive J1939 messages with external J1939 based devices; in this case the ABS ECU.

Block number one is the CAN multimessage general setup block. This block must be inserted into the Simulink model whenever multimessage RTI blocks are being implemented. Although this general setup block has internal features which can be configured, the default settings were sufficient for this project and the contents of the block will not be discussed.

Block number two is the controller setup block. This block is used to configure each dSPACE transceiver. One of these blocks must be added to the Simulink model for each transceiver being utilized; the dSPACE Midsize has a total of two transceivers. The block can be opened and parameters for the CAN network can be configured as well. These parameters include settings such as the naming of the CAN transceivers, defining the message frame format, whether it be standard or extended, and defining the baud rate of the CAN bus, in this case 250 kBaud.

Block three is the main setup block for the dSPACE transceiver and is the most important block for setting up the CAN network. This block is used to configure the CAN messages being transmitted (TX) and being received (RX) by the transceiver. Window number five illustrates the contents of block three. We can see there are options on the left hand side of window five for configuring the general settings, network nodes,

messages, signals and more. As can be seen from the figure, the general settings option at the top of the list is selected and a number six is used to point out the field for loading the CAN database file. In this database field, the user must locate the DBC file, or other database file, used to configure the CAN network. This DBC file essentially contains a list of all the nodes, messages and signals which represent the CAN network being simulated. The DBC database file will be discussed in greater detail in Section 4.3.2.

Block number four in Figure 4.20 is a Simulink subsystem which contains all the messages and signals being transmitted from the dSPACE transceiver to the ABS ECU via the J1939 bus. This block and the messages and signals it contains will be discussed in Section 4.3.2.

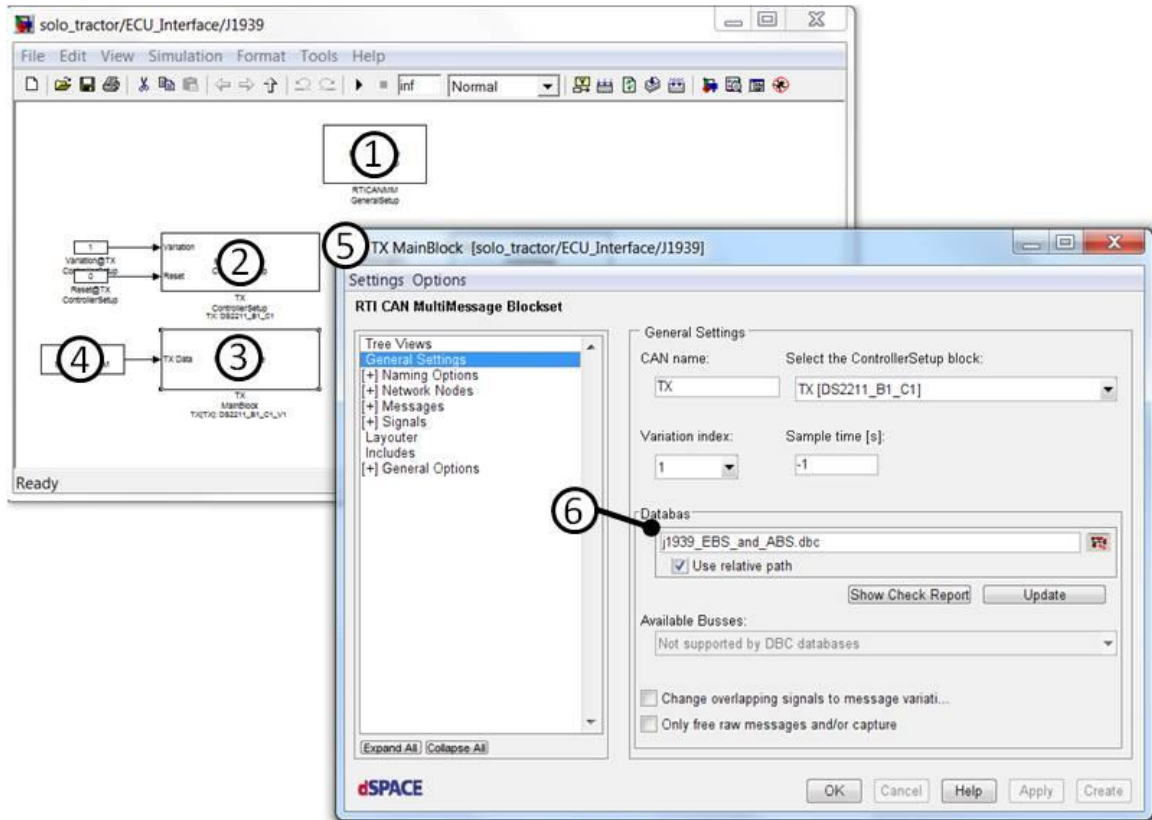


Figure 4.21: HIL Simulink Model J1939 Messaging

4.3.2 Creating the J1939 Messages

As mentioned in the previous section, a database file must be created and loaded into the database field in the TX MainBlock before CAN messages can be transmitted or received with dSPACE. The database file can be thought of as a storage bank which contains a list of messages that can be implemented on the CAN bus. In addition to this, the database file contains a list of signals which are organized into their corresponding messages. For this project, a generic SAE J1939 database file was provided by the vehicle manufacturer and it was used as a starting point for database development. This

generic database file contains hundreds of messages and signals which are all defined by SAE in document J1939-71 [7].

In order to view and modify the database file provided by the manufacturer, a program called CANdb ++ Editor was used. The CANdb software works with database files in the .dbc format and thus they are referred to as DBC database files. A screen shot of the CANdb software is given in Figure 4.22. In this figure, the DBC file developed for this project is displayed. The far left window pane, labeled with a number one, displays a list of all the messages that will be available to transmit and/ or receive with dSPACE CAN transceivers once the DBC file is loaded into the model. A number two labels the middle window pane which displays a list of signals for a particular message. In this case, we can see the message entitled CM_EBC1 is selected in window one and thus window two displays the signals contained in the CM_EBC1 message. It can be noted that the CM_EBC1 message is referred to as EBC1 by SAE standards, however, for this project the message names were modified to follow a convention in which all the messages being transmitted by the ABS ECU have a CM, short for central module, and all the messages being transmitted by the dSPACE transceiver have a REST, short for rest bus.

From within window pane two, information corresponding to each signal is given. The first column in this pane displays the names of the signals. These signal names follow the J1939-71 [7] naming convention, however, the user can modify each signal name or add new signal names if necessary. The second column displays the name of the message that each signal belongs to. In this case, the CM_EB1 message was selected so column two displays CM_EBC1 for every signal. Column three displays the start bit of

each signal. The start bit gives the order and location in which each signal appears in the message; previously discussed in Section 2.4.4. Column four gives the length of each signal in bits.

Window pane three displays configuration parameters for a particular message and appears whenever a message name from window pane one is double clicked. In this case, the CM_EBC1 message was double clicked so pane three displays the CM_EBC1 configuration parameters. From this window, the user can adjust the message type, in this case J1939, the message CAN ID, the message data length code (DLC), the transmission method, in this case cyclic at 100 millisecond intervals, and more. The user can also click on the box to the right of the CAN ID field to define the components that make up the message CAN ID such as the PGN value, the source address (SA), the destination address (DA) and the message priority; previously discussed in Section 2.4.

In order to serve as a guide for developing the CAN database, a CAN matrix document was provided by the manufacture along with the DBC file. This document lists all the ECU nodes present on the actual J1939 bus along with the message names, IDs and transmission rates as well as the signal names, start bits, lengths, factors and offsets. Essentially the DBC file was modified until it conformed to the specifications laid out in the CAN matrix document.

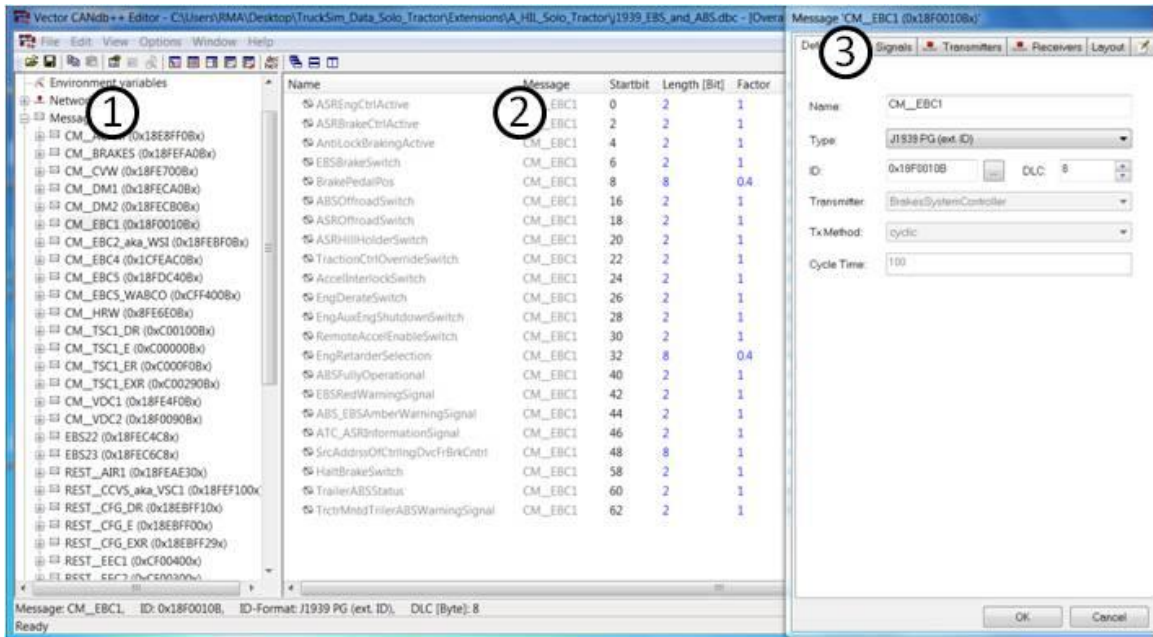


Figure 4.22: Vector DBC File Editor

After the DBC file is configured and all the desired messages and signals are accounted for, the file is loaded into the database field in the TX MainBlock, as previously mentioned, and the TX and RX messages are selected. Upon loading the database, a signal mapping block is automatically generated in the Simulink model. This signal mapping block was illustrated in Figure 4.21 and was labeled as block number four. The contents of this block are displayed in window number one of Figure 4.23.

As seen in the figure, there are a total of 17 rectangular blocks in window one which represent different J1939 messages. In this model, the TX MainBlock was configured to only transmit messages and not receive them. For this reason, each of the 17 blocks represents a TX message that is being transmitted from the dSPACE

transceiver to the ABS ECU. In addition to this, each block is labeled with its CAN message name as defined in the DBC file, this way the messages are easily identifiable.

The TX message block labeled number two is the engine configuration message; referred to as CFG_E in the J1939-71 [7] document. This message provides information regarding the torque versus speed curve for the vehicle's engine and will be used as an example to illustrate the internal structure of the TX message blocks. Upon opening this block, window three appears. This window contains 19 individual constant blocks, each of which represents a numerical value for the 19 signals found in the CFG_E message. The other 16 TX message blocks in window one have a similar internal structure, however, the name, number and value of the signal blocks will vary depending on the message.

As seen in window three, each constant block has a specific value which represents some point on the engine's torque curve. Since these values define the performance of the vehicle's engine, they will vary depending on what engine the CFG_E message is representing. For this project, the manufacturer provided a recording of the vehicle's J1939 bus while the vehicle was turned on and sitting at idle. The data in this recording was analyzed and the numerical signal values for the CFG_E message were extracted along with the signal values for the other 16 TX messages. By doing this, the CAN signals found on the actual vehicle could be replicated in the simulation. It should be noted that many signals, such as engine speed, are not constant and change with time. These are referred to as dynamic signals. Other signals are constant, such as those in the CFG_E message, and do not change with time. These are referred to as static signals. To create a proper CAN bus simulation, the dynamic signals should come from the proper

source. In the case of engine speed for example, the signal value should originate from the TruckSim S-Function which can provide the engine rpm value in real time.

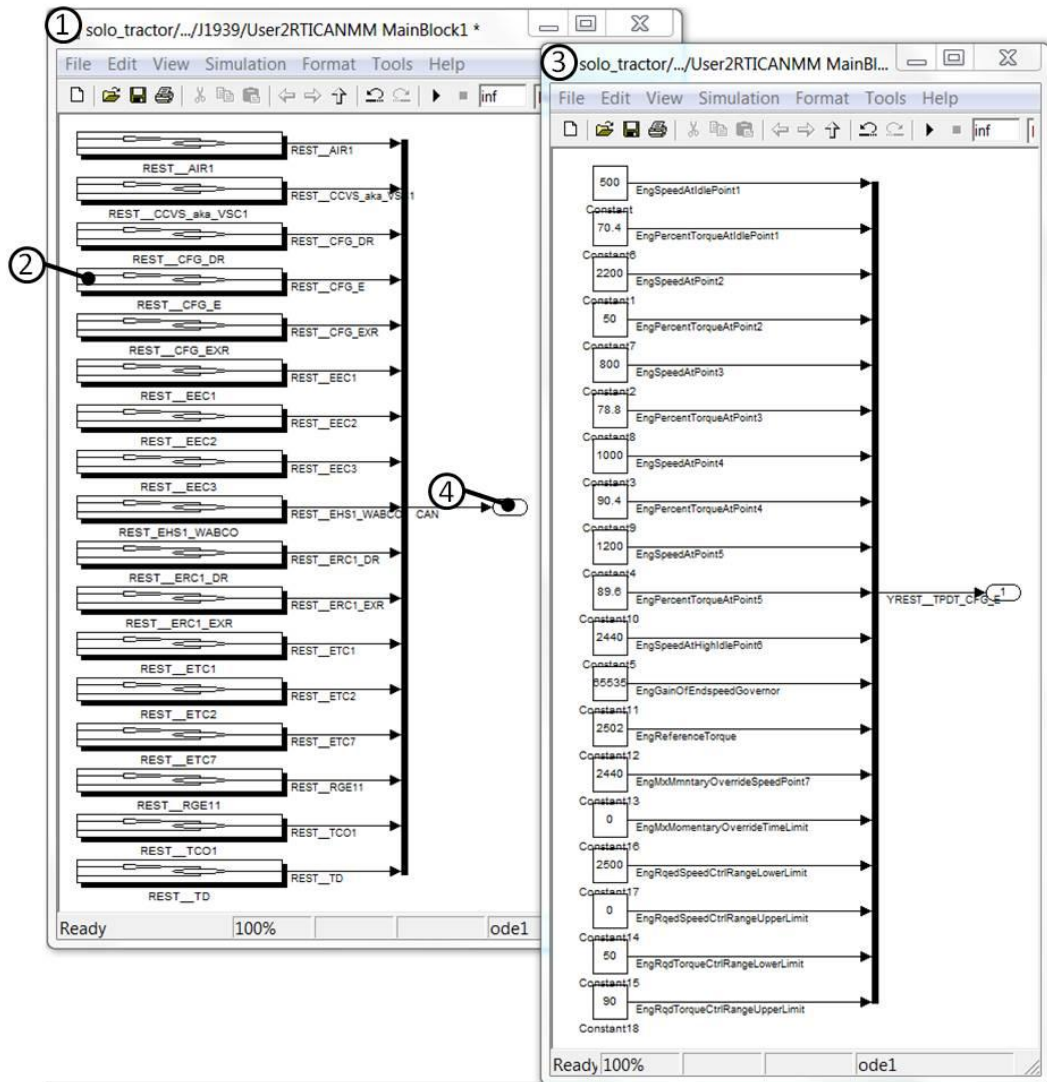


Figure 4.23: HIL Simulink Model TX Messages

In addition to the TX MainBlock, there is also an RX MainBlock which was added to the model; however, it is not pictured in any of the previous figures. This block receives all the CAN messages being transmitted by the ABS ECU. The steps taken to setup the RX MainBlock are nearly identical to those needed for the TX block. The main difference is that instead of generating messages and signals, the RX block is set to receive them. These messages can then be read in real time and/ or recorded using ControlDesk..

4.3.3 Building the Simulink Model for the dSPACE Real Time Processor

Once the Simulink model has been successfully constructed, it must be compiled into C-code for the RTP to run. In addition to this, various files must be generated that essentially describe the entire Simulink model layout and the variables within the model; these files are also needed by the RTP in order to run the model. One such example is the system description file (SDF). The SDF describes the files to be loaded to the individual components of the simulation platform; in this case the platform is the dSPACE Midsize [14].

In order to compile the Simulink model into C-code and generate the SDF file, the user must build the model. This can be accomplished by simply opening the Simulink model and pressing Ctrl + B. The dSPACE software components that run within the Simulink environment will then automatically prepare all the files needed by the RTP to run the simulation. The user can view the build log within the MATLAB command window to see the status of the build process.

After the model has been built, the simulation can be run. In order to do this, the user must open ControlDesk, the experimentation/data acquisition software that comes with dSPACE, and load the SDF file onto the dSPACE processor. This will be discussed in greater detail in the next section.

4.3.4 Running the Simulation with ControlDesk

In order to run simulations, interact with the simulation model, monitor variables and capture data, the ControlDesk experimentation software must be utilized. The ControlDesk software is installed on the host PC which is connected directly to the dSPACE unit. A screen shot of the custom made ControlDesk instrument panel, also known as a layout, for this project is illustrated in Figure 4.24. The layout was configured to monitor variables such as vehicle speed, road friction, brake torque, transmission gear, throttle, wheel speed, vertical tire loading, vehicle location and brake chamber pressure.

When running a simulation with ControlDesk for the first time, the user must first load the compiled Simulink model to the dSPACE RTP. In order to do this, the corresponding SDF file for the model must be located in the file selector window; the SDF file will be saved in the same directory as the Simulink model file. In Figure 4.24, the SDF file for this project has been located and is labeled with a number one. Next, the platform tab in the navigator bar must be selected. When the platform tab is selected, the platform navigator window will display a tree containing various platforms available for running the simulation. As seen in the figure, number two labels the platform tab and the platform navigator window directly above it shows the available platforms. In this case

there are the four ds1006 processors that can run simulations on dSPACE as well as a Simulink icon which is used for running simulations on the host PC in the Simulink environment. In addition to this, the platform navigator window displays a tree element labeled I/O. Underneath this I/O icon are elements which represent the various input/output boards for the dSPACE Midsize. In this case the ds2211 is the main input/output board in which the majority of the hardware components, such as pressure sensors and wheel speed circuits, are wired to. Label number three represents the primary ds1006 processor which was used for running simulations in this project. In order to load the compiled model to this processor, the user must click the SDF file icon (number one in the figure) and drag and drop it over the processor icon (number three).

At this point the simulation model is loaded on dSPACE and waiting to run, however, before continuing, a layout must be created in order to view the system variables as the simulation is ran, i.e. vehicle speed etc.. This is done by selecting "file" within ControlDesk and then hitting "create new layout" (the layout window is labeled with the number five). Next the user can select the desired instruments from the instrument selector (number four in the figure). The majority of the instruments pictured in layout window five are referred to as "display" blocks. These blocks display numerical values of variables defined in the Simulink model.

In order to commission a display block, the user must select the display icon from the instrument selector and then draw a rectangle in the layout window. Next, the name of the variable that will be viewed in the display block must be located in the SDF viewer tab (number six in the figure). A name will appear for each simulation variable in the Simulink model so the user must sift through all the names and find the desired variable.

Once the variable is located, for example vehicle speed or brake chamber pressure, the user must click it then drag and drop it over the display rectangle in the layout window.

In addition to viewing variables in real time via the display blocks, the user can also capture variables and save them to an excel file or MATLAB .mat file for later analysis. For this project, nearly 100 variables were captured and saved to a .mat file so they could be analyzed and plotted in MATLAB. Both the captured variables as well as display variables are transmitted from dSPACE to the host PC in real time via the Link board connection which was mentioned previously. Since there were such a large number of variables for this simulation, a down sampling factor of ten had to be used to allow the simulation to run smoothly.

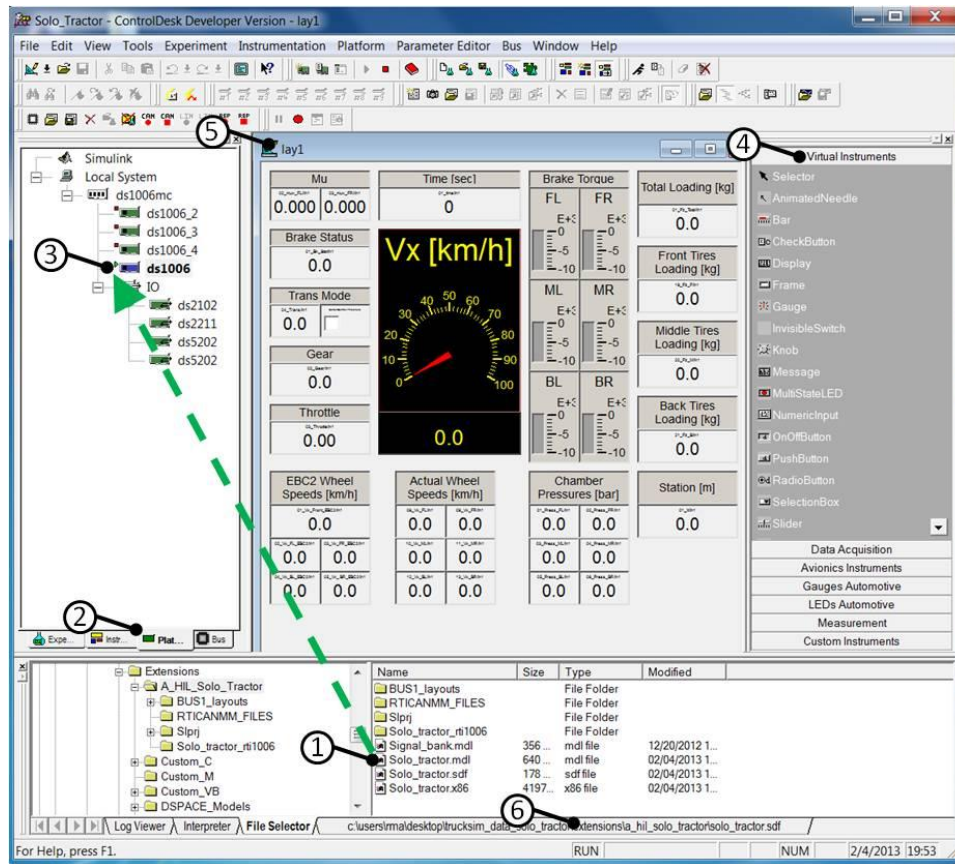


Figure 4.24: Running the HIL Simulation from ControlDesk

After the ControlDesk layout is created and the model is ready to run, the user must press the F5 key on the keyboard while in ControlDesk to enter what is known as animations mode. Finally, the main TruckSim window must be opened and the run button must be pressed. Upon clicking this button, vehicle parameter data and other files will be sent to the dSPACE RTP from the host PC and the simulation will start. This window is illustrated in Figure 4.25.

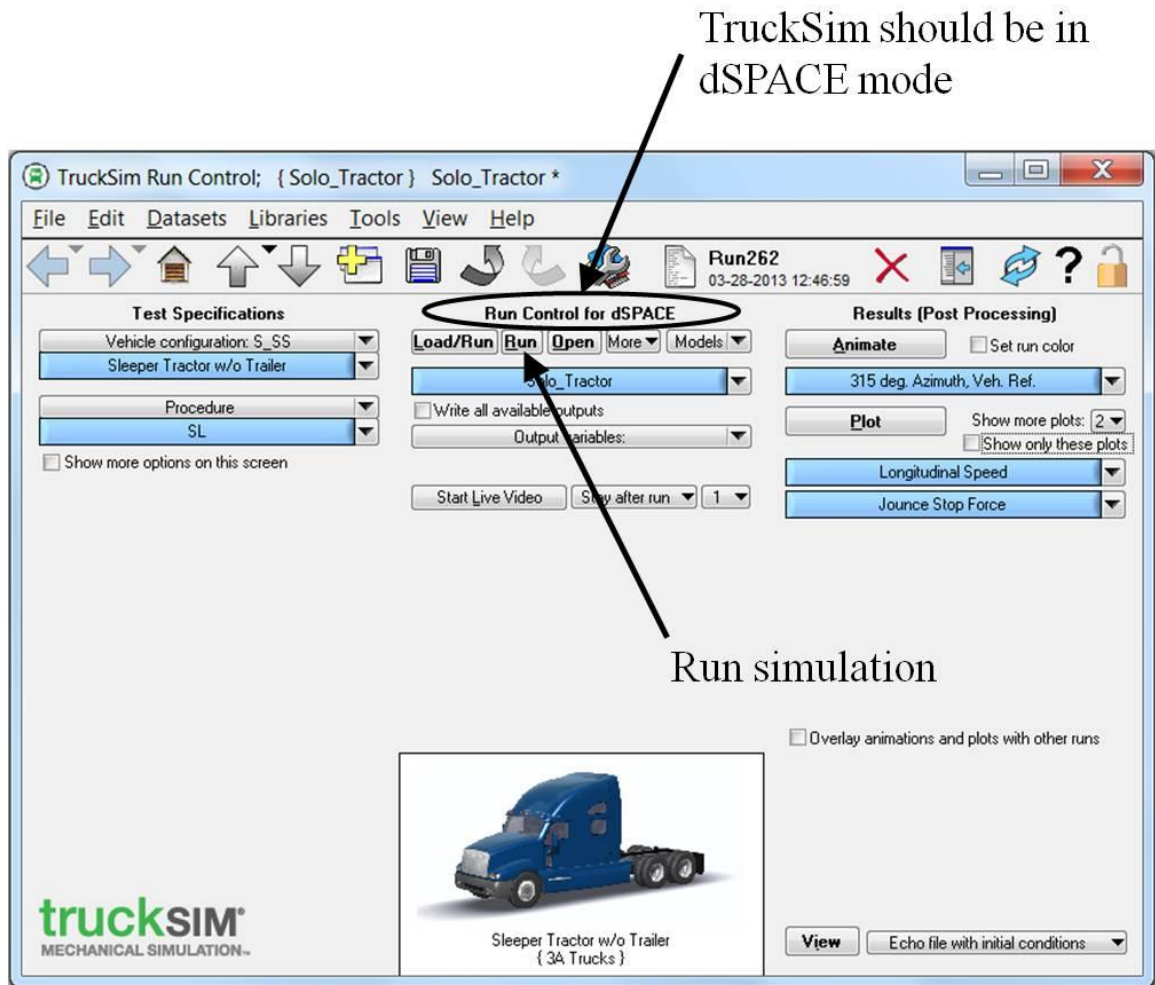


Figure 4.25: Running the HIL Simulation from TruckSim

For viewing CAN communications, the dSPACE CAN multmessage software toolbox allows the user to view all the CAN messages and signals being transmitted and/or received by the dSPACE transceivers. The software will essentially generate a bus tree within ControlDesk where each CAN node is an element on the tree. Layout windows are then automatically generated when the user selects a particular CAN node on the tree. These layouts display all the signal descriptions, signal values, message IDs

and message transmission rates for a particular message within that CAN node. A screenshot of the CAN bus running in ControlDesk is given in Figure 4.26. In the figure, the CAN bus tree is labeled number one. From here, two separate CAN message layouts have been opened and are displayed in the figure. These are the EBC 2 and EBC 1 messages which are labeled numbers two and three respectively.

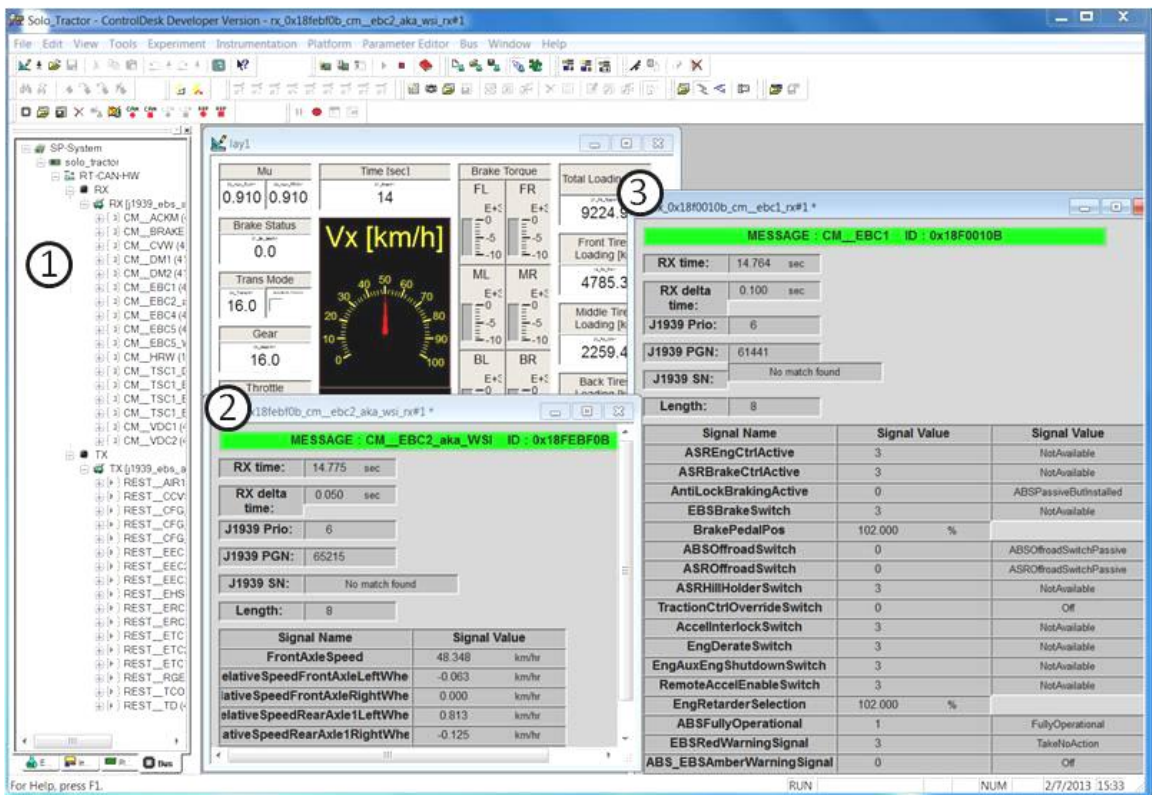


Figure 4.26: Viewing CAN Communications from ControlDesk

Chapter 5: Validation of Hardware in the Loop Simulation

5.1 HIL Braking Tests and Validation

In order to assess the stopping performance of the ABS system, the manufacturer subjected a 6x4 tractor, identical to the one being modeled, to several straight line braking maneuvers and recorded the resulting performance data. The manufacturer was able to provide this test data so it could be used for HIL validation.

Validation of the HIL simulator was accomplished by replicating the real world test maneuvers in TruckSim, running the simulation and then recording and comparing the resulting performance data. Variables including the ABS modulation time, average brake chamber pressure, stopping time and stopping distance were chosen as validation metrics since they directly measure how the ABS system controls the brake chambers, and vehicle speed during braking. By analyzing these metrics we can sufficiently evaluate how well the HIL simulator emulates the HTM tractor during braking. For some tests, the slip ratio was plotted and analyzed as well. The calculation for slip ratio used in this section is slightly different than Equation 2.2 in the background section. For this section, slip ratio is calculated using Equation 5.1. All that has changed here is the sign convention.

$$s = \frac{\omega \cdot r - V}{V} \quad \text{Equation 5.1}$$

5.1.1 Braking Test Procedures

When the manufacturer conducted the ABS braking tests, four different road conditions were tested along with two different vehicle loading conditions. The manufacturer also conducted the braking tests at multiple speeds, however, the results of some of the high speed tests appear to be compromised due to the vehicle running out of track at the testing facility. For this reason, only the low speed test data, i.e. 50 kilometer per hour, will be used for HIL validation.

The first road condition the vehicle was tested on was a homogeneous low μ surface. Essentially this means the road conditions were constant for this test, i.e. homogeneous, and the friction of the surface was low, i.e. an icy or snowy surface. The second road condition tested was a homogenous high μ surface. This road consisted of a dry or fairly dry pavement type material. The third road condition tested was a low to high jump μ surface. This road surface included a transition point from low μ to high μ as the vehicle underwent the braking maneuver. Finally, the fourth road condition tested was a split μ surface. On this surface, all of the tires on the left side of the vehicle were on a low μ surface while all the tires on the right side of the vehicle were on a high μ surface during braking.

These four surfaces were tested with the tractor subjected to two different loading conditions; unladen and laden. The unladen condition consisted of the 6x4 tractor by itself with no additional loads applied. Under this condition the vehicle had a total mass of 9,320 kilograms. For the laden condition, a total of 9,428 kilograms of loading blocks were positioned atop the second and third axels. This load was applied in order to emulate the weight the tractor would experience if a trailer were coupled to it and loaded

to the full gross vehicle weight (GVW) capacity. The engineers conducting the testing decided to use loading blocks as opposed to an actual trailer because they were interested in assessing the braking performance of laden tractor alone without any lateral inertial effects that may be caused by the addition of a trailer.

5.1.2 Simulating Road Friction Characteristics

In order to accurately validate the HIL simulator, it was crucial that the values entered into TruckSim for road friction were as accurate as possible with respect to the real world testing conditions. Even a small deviation in road friction can cause a significant change in the stopping time and stopping distance of the HIL simulation. Fortunately, the test engineers that conducted the testing had a method in place to evaluate the friction of the high and low μ surfaces before conducting the actual braking tests. The procedure was as follows:

1. Position the test vehicle on the surface for which the friction needs to be determined, i.e. high μ or low μ surface, and deactivate ABS functionality.
2. Disconnect the rear four brake chambers on the test vehicle while leaving the front two connected.
3. Accelerate vehicle to 50 kilometers per hour and apply brakes once this speed is achieved.
4. While monitoring the front wheel speeds via instrumentation, manually modulate the brake treadle so the front wheels have ideal slip for maximum adhesion; i.e. keep front wheels on the verge of lockup.

5. Record the time it takes the vehicle to decelerate from 40 kilometers per hour to 20 kilometers per hour and calculate this deceleration in g's.
6. Repeat steps two through five, however, this time disconnect the front brake chambers and connect only the rear four brake chambers.
7. After the deceleration from the brakes (Ax_{front}) and the deceleration from the rear brakes (Ax_{rear}) are determined, add these two values together to get the maximum vehicle deceleration (Ax_{total}) in g's. This value is equal to the peak road friction coefficient.

Although this procedure seems arbitrary, there is actually much logic and practicality behind it. Essentially, the test engineers wanted to determine the maximum deceleration that the test vehicle could achieve on a particular surface. Coincidentally, the maximum deceleration in g's that any object can achieve on a surface is also equal to the peak coefficient of friction for that surface, assuming there are no other external forces acting on the object in motion.

In order to achieve the maximum deceleration for the six wheeled tractor, all six wheels had to be kept at an ideal slip ratio of around 0.10 to 0.60 during braking. However, when manually modulating the brakes, this can be rather difficult since the vertical load on each of the front two wheels is much greater than the vertical load on each of the rear four wheels. For this reason, the rear wheels are prone to lockup before the front wheels during manual braking. This is why only the front wheels were subjected to driver modulated braking for one test and then only the rear wheels were subjected to driver modulated braking for the other test. Then the total deceleration is calculated by adding the deceleration produced by the front tires and rear tires. By

calculating the maximum vehicle deceleration in this fashion, an estimate of the peak road friction could be determined.

Even though the peak friction is known, TruckSim requires the value for sliding friction ($\mu_{sliding}$) be entered for each road surface. This value is greater than the peak friction and can be calculated by dividing the peak friction coefficient (μ_{peak}) by the friction efficiency ($\eta_{friction}$); refer to Equation 5.2. The friction efficiency is essentially the relationship between the peak friction and sliding friction coefficients and is equal to the ratio between the two; refer to Equation 5.3.

$$\mu_{sliding} = \frac{\mu_{peak}}{\eta_{friction}} \quad \text{Equation 5.2}$$

$$\eta_{friction} = \frac{\mu_{peak}}{\mu_{sliding}} \quad \text{Equation 5.3}$$

The value for the friction efficiency was calculated from lab tested tire data supplied by the manufacturer. This data was collected through the use of a rolling road tire force meter in which the longitudinal force generated by the tire at varying slip ratios and varying vertical loads could be measured. According to the test engineers that conducted these measurements, the sliding friction produced by the tire and rolling road surface was equal to 0.9, however, as can be seen in the longitudinal force plot given in Figure 5.1, the average peak tire friction only reached a value of 0.7419. Thus, upon implementing Equation 5.3, the friction efficiency was determined to equal 0.8243 or 82.43%; this calculation is given in Equation 5.4.



Figure 5.1: TruckSim Tire Efficiency

$$\eta_{friction} = \frac{\mu_{peak}}{\mu_{sliding}} = \frac{0.7419}{0.9} = 0.8243 \rightarrow 82.43\% \quad \text{Equation 5.4}$$

Now that the friction efficiency is known and the maximum peak frictions for all test surfaces are known, provided by HTM, the sliding friction values for all road surfaces can be determined upon implementing Equation 5.2. These sliding friction values are calculated in Table 5.1. In addition to this, a list of all the tests conducted with the HIL simulation and the corresponding vehicle configurations are given in Table 5.2.

<u>Surface Type</u>	<u>Vehicle Mass [kg]</u>	$\mu^{kinetic_max}$ (Provided by HTM)	<u>Equation 5.2</u>	$\mu_{sliding}$
Low μ	Unladen; 9320	0.1289	$\mu_{sliding} = \frac{0.1289}{0.8243}$	0.16
Low μ	Laden; 18748	0.1111	$\mu_{sliding} = \frac{0.1111}{0.8243}$	0.13
High μ	Unladen; 9320	0.7521	$\mu_{sliding} = \frac{0.7521}{0.8243}$	0.91
High μ	Laden; 18748	0.6207	$\mu_{sliding} = \frac{0.6207}{0.8243}$	0.75

Table 5.1: Calculating Friction for the HIL Simulation

<u>Test No.</u>	<u>Vehicle Mass [kg]</u>	<u>Description</u>	<u>Brake Application Speed [kph]</u>
1	Unladen; 9320	ABS On; Homogeneous; Low μ (0.16)	50
2	Unladen; 9320	ABS On; Homogeneous; High μ (0.91)	50
3	Unladen; 9320	ABS On; Jump; Low μ (0.16) to High μ (0.91)	55
4	Unladen; 9320	ABS On; Split; Left Side Low μ (0.16) Right Side High μ (0.91)	50
5	Laden; 18748	ABS On; Homogeneous; Low μ (0.13)	50
6	Laden; 18748	ABS On; Homogeneous; High μ (0.75)	50
7	Laden; 18748	ABS On; Jump; Low μ (0.13) to High μ (0.75)	55
8	Laden; 18748	ABS On; Split; Left Side Low μ (0.13) Right Side High μ (0.75)	50

Table 5.2: Test Configuration for HIL Validation

5.1.3 Stationary Brake Chamber Pressure Test

Before the actual HIL braking tests could take place, the pressure rise performance of the brake hardware was evaluated and compared to similar data provided by the brake system manufacturer. This test consisted of applying a step brake command, accomplished by actuating the brake treadle as fast as possible, with full pressure in the air reservoirs, in this case about 9 bar, while recording the pressure rise curve for the brake chambers. This test was conducted while the vehicle was stationary and without any ABS intervention.

The purpose of this test is to assess how the transport delays and first-order time delays of the HIL brake hardware compare to bench test data from the braking system manufacturer. The pressure rise curves for the HIL testing are given in Figure 5.2. It should be noted that only results for the front left chamber are given since the front right chamber is configured identically to the front left. Similarly, only results for the back left chamber are given since the other three rear chambers are configured identically as well.

As illustrated in the figure, the chamber rise times for the HIL simulator are calculated by determining the time it takes for the chamber pressure to rise from ten percent of its maximum value ($10\% \times 8 \text{ bar}$) to 90 percent of its maximum value ($90\% \times 8 \text{ bar}$). It can be noted that although the pressure reservoirs are filled to nine bar, the treadle has an internal regulator which allows the chambers to reach only eight bar.

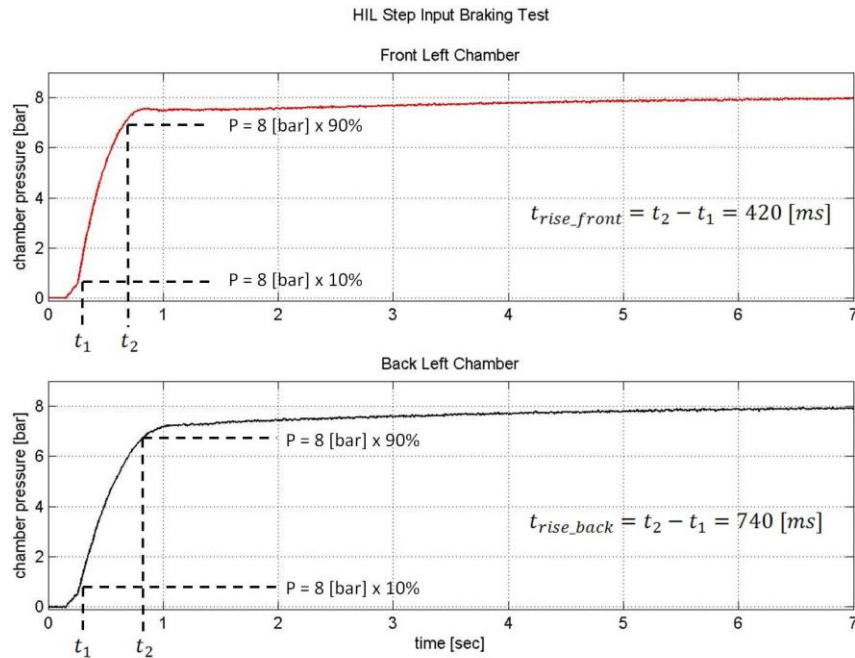


Figure 5.2: HIL Step Input Pressure Test

Table 5.3 compares the pressure rise times from the brake system manufacturer (BSM) and HIL test data. We can see from the table that the front brake chambers for the HIL test produced a rise time of 420 milliseconds while the front chambers for the BSM test produced a rise time of 390 milliseconds. These values differ by only 7.7 percent which is relatively low. However, the rise times for the rear chambers differ significantly more. As we can see from the table, the rear brake chambers for the HIL test produced a rise time of 740 milliseconds while the rear chambers for the BSM test produced a rise time of only 410 milliseconds. These values differ by 80.5 percent! This deviation may be due to the fact that the rear relay valve was not utilized in the HIL simulator as there was a long lead time required to obtain it. Had the valve been implemented, it mostly likely would have reduced the rear chamber rise time due to its large flow orifice and

ability to deliver air at a greater flow rate than the treadle. For future HIL projects, the pneumatic hardware used on the real vehicle should also be utilized on the simulator in its entirety. This includes the rear relay valve as well as the quick release valve which is connected in line with the front chambers.

<u>Brake Chamber</u>	<u>BSM</u>	<u>HIL</u>	<u>% Difference</u>
Front Left	390 [ms]	420 [ms]	+7.7 [%]
Back Left	410 [ms]	740 [ms]	+80.5 [%]

Table 5.3: Brake Chamber Pressure Rise Times

5.1.4 Braking Tests

TEST 1: UNLADEN TRACTOR on LOW MU SURFACE

For the initial HIL braking test, the tractor was unladen (9,320 kilograms) and the road conditions were set to homogeneous low μ (0.16 friction coefficient). The vehicle model started from a stop and was accelerated to a velocity of 50 kilometers per hour in accordance with the HTM test velocity. After maintaining the desired velocity for a few seconds, the brake treadle was manually pressed to 100 percent stroke and held there until the vehicle came to a complete stop. Upon pressing the treadle, the Simulink model was configured to automatically shift the transmission to neutral so torque and inertial effects from the engine were not experienced by the wheels. The resulting validation variables for the HIL and HTM tests are plotted in the proceeding figures. In addition to

this, Table 5.4 contains the validation metrics which are used to compare the overall performance of the HIL simulator and HTM tractor for this test.

Figure 5.3 illustrates pressure versus time for the front left brake chamber and wheel speed versus time for the front left wheel of the HTM tractor and HIL simulator. The subplots in this figure as well as those in proceeding figures have been adjusted so that brake application occurs near time equals zero. This was done to make comparison between the HTM and HIL data easier.

As we can see from subplots a and b, there are strong similarities in the pressure curves for the HTM and HIL data. We can first notice the pressures rises quickly upon initial brake application until a pressure of around 2.2 bar is reached. At this point, ABS modulation begins for both the HTM tractor and HIL simulator resulting in a rapid pressure dump. Similarly in subplots c and d, the wheel speeds drop by roughly 15 kilometers per hour as this initial ABS modulation cycle takes place. For this test we can conclude the initial braking behavior for the front wheels of the HTM tractor and HIL simulator are quite similar and ABS intervention initializes at the same instance.

As we further asses Figure 5.3 along with the numerical data in Table 5.4, we can see a small discrepancy exists in the ABS modulation time for the HTM and HIL data. The modulation time is essentially the amount of time that passes from the initial ABS modulation to the time when the wheel comes to a complete stop. For this test, the HTM tractor has a modulation time of 11.04 seconds while the HIL simulator has a modulation time of 11.98 seconds. In addition to this, the average chamber pressure for the HTM data is 0.96 bar while the HIL data is lower at 0.87 bar. These discrepancies could possibly be due to a slight difference in the simulated road friction and the actual road

friction. If the actual road friction were slightly greater than the simulated friction, the HTM tractor would brake slightly faster and with greater chamber pressure due to the greater adhesion ability of the tires.

Figure 5.4 illustrates pressure versus time for the back left brake chamber and wheel speed versus time for the back left wheel of the HTM tractor and HIL simulator. We can see from subplots a and b that the pressures rise quickly upon initial brake application until a pressure of around 2.2 bar is reached. From this figure, it appears that even without the use of the rear relay valve on the HIL brake hardware, the rear chambers are able to build pressure as quickly as those on the HTM tractor. This suggests that the 80.5 percent rise time discrepancy found in the stationary brake chamber test for the rear chamber does not significantly effect the overall performance of the HIL simulator during ABS intervention; refer to Table 5.3. We can also see from Figure 5.4 and Table 5.4 that the HTM data has a shorter modulation time at 11.01 seconds while the HIL data has a modulation time of 11.94 seconds. This difference is similar to what was experienced with the front brakes and again may be caused by a slight difference in the simulated road friction value.

Front Left Chamber Pressures and Wheel Velocities
(Unladen, ABS On, Low μ , 50 kmph)

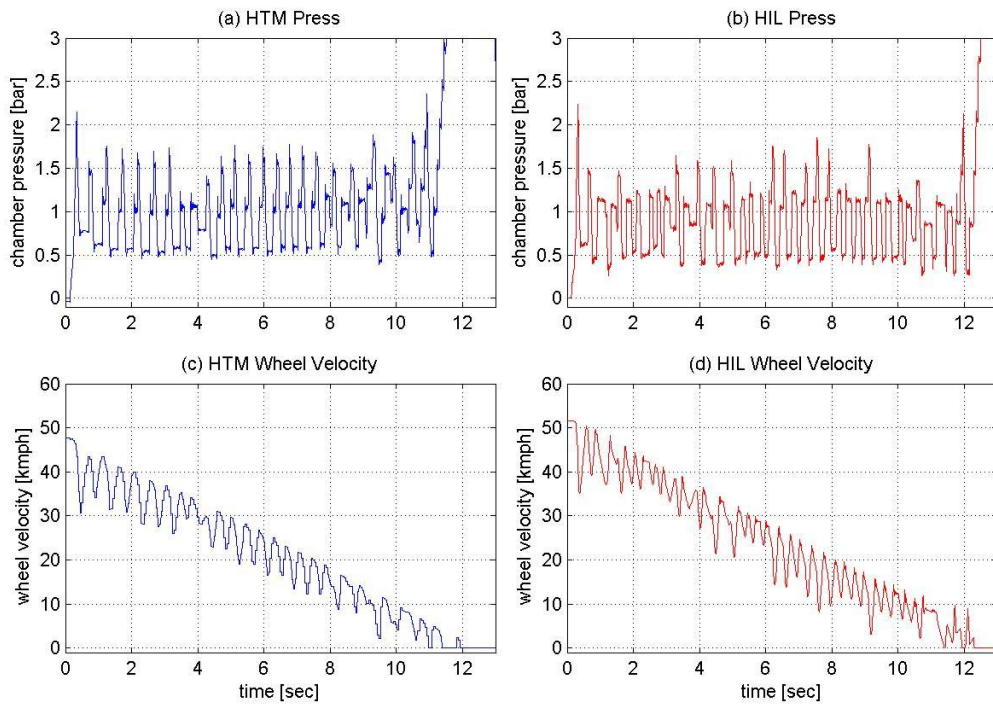


Figure 5.3: HIL Test 1 Front Left Pressure and Wheel Speed

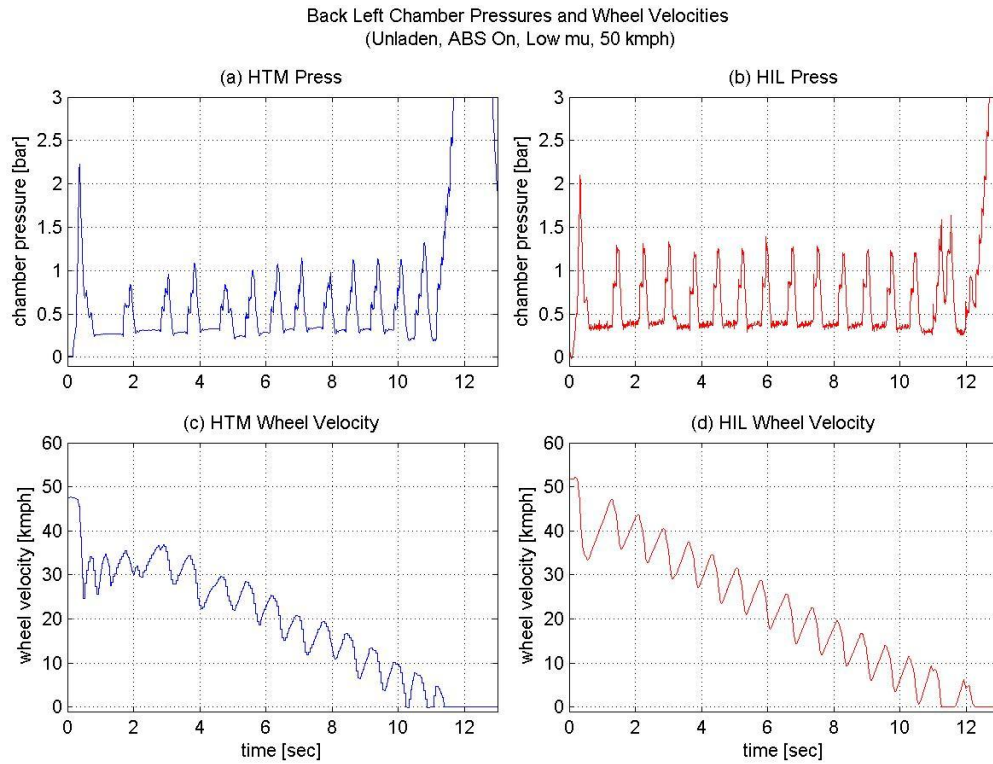


Figure 5.4: HIL Test 1 Back Left Pressure and Wheel Speed

Figure 5.5 illustrates the front left wheel speed (V_{x_FL}), back left wheel speed (V_{x_BL}) and vehicle C.G. speed (V_x) versus time as well as the vehicle C.G. speed versus distance for the HTM tractor and HIL simulator. We can see from subplots a and b along with the numerical data in Table 5.4 that the HTM tractor comes to a complete stop at 11.73 seconds while the HIL simulator stops after 13.03 seconds (a difference of +11.1 percent). Similarly, we can see from subplots c and d that the HTM tractor stops at 88.96 meters while the HIL simulator stops further at 95.02 meters (a difference of +6.8 percent). As previously mentioned, this increased stopping time and distance may be attributed to small differences in road friction, however, the differences are relatively

minimal and we can conclude the simulator effectively emulates the braking performance of the unladen HTM tractor on a homogeneous low μ surface.

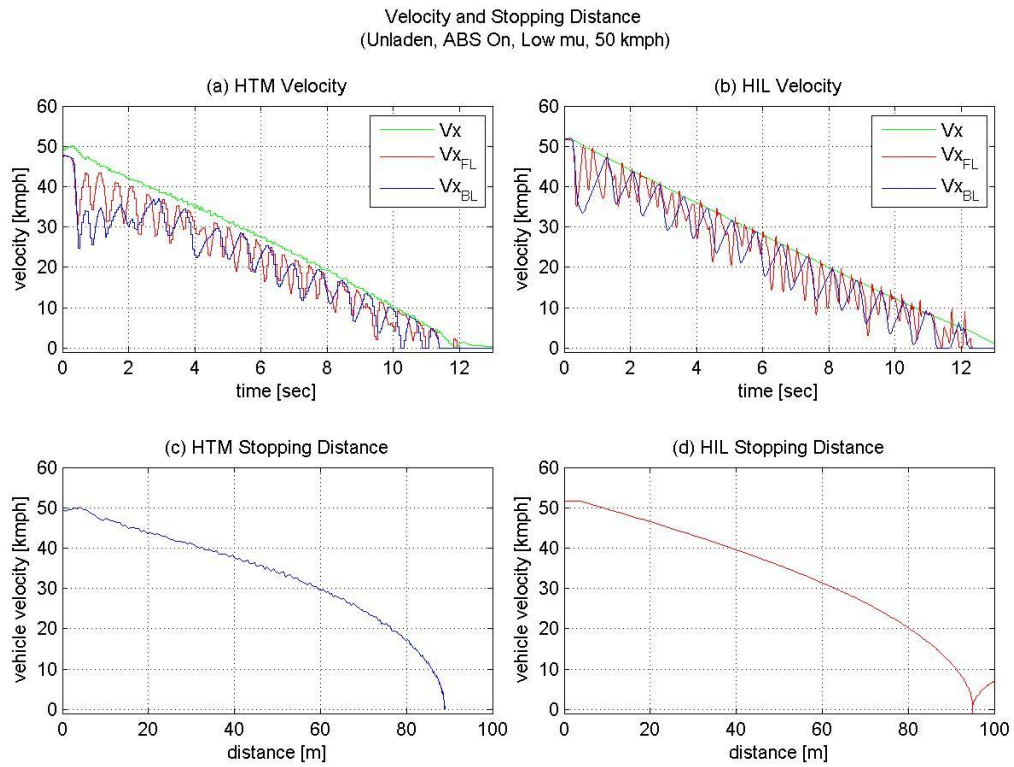


Figure 5.5: HIL Test 1 Stopping Performance

<u>Validation Metrics</u>	<u>HTM</u>		<u>HIL</u>		<u>% Difference</u>	
	Front Left Wheel	Back Left Wheel	Front Left Wheel	Back Left Wheel	Front Left Wheel	Back Left Wheel
ABS Modulation Time	11.04 [sec]	11.01 [sec]	11.98 [sec]	11.94 [sec]	+8.5 [%]	+8.4 [%]
Avg. Pressure	0.96 [bar]	0.48 [bar]	0.87 [bar]	0.57 [bar]	-9.4 [%]	+18.8 [%]
Stopping Time	11.73 [sec]		13.03 [sec]		+11.1 [%]	
Stopping Distance	88.96 [m]		95.02 [m]		+6.8 [%]	

Table 5.4: HIL Test 1 Validation Metrics

TEST 2: UNLADEN TRACTOR on HIGH MU SURFACE

For the second braking test, the road conditions were set to homogeneous high μ (0.91 friction coefficient) and the brakes were applied at 50 kilometers per hour. Figure 5.6 illustrates the front left brake chamber pressures and wheel speeds versus time for this test. We can see from subplots a and b in the figure there are significant differences between the HTM and HIL pressure curves. If we first analyze the HIL pressure curve in subplot b, we can see the pressure rises to around six bar before the first ABS modulation occurs and the pressure is dumped. As modulation of the brake chamber continues, the pressure fluctuates rapidly between plus or minus 1.4 bar from the average (5.37 bar); given in Table 5.5. Now if we refer to subplot a, we notice that the first ABS modulation also occurs around six bar, however, in this case only two large pressure fluctuations occur with an amplitude of around 2.5 bar from the average pressure (5.09 bar). We can see from subplot c that at 1.8 seconds a significant wheel deceleration occurs in conjunction with the second pressure spike of the HTM brake chamber.

Due to the high μ and high adhesion road conditions in this test, the brake chamber pressures and internal forces acting on the brake drum components are much larger than what was experienced in test one. For this reason, it is possible that the brakes on the HTM test vehicle experienced self-energizing effects. These self-energizing effects can result in the brake shoe "self-generating" brake actuation force from the friction produce by the brake lining. This can ultimately lead to the generation of brake torque even with minimal brake chamber pressure. This phenomenon seems to explain the unusual wheel deceleration and pressure drop that occurs between 1.65 seconds and 1.80 seconds in the HTM data. We can see that as the HTM chamber pressure peaks at 1.65 seconds, the wheel speed begins to drop rapidly. In response to this, the ABS ECU dumps the pressure as would be expected, however, what is unusual is that even after four bars of pressure have been released, the wheel continues to decelerate. It isn't until after a five bar pressure drop that the wheel deceleration is finally stabilized and the ECU decides to stop dumping pressure. Self-energizing effects may explain why this behavior occurs in the HTM data and not the HIL data.

From this initial analysis it appears the HTM front brakes behave more erratically than the HIL front brakes under severe high μ braking. While the HIL brake chambers experience rapid and constrained pressure modulation, the HTM brake chambers experience large spaced out pressure fluctuations with one region of significantly large wheel deceleration. After assessing various possible causes for these discrepancies, including road friction, vertical tire loading and dynamic load transfer, it was determined that the most likely cause for inconsistencies in the HIL data arise from the dynamic behavior of the drum brakes on the HTM test vehicle. This dynamic behavior can

potentially consist of brake torque delay and self-energizing effects, as previously mentioned.

Figure 5.7 illustrates the back left brake chamber pressures and wheel speeds versus time. We can see the initial pressure rises for the HTM and HIL data are very similar with the initial ABS modulation occurring around a 0.4 seconds and a pressure just over 2.5 bar. For some reason, after the ABS modulation occurs, the average pressure of the HIL chamber remains greater than that of the HTM chamber with pressures of 1.83 bar and 1.50 bar respectively. We can also see the HIL pressure fluctuates more consistently with a smaller amplitude of oscillation. It was not determined exactly what caused these differences, however, it is assumed they result from some inaccuracies in the brake torque model in which dynamic braking effects have not been properly accounted for. Despite these differences, the back left wheel speeds for the HTM and HIL data seem to behave similarly. As seen in subplots c and d, both wheels come to a stop around 2.25 seconds and upon referring to Table 5.5 we can see the ABS modulation times differ by only -3.6 percent.

Upon comparing figures 5.6 and 5.7, the front brake chambers operate at higher pressures than the rear chambers. This is due to the greater vertical loading on the front axle which allows the front tires to achieve greater longitudinal grip and ultimately handle larger braking forces without locking up. This same loading configuration was also used in test one, however, since that test was conducted on a low μ surface and the chambers were modulated at low pressure, it was difficult to notice significant differences between the front and rear pressure magnitudes.

Front Left Chamber Pressures and Wheel Velocities
(Unladen, ABS On, High μ , 50 kmph)

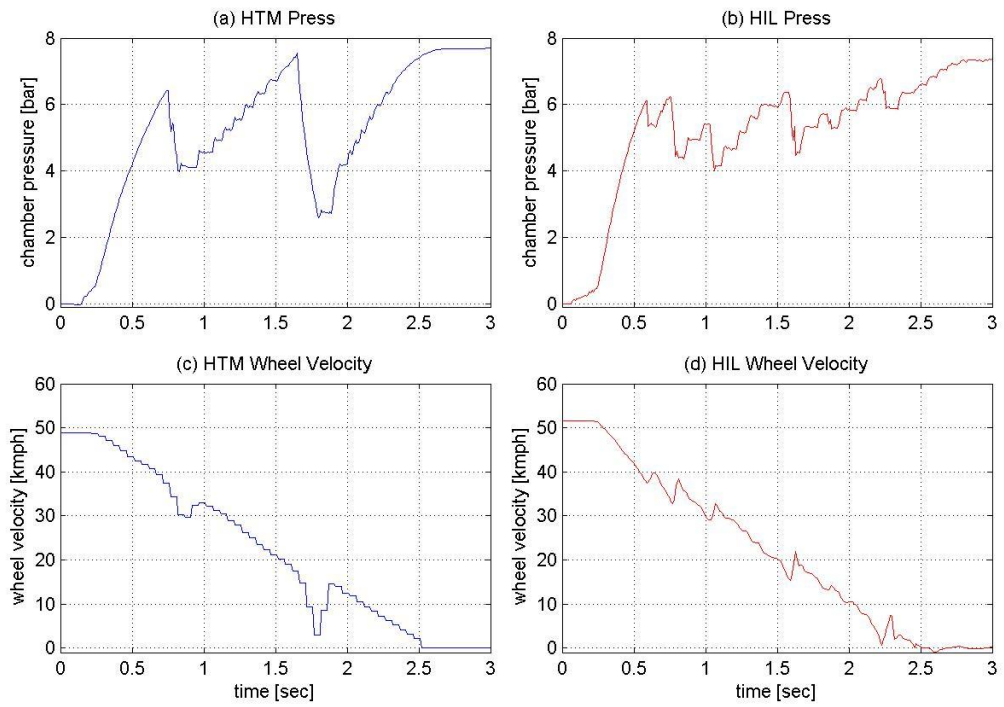


Figure 5.6: HIL Test 2 Front Left Pressure and Wheel Speed

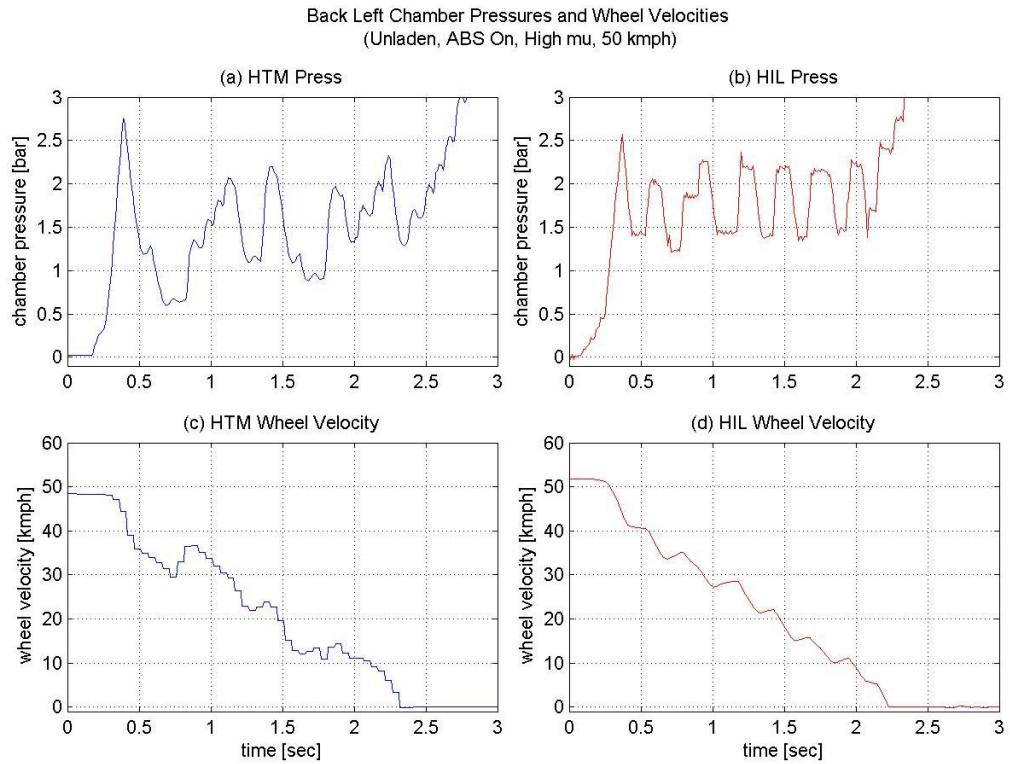


Figure 5.7: HIL Test 2 Back Left Pressure and Wheel Speed

Despite the differences in the front brake chamber pressures and wheel speeds, the HIL simulator was able to accurately emulate the HTM tractor stopping performance. If we refer to Figure 5.8 and Table 5.5, we can see the stopping times match with both tests reaching zero velocity at 2.48 seconds. The stopping distances were close as well with the HTM tractor stopping at 20.65 meters and the simulator stopping at 20.72 meters (a difference of only +0.3 percent).

Velocity and Stopping Distance
(Unladen, ABS On, High mu, 50 kmph)

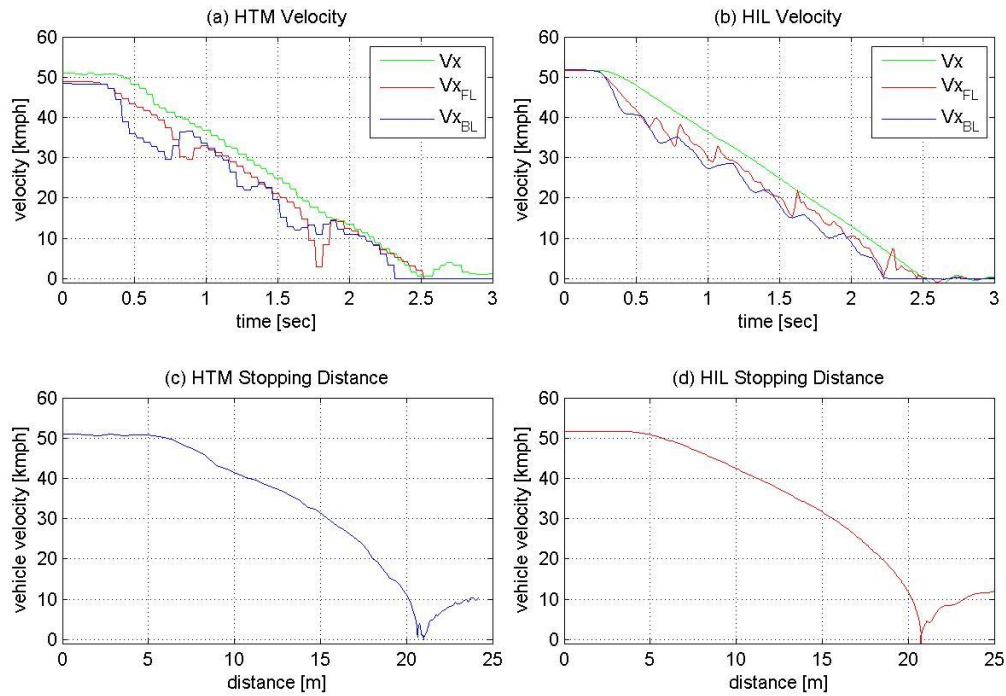


Figure 5.8: HIL Test 2 Stopping Performance

<u>Validation Metrics</u>	<u>HTM</u>		<u>HIL</u>		<u>% Difference</u>	
	Front Left Wheel	Back Left Wheel	Front Left Wheel	Back Left Wheel	Front Left Wheel	Back Left Wheel
ABS Modulation Time	1.77 [sec]	1.93 [sec]	1.93 [sec]	1.86 [sec]	+9.0 [%]	-3.6 [%]
Avg. Pressure	5.09 [bar]	1.50 [bar]	5.37 [bar]	1.83 [bar]	+5.5 [%]	+22.0 [%]
Stopping Time	2.48 [sec]		2.48 [sec]		0.0 [%]	
Stopping Distance	20.65 [m]		20.72 [m]		+0.3 [%]	

Table 5.5: HIL Test 2 Validation Metrics

TEST 3: UNLADEN TRACTOR on JUMP MU SURFACE

For the third braking test, the road conditions were set to jump μ in which a low to high friction transition occurred (0.16 to 0.91 friction coefficient). For this test, the HTM tractor was accelerated to 55 kilometers per hour while on the low μ surface and the brakes were applied. As the vehicle was decelerating, a transition to high μ occurred. The exact distance, also referred to as station, at which the braking and surface transition took place was determined from GPS data supplied by the HTM test engineers. By analyzing this data, the braking procedure could be properly repeated with the HIL simulator.

Figure 5.9 illustrates the front left brake chamber pressures and wheel speeds for this test. As seen in subplots a and b, the chambers are modulated at a low pressure, around one bar, for the first second of the brake procedure. In this region, the road surface is low adhesion and therefore the pressure must be kept low in order to prevent wheel lockup. As the brake procedure continues, the chamber pressures rise to a level of around five bar. This increase in pressure represents the road surface transition point from low μ to high μ . On the high μ surface, the ABS modulators allow more pressure to enter the chambers since the wheels can handle more braking force without lockup occurring. We can also see from subplots c and d that the ABS ECU has greater difficulty preventing large wheel decelerations on the low μ surface than on the high μ surface. This behavior is characterized by the two large drops in wheel speed that occur between zero and one seconds in the HTM and HIL data.

In Figure 5.10 the back left chamber pressures and wheel speeds are given. When comparing these chamber pressures to those in Figure 5.9, we can see the overall

behavior is fairly similar. Initially there is a region of low chamber pressure, this signifies low μ braking, and then there is a region of high pressure, this signifies high μ braking. The main differences between the front and rear chambers are that the pressure magnitudes are larger in the front due to the greater vertical loading. Another difference between the figures is that the rear chamber pressures begin to rise at around 1.5 seconds while the front chambers rise at around one second. This difference is due to the fact that the rear tires don't cross the friction transition point until around 0.5 seconds after the front tires. As a result, the ABS ECU keeps the rear chambers at a lower pressure for a slightly longer time period.

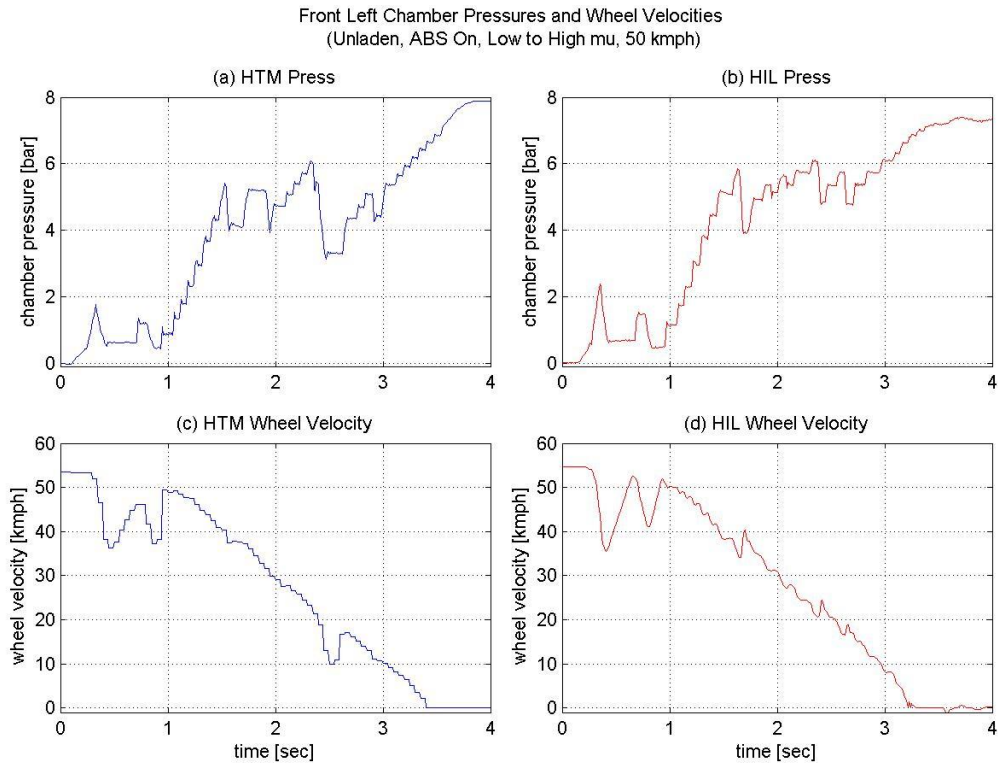


Figure 5.9: HIL Test 3 Front Left Pressure and Wheel Speed

Back Left Chamber Pressures and Wheel Velocities
(Unladen, ABS On, Low to High μ , 50 kmph)

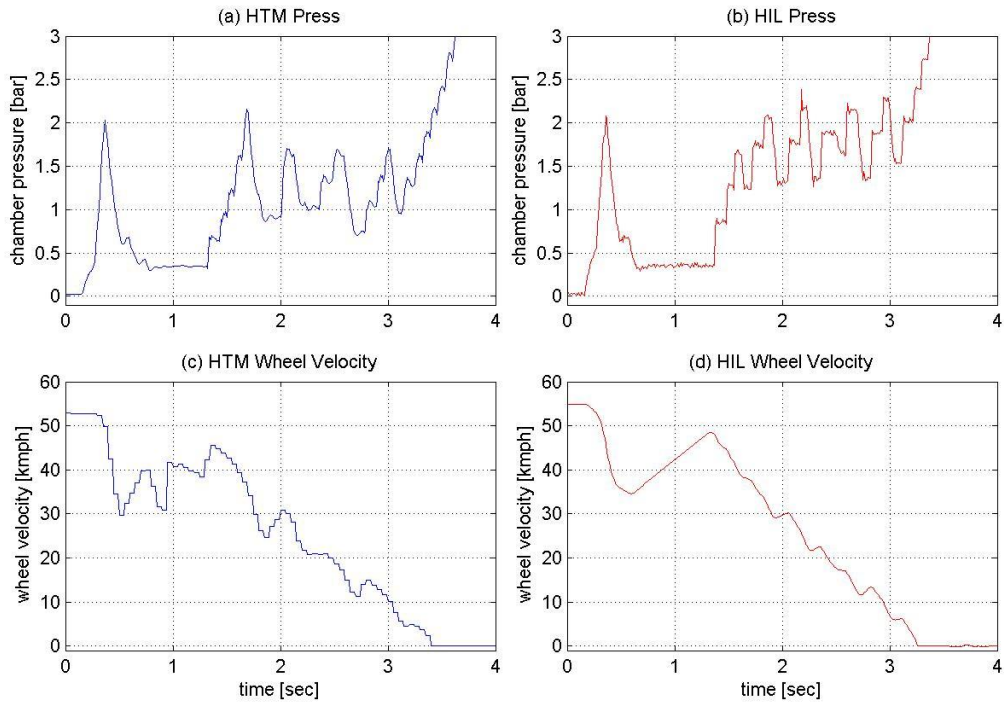


Figure 5.10: HIL Test 3 Back Left Pressure and Wheel Speed

Upon referring to Figure 5.11 and Table 5.6, we can see the HIL simulator was able to accurately emulate the vehicle speed versus time and vehicle speed versus stopping distance. The stopping times for the HTM and HIL data were 3.44 seconds and 3.42 seconds respectively (a difference of only -0.6 percent). The stopping distances were 35.04 meters and 34.61 meters (a difference of -1.2 percent).

Velocity and Stopping Distance
(Unladen, ABS On, Low to High μ , 50 kmph)

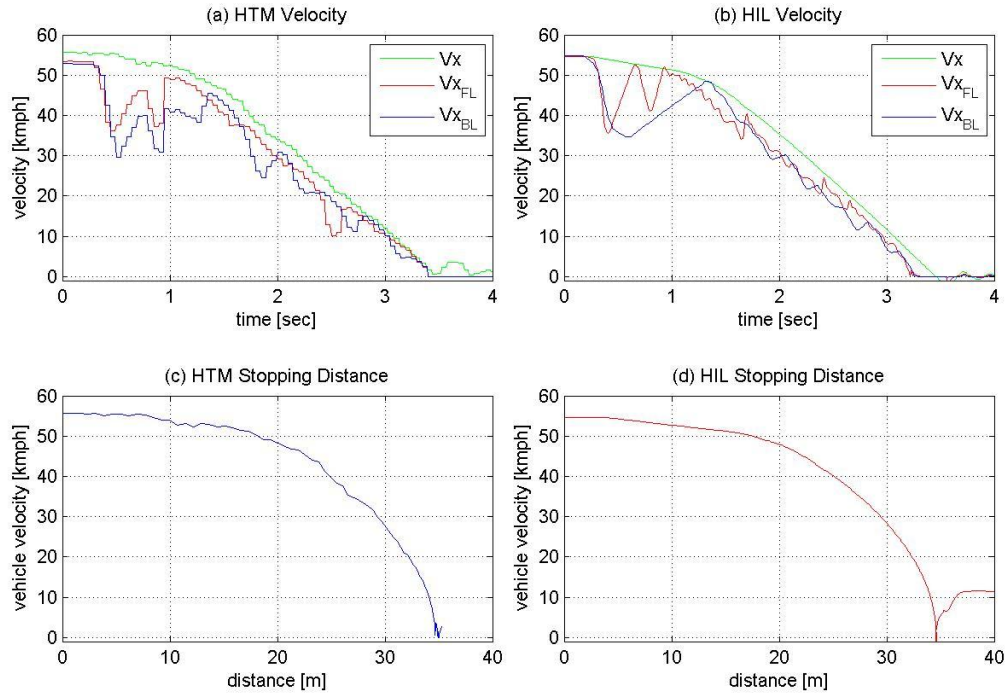


Figure 5.11 HIL Test 3 Stopping Performance

<u>Validation Metrics</u>	<u>HTM</u>		<u>HIL</u>		<u>% Difference</u>	
	Front Left Wheel	Back Left Wheel	Front Left Wheel	Back Left Wheel	Front Left Wheel	Back Left Wheel
ABS Modulation Time	3.05 [sec]	3.03 [sec]	2.89 [sec]	2.90 [sec]	-5.2 [%]	-4.3 [%]
Avg. Pressure	4.73 [bar]	1.20 [bar]	5.48 [bar]	1.78 [bar]	+15.9 [%]	+48.3 [%]
Stopping Time	3.44 [sec]		3.42 [sec]		-0.6 [%]	
Stopping Distance	35.04 [m]		34.61 [m]		-1.2 [%]	

Table 5.6: HIL Test 3 Validation Metrics

TEST 4: UNLADEN TRACTOR on SPLIT MU SURFACE

For the fourth braking test, the road conditions were set to split μ with the left half of the test road being low μ (0.16 coefficient of friction) and the right half being high μ (0.91 coefficient of friction). For this test the vehicle was accelerated to 50 kilometers per hour and the brakes were applied.

Upon referring to Figure 5.12, we can see the chamber pressure and wheel speed data for the HTM and HIL tests are very similar. The HTM chambers have an average pressure of 0.86 bar while the HIL chambers have an average pressure of 0.90 bar (a difference of only +4.7 percent). The ABS modulation times are very close as well with the HTM chambers taking 4.60 seconds to bring the front left wheel to a stop and the HIL chambers taking 4.82 seconds (a difference of +5.8 percent).

In Figure 5.13 the rear chamber pressures and wheel speeds are given. The HIL data in this figure is very comparable to the HTM data, however, again the average HIL rear chamber pressure is larger; in this case by +28.6 percent. If we compare this figure to Figure 5.12, we can see the frequency of pressure oscillation and wheel speed oscillation is significantly faster for the front wheels than for the rear. This behavior is also apparent in test one and is most likely due to the greater rotational inertia of the rear wheels caused by the mass of the drive train. In addition to this, the rear tires do not generate as much longitudinal force as the front tires since they have a smaller vertical loading. This large rotational inertia combined with low longitudinal force generation means the rear wheels cannot accelerate or decelerate as fast as the front wheels when subjected to ABS braking. This may explain the difference in the pressure and wheel velocity fluctuation frequency.

Front Left Chamber Pressures and Wheel Velocities
(Unladen, ABS On, Left-Low Right-High μ , 50 kmph)

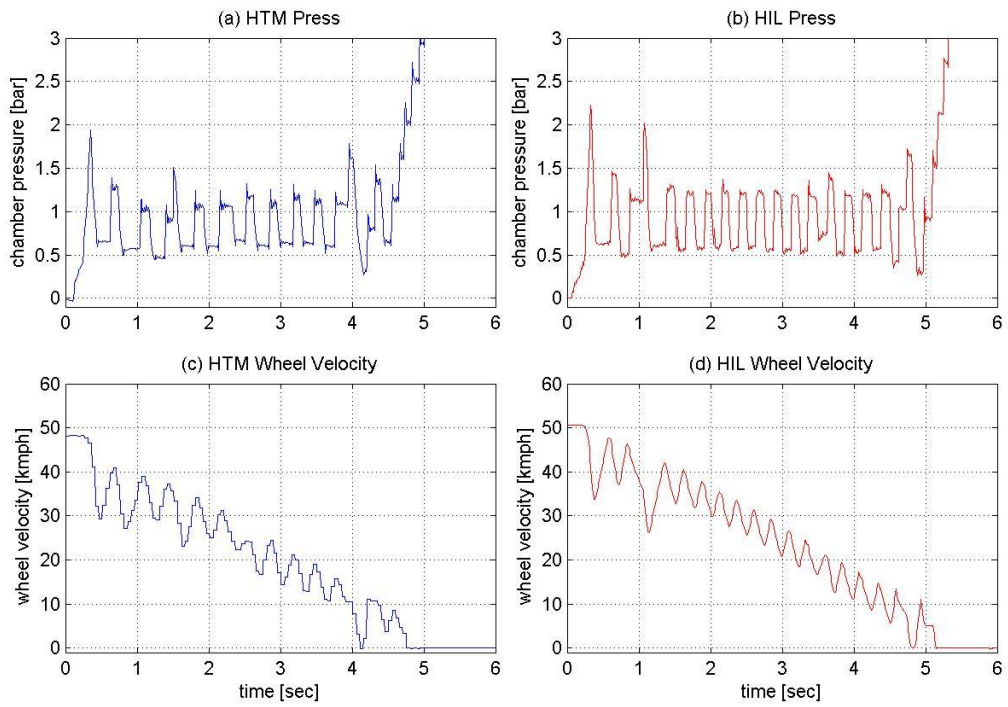


Figure 5.12: HIL Test 4 Front Left Pressure and Wheel Speed

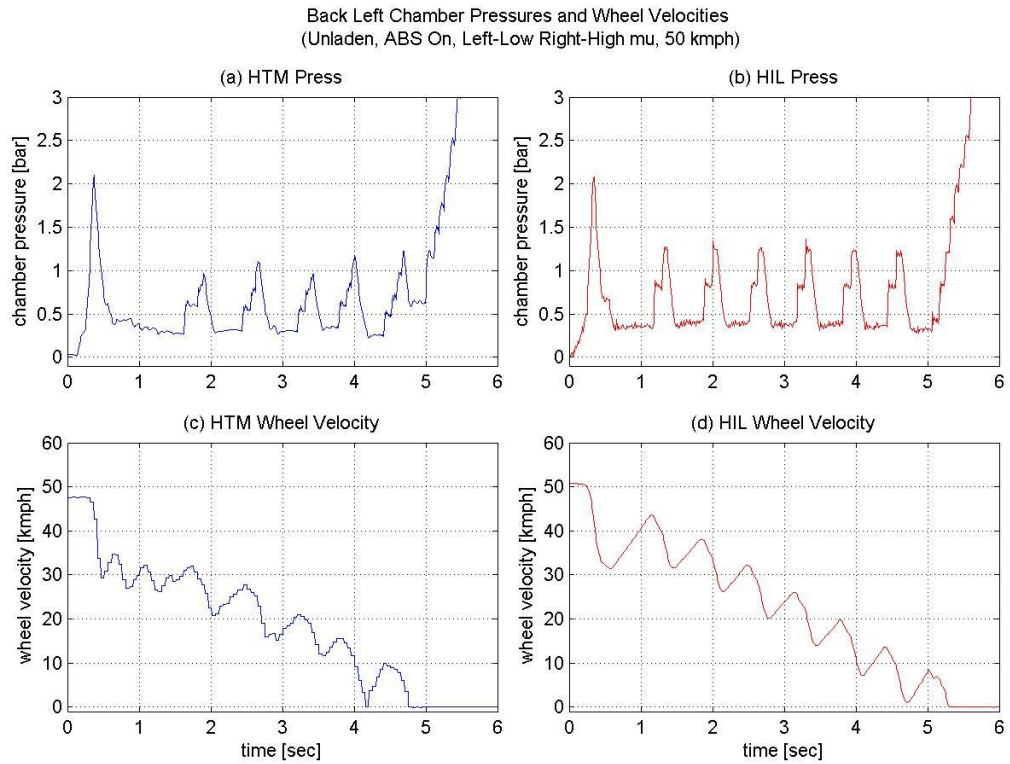


Figure 5.13: HIL Test 4 Back Left Pressure and Wheel Speed

The overall stopping times and distances for this test are given in Figure 5.14 and Table 5.7. For this test, the stopping times for the HTM tractor and simulator were 5.21 seconds and 5.63 seconds respectively (a difference of +8.1 percent). If we compare these stopping times to those given in test one (11.73 and 13.03 seconds respectively) and test two (2.48 seconds and 2.48 seconds respectively) we can notice they fall roughly in between the two sets. This is due to the fact that the split μ surface consists of one half low μ and one half high. Therefore, the surface conditions for this test are effectively a combination of those used in tests one and two so the stopping ability of the vehicle falls in between.

Velocity and Stopping Distance
(Unladen, ABS On, Left-Low Right-High mu, 50 kmph)

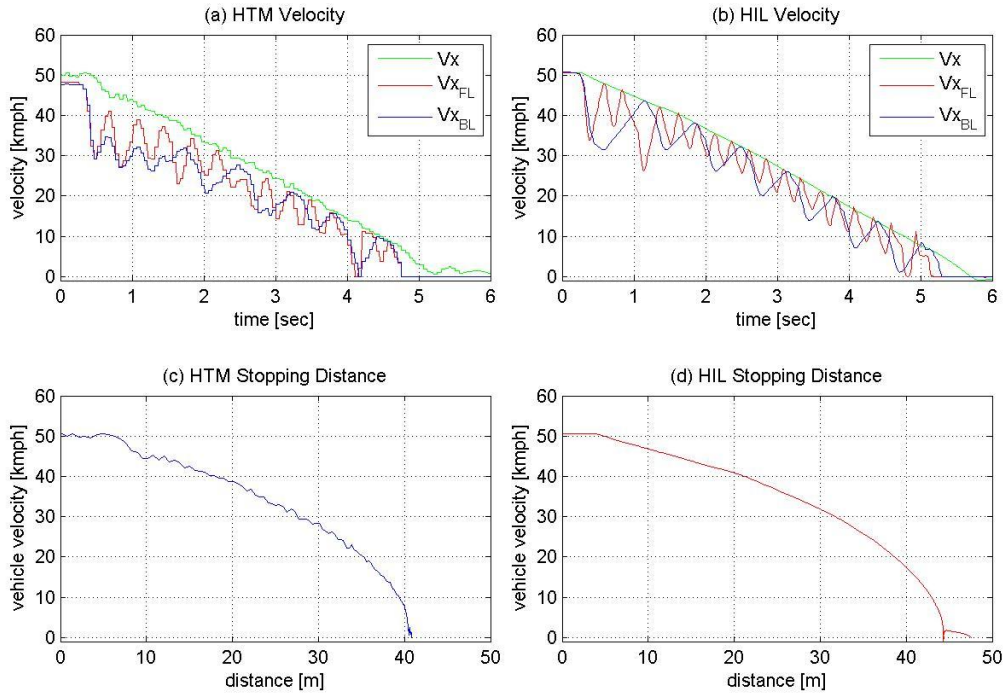


Figure 5.14: HIL Test 4 Stopping Performance

<u>Validation Metrics</u>	<u>HTM</u>		<u>HIL</u>		<u>% Difference</u>	
	Front Left Wheel	Back Left Wheel	Front Left Wheel	Back Left Wheel	Front Left Wheel	Back Left Wheel
ABS Modulation Time	4.60 [sec]	4.39 [sec]	4.82 [sec]	4.95 [sec]	+5.8 [%]	+12.8 [%]
Avg. Pressure	0.86 [bar]	0.49 [bar]	0.90 [bar]	0.63 [bar]	+4.7 [%]	+28.6 [%]
Stopping Time	5.21 [sec]		5.63 [sec]		+8.1 [%]	
Stopping Distance	40.82 [m]		44.35 [m]		+8.6 [%]	

Table 5.7: HIL Test 4 Validation Metrics

TEST 5: LADEN TRACTOR on LOW MU SURFACE

For the fifth test, the same braking procedure from test one was followed, however, this time a 9,428 kilogram load was added to the tractor. In addition to this, the HTM test engineers remeasured the road surface friction using the process explained in Section 4.4.2. This was done in order to account for any changes that occurred with the road conditions since the initial measurements for tests one through four were taken. The resulting friction coefficient for this test was 0.13.

Figure 5.15 illustrates pressure versus time for the front left brake chamber and wheel speed versus time for the front left wheel of the HTM tractor and HIL simulator. As seen in the figure, the test vehicle and the simulator both experience an initial pressure dump at nearly the same instance (0.32 seconds and 0.33 seconds respectively). The average brake chamber pressures are very close as well at 0.76 bar and 0.83 bar respectively (a difference of only +9.2 percent); refer to Table 5.8.

Figure 5.16 illustrates pressure versus time for the back left brake chamber and wheel speed versus time for the back left wheel of the HTM tractor and HIL simulator. From this figure we can see the test vehicle and the simulator both experience an initial pressure dump at nearly the same instance (0.37 seconds and 0.35 seconds respectively). In addition to this, the average back left brake chamber pressures differ by only +8.3 percent. This is an improvement when compared to the +18.8 percent pressure difference calculated in test one.

Front Left Chamber Pressures and Wheel Velocities
(Laden, ABS On, Low μ , 50 kmph)

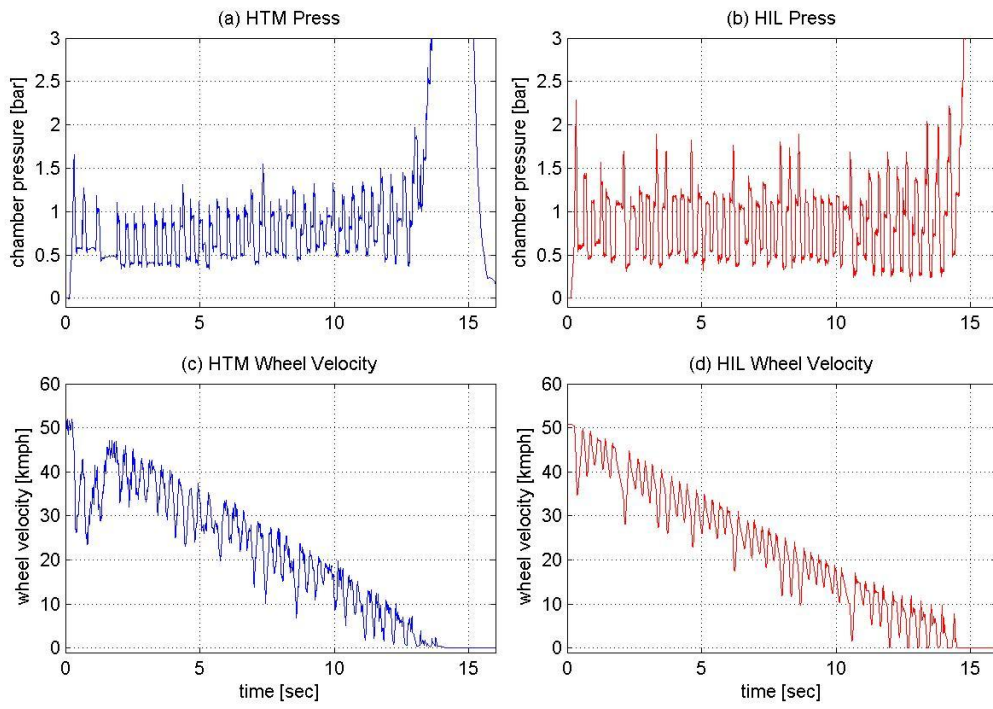


Figure 5.15: HIL Test 5 Front Left Pressure and Wheel Speed

Back Left Chamber Pressures and Wheel Velocities
(Laden, ABS On, Low μ , 50 kmph)

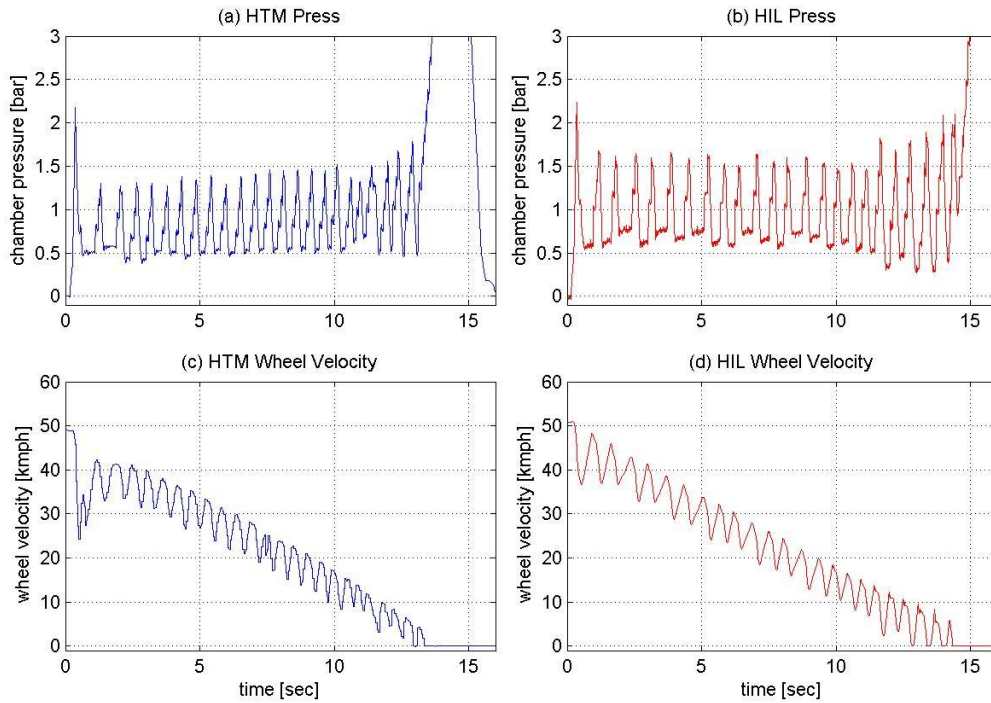


Figure 5.16: HIL Test 5 Back Left Pressure and Wheel Speed

The overall stopping times and distances for this test are given in Figure 5.17 and Table 5.8. For this test, the stopping times for the HTM tractor and simulator were 13.69 seconds and 15.37 seconds respectively (a difference of +12.3 percent). If we compare these stopping times to those given in test one (11.73 and 13.03 seconds respectively) we can notice they are slightly larger. This is due to the decrease in road friction from 0.16 to 0.13. For this same reason, the stopping distances for this test were larger as well at 109.30 meters for the HTM tractor and 110.20 meters for the simulator compared to 88.96 meters and 95.02 meters for test one.

Velocity and Stopping Distance
(Laden, ABS On, Low mu, 50 kmph)

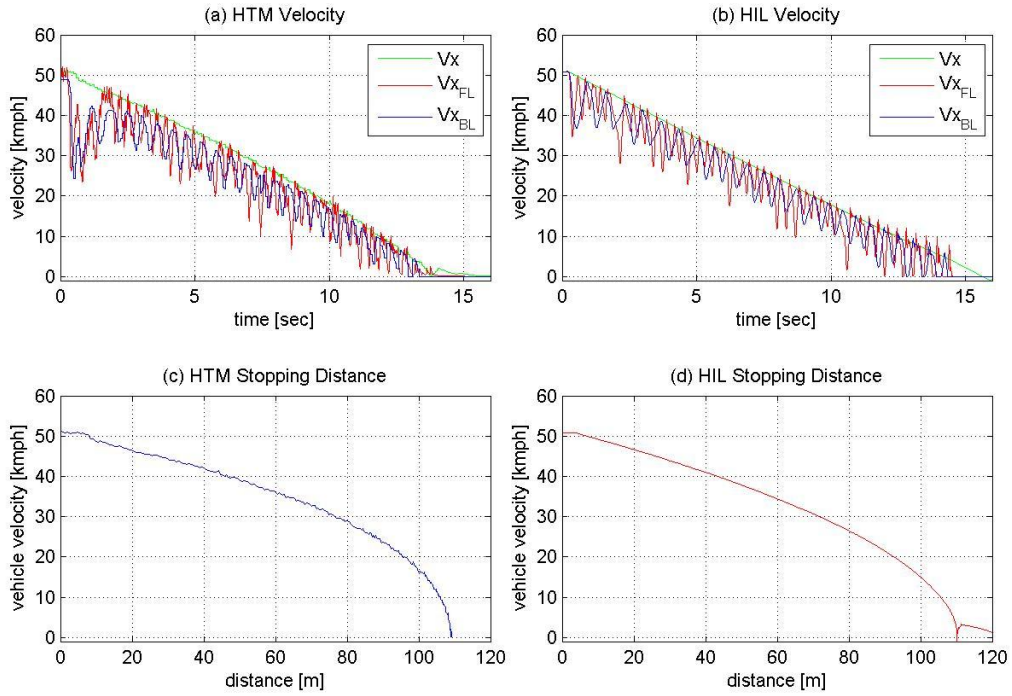


Figure 5.17: HIL Test 5 Stopping Performance

<u>Validation Metrics</u>	<u>HTM</u>		<u>HIL</u>		<u>% Difference</u>	
	Front Left Wheel	Back Left Wheel	Front Left Wheel	Back Left Wheel	Front Left Wheel	Back Left Wheel
ABS Modulation Time	13.63 [sec]	12.98 [sec]	14.11 [sec]	13.99 [sec]	+3.5 [%]	+7.8 [%]
Avg. Pressure	0.76 [bar]	0.84 [bar]	0.83 [bar]	0.91 [bar]	+9.2 [%]	+8.3 [%]
Stopping Time	13.69 [sec]		15.37 [sec]		+12.3 [%]	
Stopping Distance	109.30 [m]		110.20 [m]		+0.8 [%]	

Table 5.8: HIL Test 5 Validation Metrics

TEST 6: LADEN TRACTOR on HIGH MU SURFACE

For the sixth braking test, the laden tractor was placed on a homogeneous high μ surface and the road friction was again measured by the HTM test engineers. In this case, the friction coefficient was only 0.75; a significant drop from the high μ value of 0.91 for the unladen tractor in test two. Most likely, this was caused by precipitation on the test track or some other effects from changing weather conditions.

Figure 5.18 illustrates the front left brake chamber pressures and wheel speeds for this test. Upon referring to subplots a and b, we can see there are significant differences between the HTM and HIL pressure curves. For example, in subplot a, the HTM tractor experiences one large pressure dump which occurs between 0.80 and 0.95 seconds. After this dump command, the modulator proceeds to build pressure in the chamber until eventually the wheel comes to a stop at three seconds. On the other hand, in subplot b, the simulator experiences several pressure modulation cycles between 0.57 and two seconds and the wheel comes to a stop earlier at 2.5 seconds. If we now refer to subplots a and b in Figure 5.20 we can see for the majority of the braking maneuver, the test vehicle has a lower slip ratio magnitude than the simulator.

Essentially, the HTM front left brake is able to sufficiently decelerate the wheel at the beginning of the maneuver causing the modulator to dump the pressure (occurs between 0.80 and 0.95 seconds), however, after this period the brakes are no longer capable of producing sufficient brake torque to decelerate the wheel. This is why the front left wheel velocity, given in subplot c, decreases steadily in a linear fashion even when the chamber pressure rises to eight bar. After much deliberation, it was determined

that these differences in pressure modulation and slip ratio may be attributed to discrepancies in the simulation brake torque model.

Another observation to make in Figure 5.18 subplot a is that a severe wheel deceleration occurs between 0.80 and 0.95 seconds even after a large amount of chamber pressure is dumped by the ABS modulator. This type of deceleration was also observed in the HTM data for test two and was determined to be the result of self-energizing effects within the drum brakes. If we now refer to Figure 5.19, the pressure versus time and wheel velocity versus time for the rear wheels is given. From this figure we can see the pressure fluctuations and wheel velocities for the two tests agree more so than those in Figure 5.18.

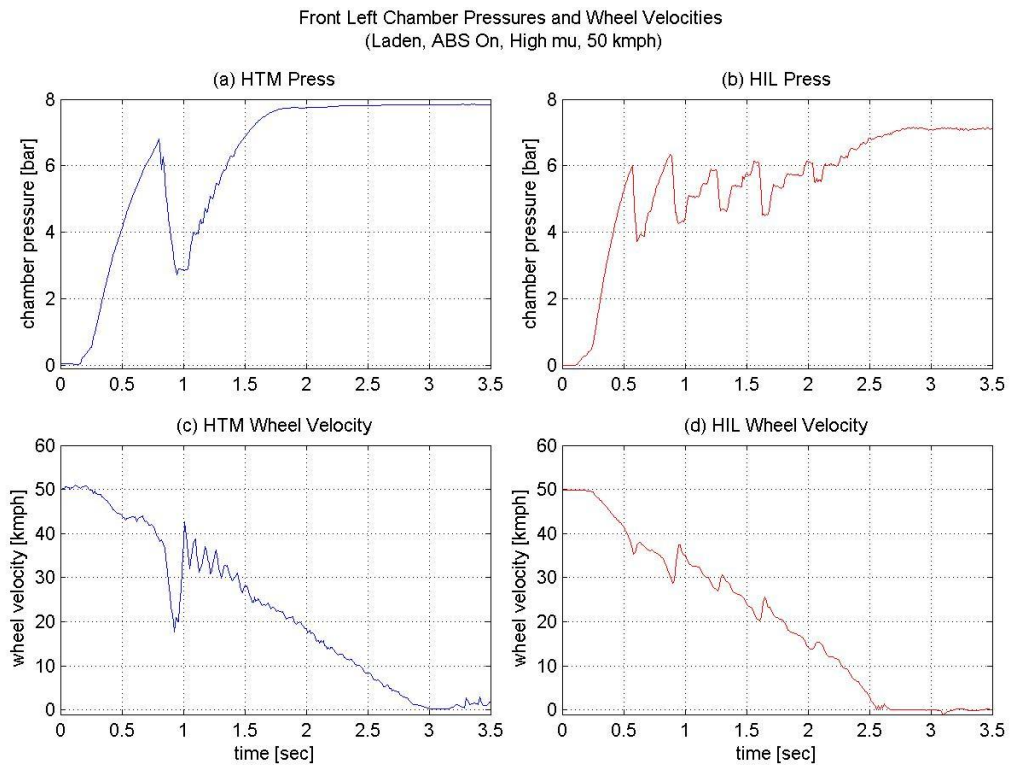


Figure 5.18: HIL Test 6 Front Left Pressure and Wheel Speed

Back Left Chamber Pressures and Wheel Velocities
(Laden, ABS On, High μ , 50 kmph)

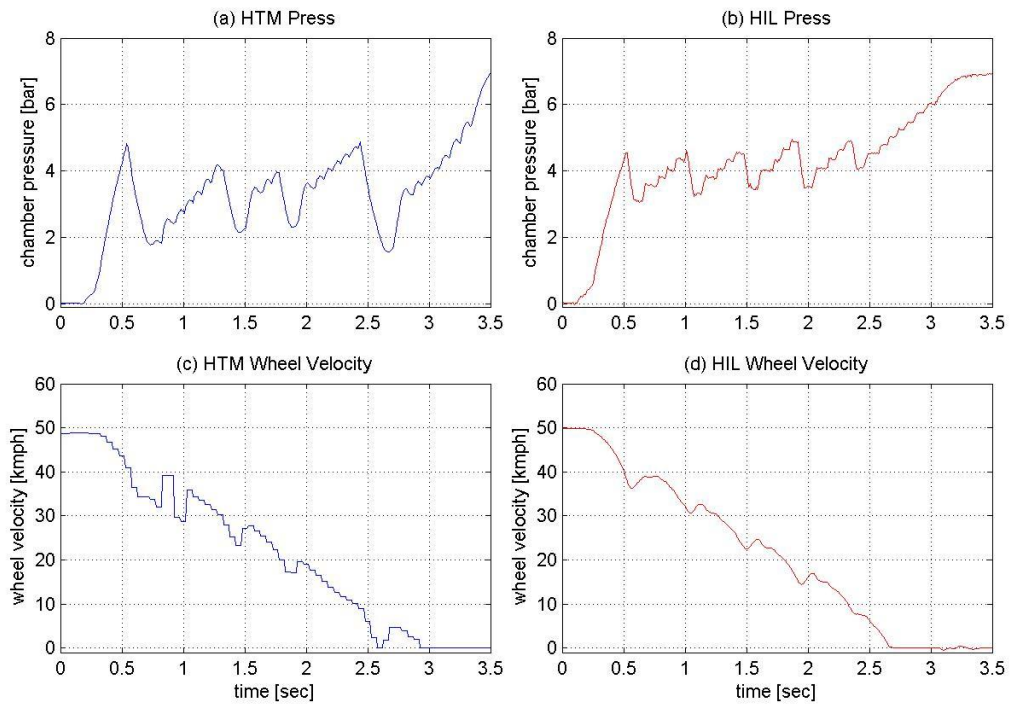


Figure 5.19: HIL Test 6 Back Left Pressure and Wheel Speed

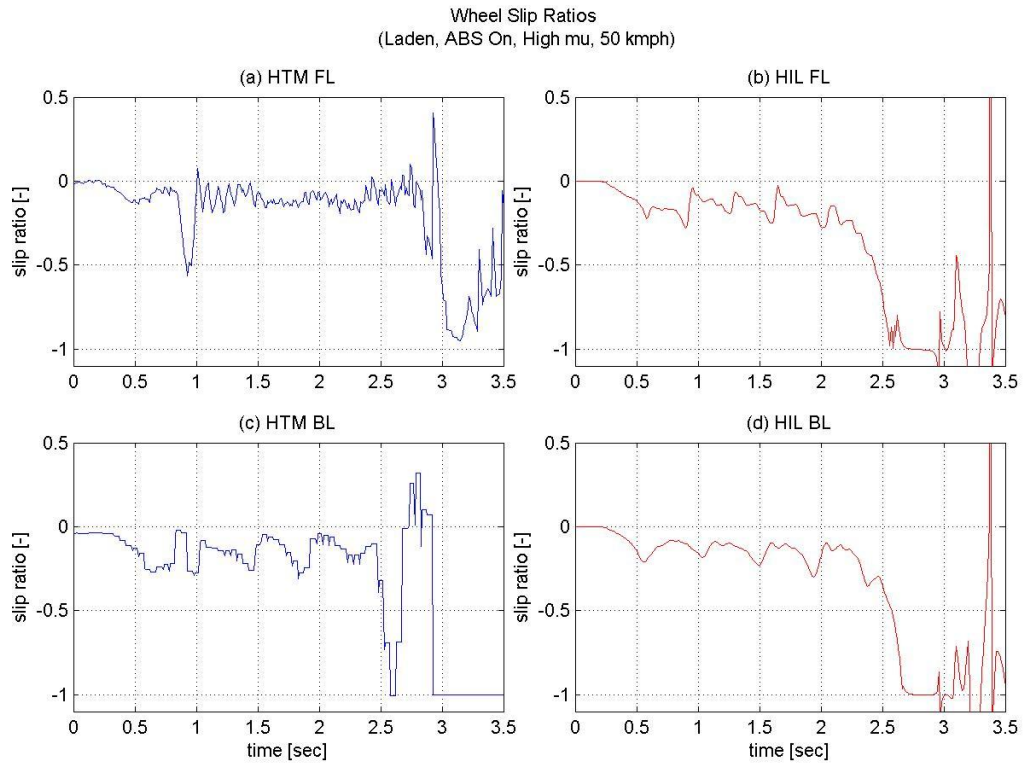


Figure 5.20: HIL Test 6 Wheel Slip Ratio

Despite the discrepancies with the front left chamber pressures and wheel speeds, the overall stopping performances for the test vehicle and simulator, given in Figure 5.21 and Table 5.9, agree closely. The stopping times for the HTM tractor and simulator were 2.93 seconds and 2.92 seconds respectively (a difference of -0.3 percent). The stopping distances were 24.31 meters and 23.47 meters respectively (a difference of only -3.5 percent).

Velocity and Stopping Distance
(Laden, ABS On, High mu, 50 kmph)

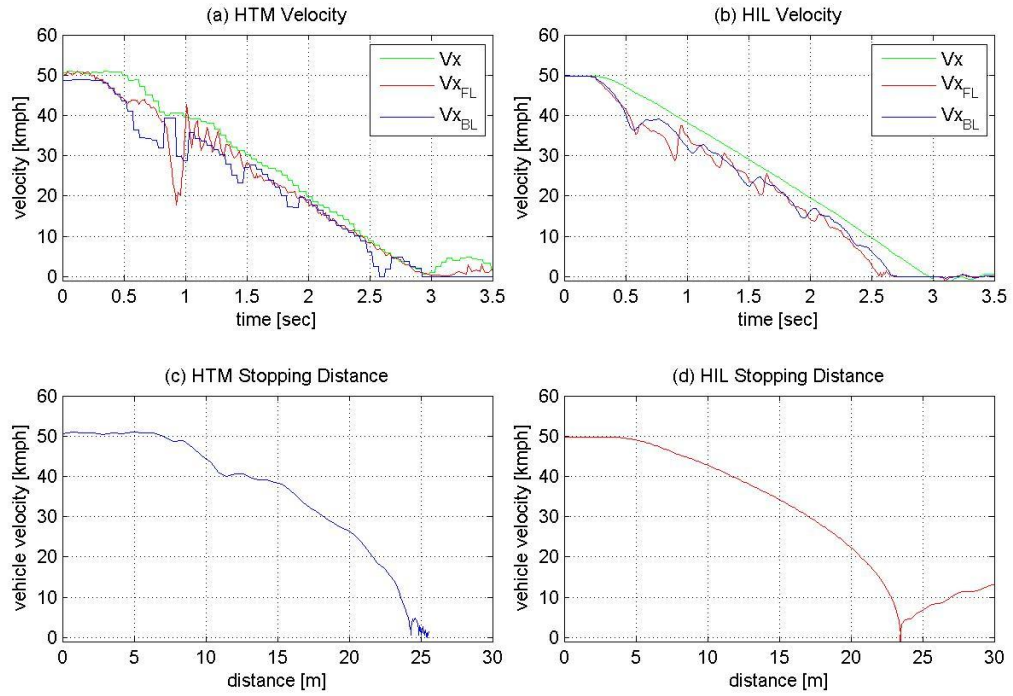


Figure 5.21: HIL Test 6 Stopping Performance

Validation Metrics	HTM		HIL		% Difference	
	Front Left Wheel	Back Left Wheel	Front Left Wheel	Back Left Wheel	Front Left Wheel	Back Left Wheel
ABS Modulation Time	2.20 [sec]	2.39 [sec]	2.01 [sec]	2.13 [sec]	-8.6 [%]	-10.9 [%]
Avg. Pressure	6.72 [bar]	3.47 [bar]	5.59 [bar]	4.15 [bar]	-16.8 [%]	+19.6 [%]
Stopping Time	2.93 [sec]		2.92 [sec]		-0.3 [%]	
Stopping Distance	24.31 [m]		23.47 [m]		-3.5 [%]	

Table 5.9: HIL Test 6 Validation Metrics

TEST 7: LADEN TRACTOR on JUMP MU SURFACE

For the seventh braking test, the laden tractor underwent a jump μ braking procedure just as in test three. The updated friction values from tests five and six were used for the low and high μ surfaces (0.13 and 0.75 respectively). Figure 5.22 illustrates the front left brake chamber pressures and wheel speeds for this test. Upon referring to subplots a and b, we can see there are significant differences between the HTM and HIL pressure curves just as in the previous test.

For the first second after braking begins, both pressure curves behave similarly and each chamber experiences two to three modulations; this is the region in which the front wheels are on the low μ surface. As the maneuver proceeds and the transition to high μ occurs, the HIL simulation pressure rises to around five bar and several modulations occur about this level. On the other hand, the chamber pressure for the HTM tractor rises all the way to eight bar and even at this high pressure, only one significant pressure modulation occurs. We can also see from subplot c that the wheel velocity for the HTM tractor decreases steadily and in a linear fashion when compared to the HIL wheel velocity in subplot d. Finally, if we refer to the front wheel slip ratios plotted in subplots a and b of Figure 5.24, it is apparent that the test vehicle does not experience as much slip as the simulator. The HTM wheel slip tends towards zero starting around 2.5 seconds, on the other hand, the HIL wheel slip consistently fluctuates throughout the brake maneuver. If we now refer to Figure 5.23, the pressure versus time and wheel velocity versus time for the rear wheels is given. From this figure we can see the pressure fluctuations and wheel velocities for this test agree more so than those in Figure 5.22.

Front Left Chamber Pressures and Wheel Velocities
(Laden, ABS On, Low to High μ , 50 kmph)

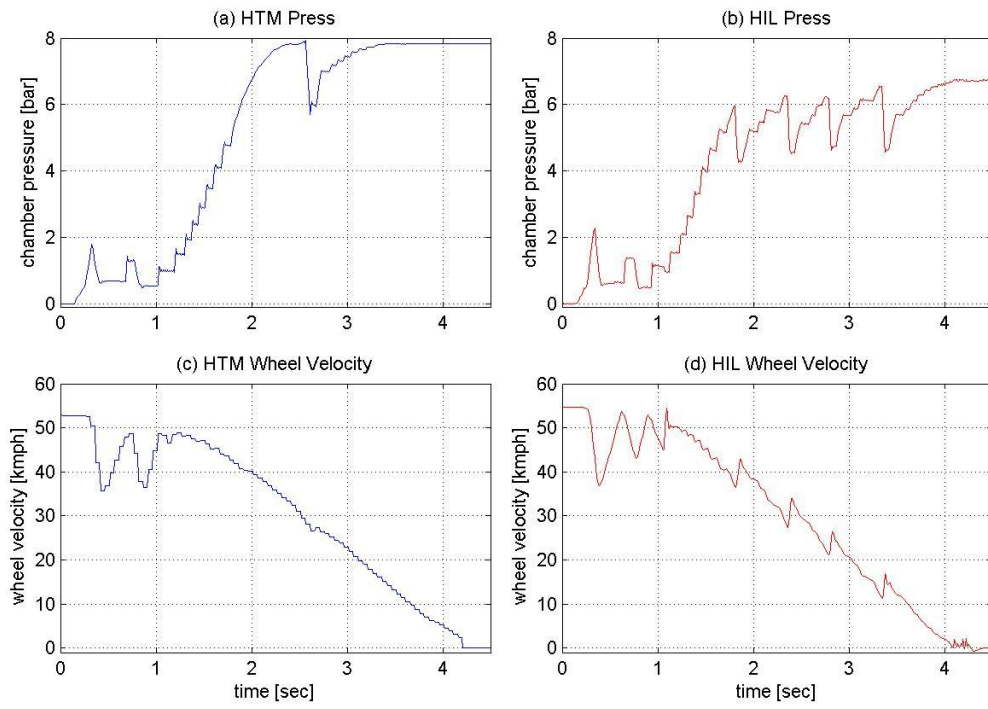


Figure 5.22: HIL Test 7 Front Left Pressure and Wheel Speed

Back Left Chamber Pressures and Wheel Velocities
(Laden, ABS On, Low to High μ , 50 kmph)

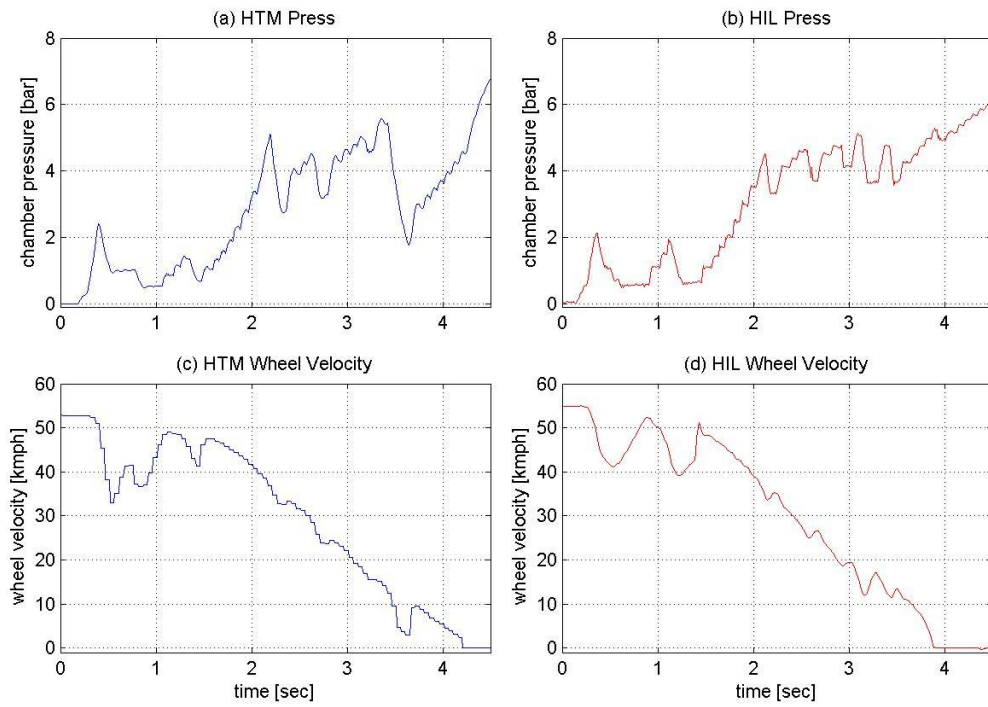


Figure 5.23: HIL Test 7 Back Left Pressure and Wheel Speed

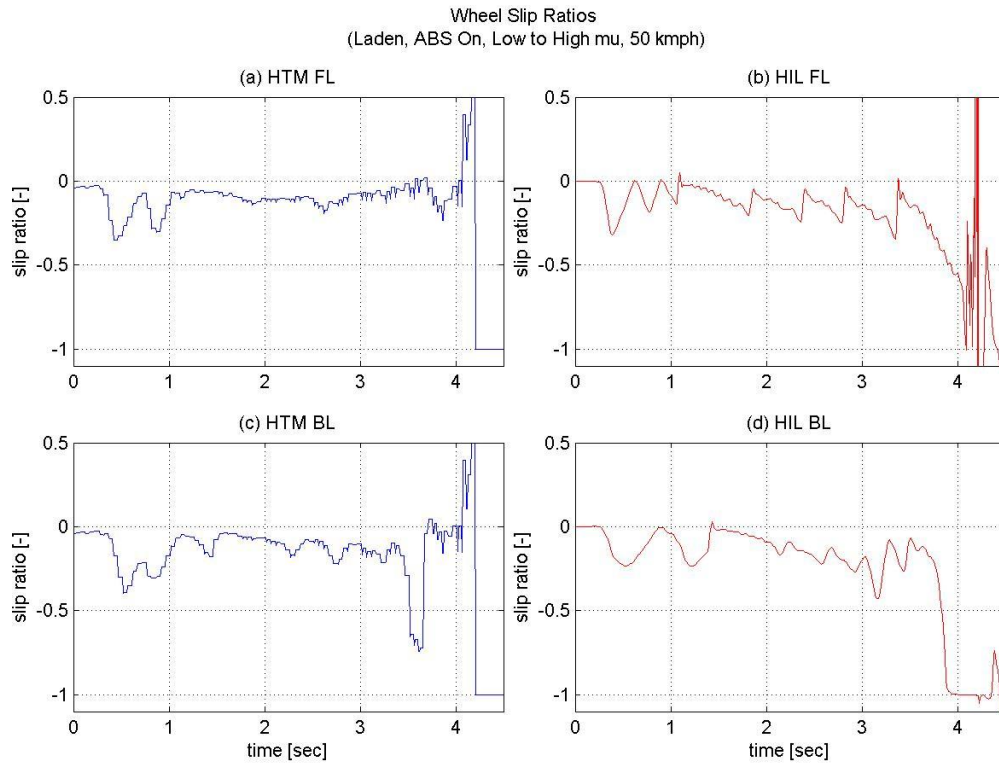


Figure 5.24: HIL Test 7 Wheel Slip Ratio

Overall, the stopping performances for the test vehicle and simulator, given in Figure 5.25 and Table 5.10, agree closely. The stopping times for the HTM tractor and simulator were 4.22 seconds and 4.18 seconds respectively (a difference of -0.9 percent). The stopping distances were 42.93 meters and 41.99 meters respectively (a difference of -2.2 percent).

Velocity and Stopping Distance
(Laden, ABS On, Low to High μ , 50 kmph)

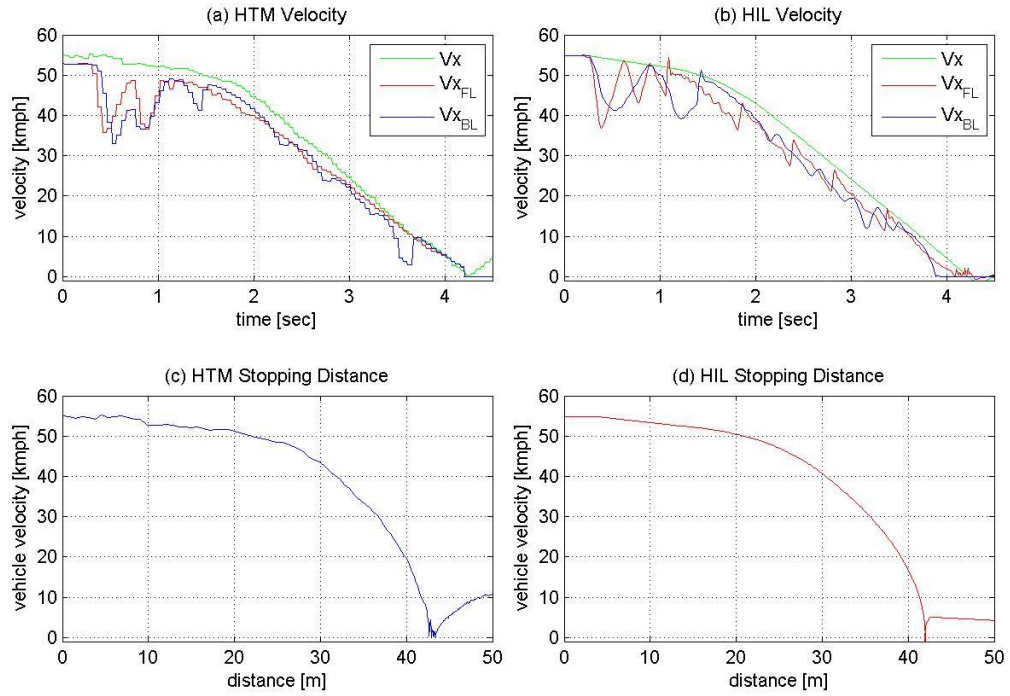


Figure 5.25: HIL Test 7 Stopping Performance

Validation Metrics	HTM		HIL		% Difference	
	Front Left Wheel	Back Left Wheel	Front Left Wheel	Back Left Wheel	Front Left Wheel	Back Left Wheel
ABS Modulation Time	3.88 [sec]	3.81 [sec]	3.79 [sec]	3.53 [sec]	-2.3 [%]	-7.3 [%]
Avg. Pressure	7.49 [bar]	4.04 [bar]	5.68 [bar]	4.22 [bar]	-24.2 [%]	+4.5 [%]
Stopping Time	4.22 [sec]		4.18 [sec]		-0.9 [%]	
Stopping Distance	42.93 [m]		41.99 [m]		-2.2 [%]	

Table 5.10: HIL Test 7 Validation Metrics

TEST 8: LADEN TRACTOR on SPLIT MU SURFACE

For the eighth braking test, the road conditions were set to split μ with the left half of the test road being low μ (0.13 coefficient of friction) and the right half being high μ (0.75 coefficient of friction). For this test the vehicle was accelerated to 50 kilometers per hour and the brakes were applied.

In Figure 5.26 and Table 5.11, the front left chamber pressures and wheel velocities for the HTM and HIL tests are given. From the figure we can see these brakes behave similarly with the average chamber pressures being 1.02 bar and 0.68 bar respectively (a difference of -33.3 percent) and the ABS modulation times being 5.04 seconds and 5.27 seconds respectively (a difference of +4.6 percent). In Figure 5.27, the rear chamber pressures and wheel velocities are given. These brakes also behave similarly with the average chamber pressures being 0.99 bar and 0.95 bar respectively (a difference of only -4.0 percent) and the ABS modulation times being 4.71 seconds and 5.07 seconds respectively (a difference of +7.6 percent). If we refer to Figure 5.28, we can see the overall results for this test were fairly good with the stopping times and distances differing by +7.3 percent and +10.3 percent respectively.

Front Left Chamber Pressures and Wheel Velocities
(Laden, ABS On, Left-Low Right-High μ , 50 kmph)

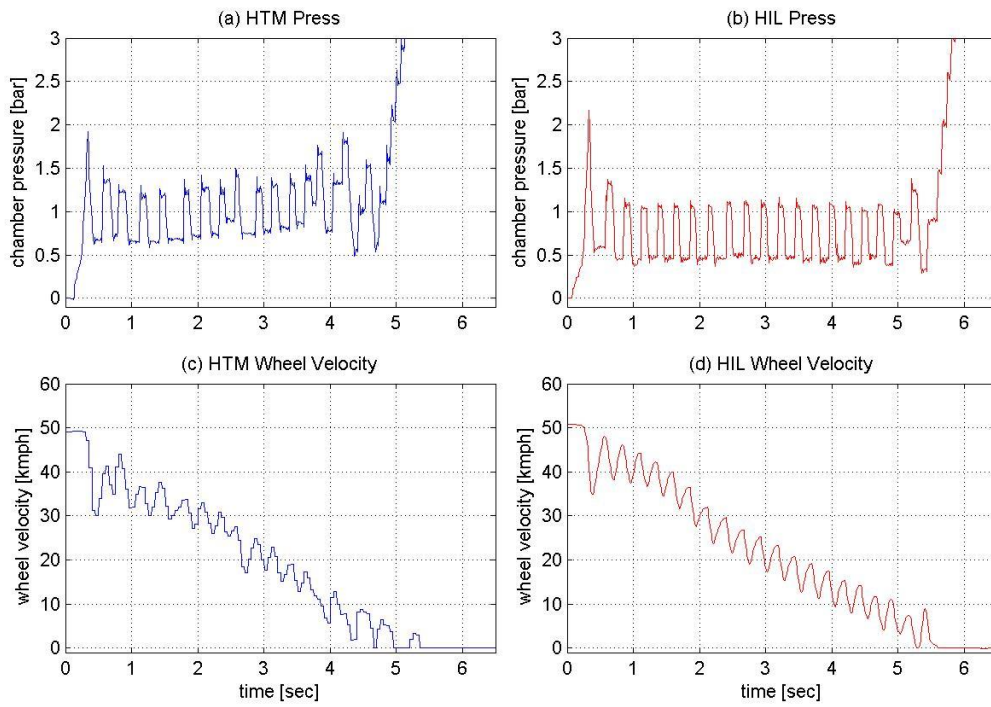


Figure 5.26: HIL Test 8 Front Left Pressure and Wheel Speed

Back Left Chamber Pressures and Wheel Velocities
(Laden, ABS On, Left-Low Right-High μ , 50 kmph)

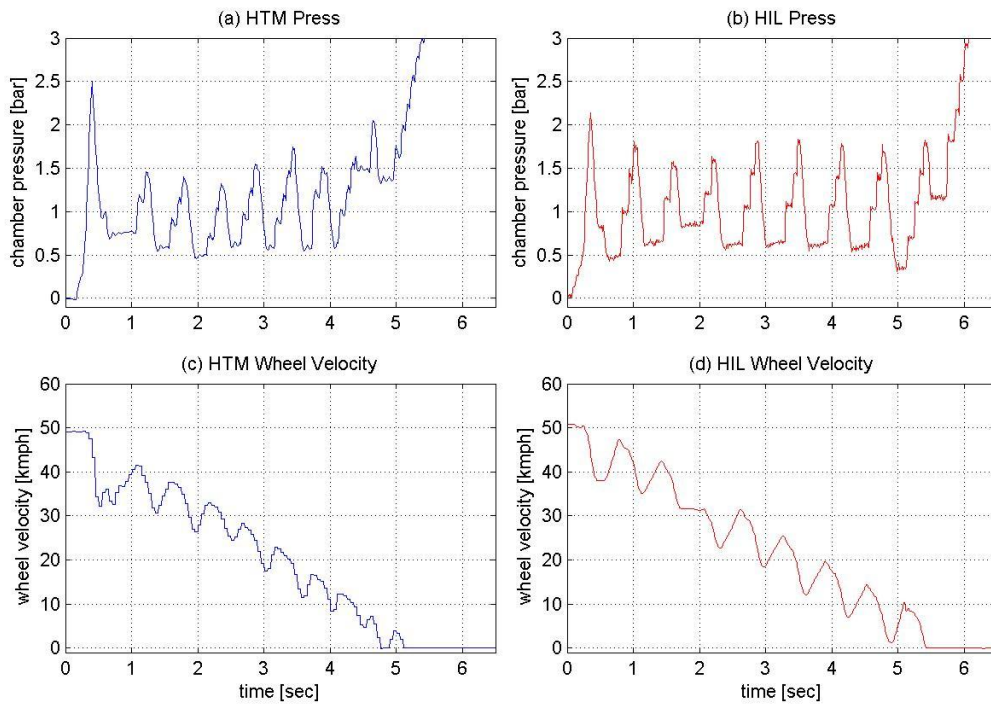


Figure 5.27: HIL Test 8 Back Left Pressure and Wheel Speed

Velocity and Stopping Distance
(Laden, ABS On, Left-Low Right-High μ , 50 kmph)

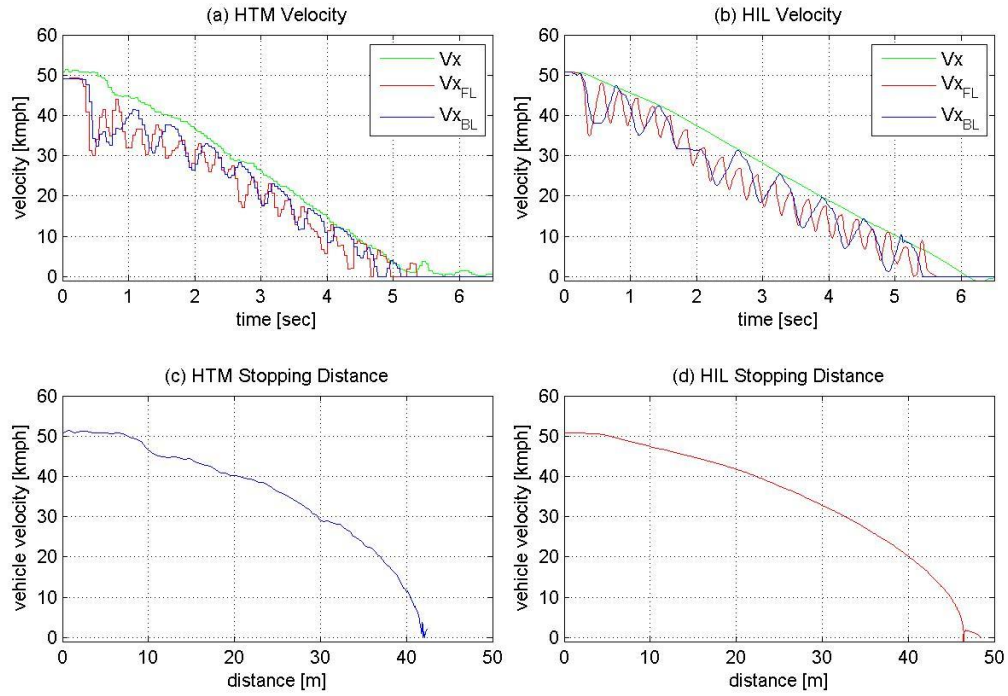


Figure 5.28: HIL Test 8 Stopping Performance

<u>Validation Metrics</u>	<u>HTM</u>		<u>HIL</u>		<u>% Difference</u>	
	Front Left Wheel	Back Left Wheel	Front Left Wheel	Back Left Wheel	Front Left Wheel	Back Left Wheel
ABS Modulation Time	5.04 [sec]	4.71 [sec]	5.27 [sec]	5.07 [sec]	+4.6 [%]	+7.6 [%]
Avg. Pressure	1.02 [bar]	0.99 [bar]	0.68 [bar]	0.95 [bar]	-33.3 [%]	-4.0 [%]
Stopping Time	5.60 [sec]		6.01 [sec]		+7.3 [%]	
Stopping Distance	42.14 [m]		46.47 [m]		+10.3 [%]	

Table 5.11: HIL Test 8 Validation Metrics

5.2 Overall Results for HIL Simulation

Overall, the HIL simulator effectively emulated the behavior of the test vehicle. Upon referring to Figure 5.42, the percent difference for the ABS modulation times are given. As we can see, the deviations never exceeded plus or minus 15 percent. In Figure 5.43, the percent difference for the average brake chamber pressures are given. Typically the deviations remained within +30 percent and -30 percent. In the case of the unladen jump μ and laden split μ tests, the largest deviations were produced with values of +48.3 percent and -33.3 percent respectively. Finally, in Figure 5.44, the differences in stopping time and distance are given. These metrics were most important in understanding how well the HIL simulator emulated the actual vehicle since the main goal of the ABS system is to decelerate the vehicle in a quick and controlled manner. We can see that both the stopping times and distances for all eight tests were well simulated. On average, these deviations remained under 10 percent with the maximum deviations for time and distance being +12.3 percent and +10.3 percent respectively.

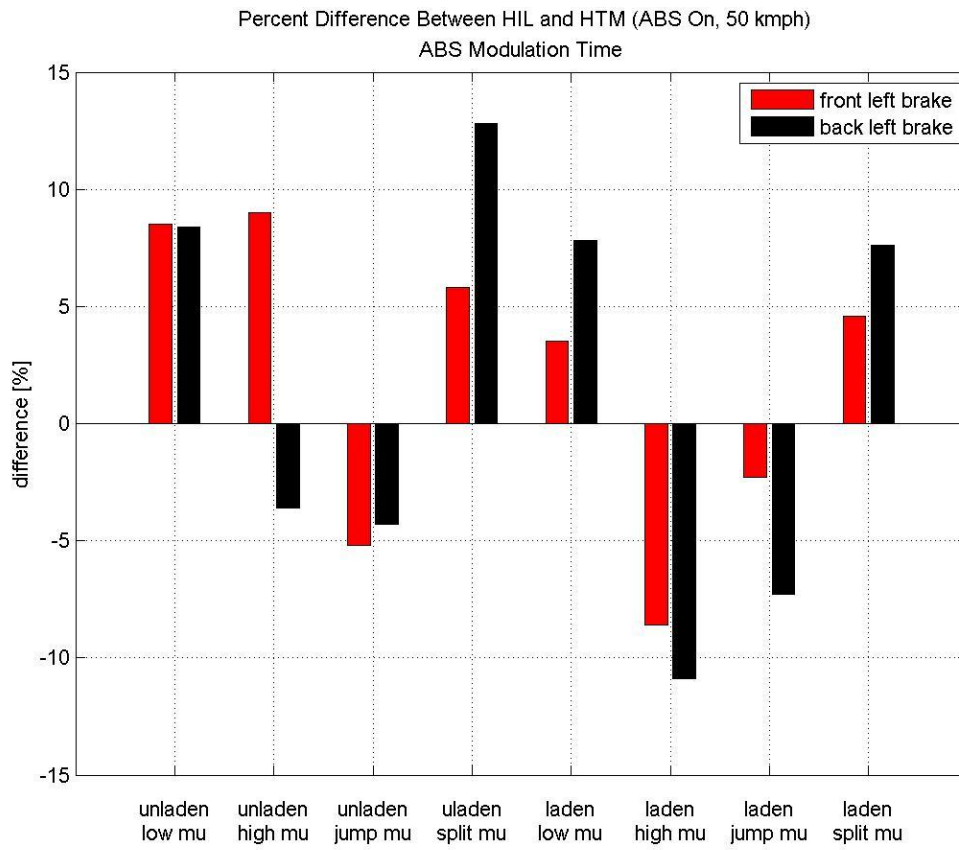


Figure 5.29: HIL ABS Modulation Time Differences

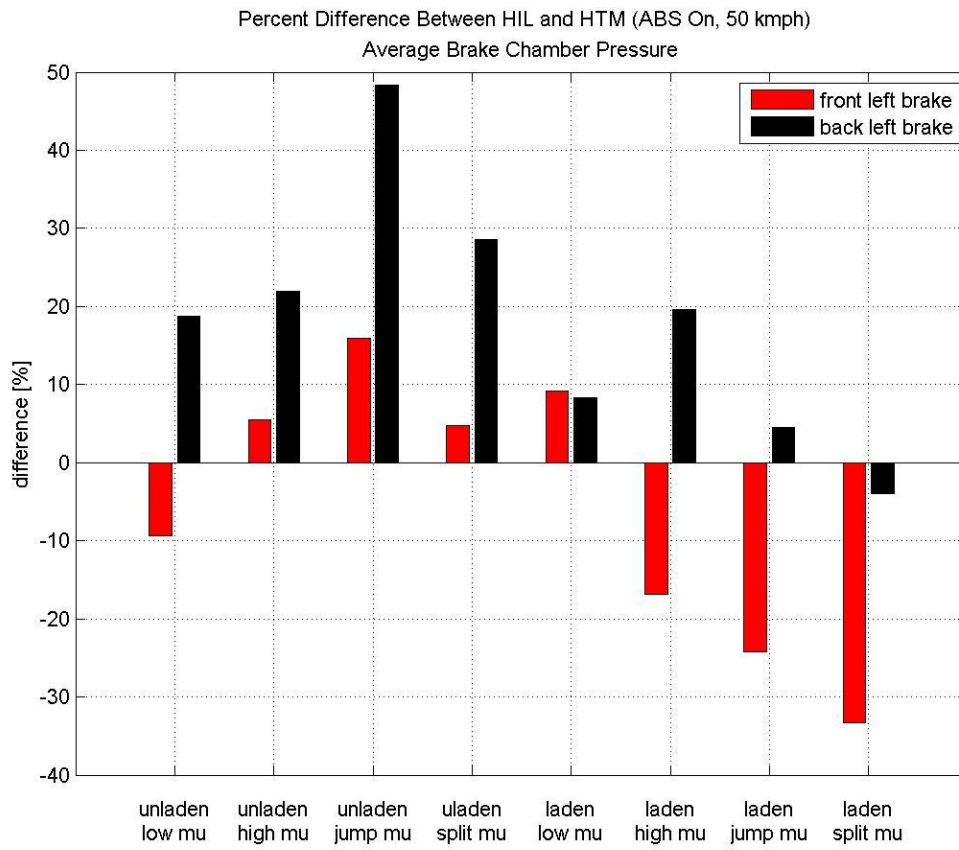


Figure 5.30: HIL Average Pressure Differences

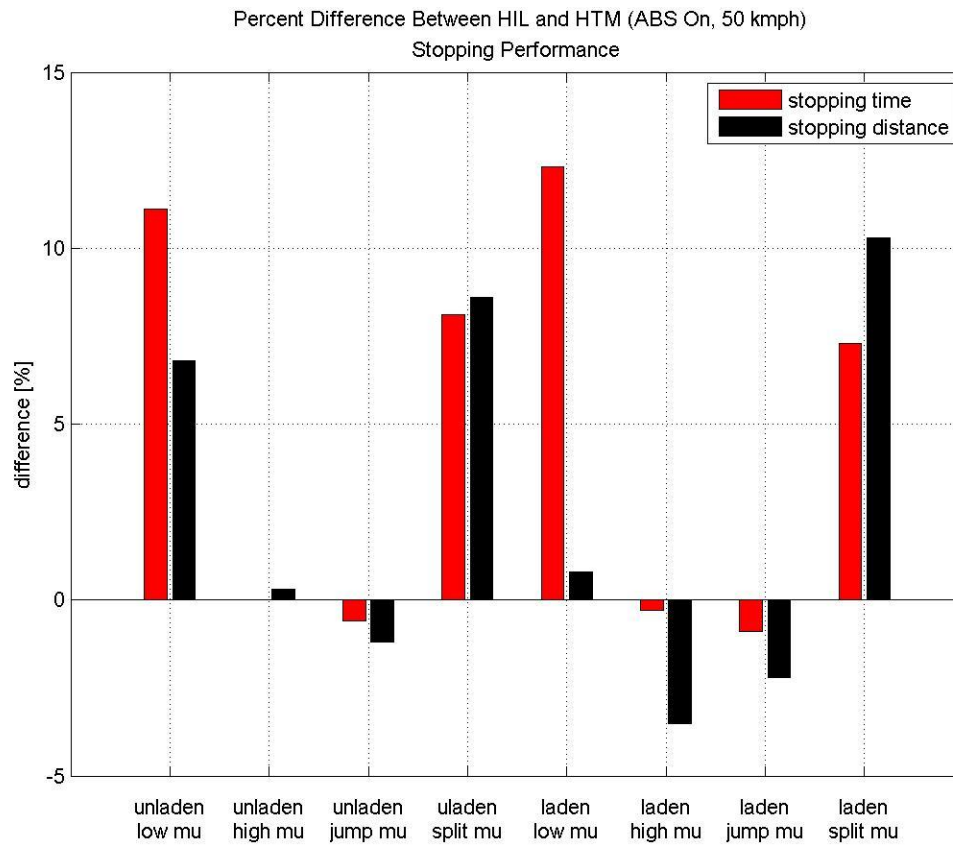


Figure 5.31: HIL Stopping Performance Differences

Chapter 6: Software in the Loop Simulation

6.1 SIL Simulation Concept

Within an SIL simulation, a plant model runs on a processor at a rate dependent on the speed of the processor. The plant model then interacts with peripheral software subsystems. With SIL simulations, control strategies can be rapidly developed entirely within the computer realm. In Figure 6.1, we can see a simplified illustration which represents the overall working principal of the SIL simulation for this project. In this case, the entire simulation was developed within MATLAB Simulink. The plant is the tractor-trailer vehicle dynamics model which was developed in TruckSim and is represented in Simulink as an S-Function. The main peripheral subsystems are the vehicle mass estimator, the roll stability controller and the anti-lock brake controller.

The goal with this SIL simulation was to develop ABS and RSC algorithms comparable to the ones implemented by the vehicle manufacturer. Information on the basic working principals of the ABS and RSC systems was obtained from the manufacturer and the concepts were implemented here. These basic principles are illustrated in Figure 6.1. From the figure, we can see the vehicle model continuously sends variables to the subsystems such as wheel speed, lateral acceleration, steer angle and power train tractive force. During severe braking and handling maneuvers, these subsystems intervene and keep the vehicle model performing in an optimal manner.

Essentially, the mass estimator subsystem continually estimates the mass of the

vehicle in order to determine how severe a turn the vehicle should be allowed to make. The roll stability control subsystem takes this mass estimation into account along with wheel speed, lateral acceleration and steer angle data in order to determine if the vehicle is on the verge of rollover. The subsystem then develops a braking strategy to mitigate rollover and passes this command through the anti-lock brake controller. The brake controller then proceeds to slow the vehicle in a manner that will keep wheel lockup from occurring. In addition to this, the roll stability controller sends commands to the vehicle model to reduce engine power.

If we refer to Figure 6.2, a screenshot of the entire SIL Simulink model is given. The various subsystems within this model and the steps taken to develop them will be discussed in the proceeding sections. In addition to this, the ABS and RSC control strategies will be tested and validated using real world test data provided by the tractor manufacturer. If after reviewing this chapter the reader wishes to obtain more detailed information on the SIL simulation process, please refer to "Development of a Heavy Truck Vehicle Dynamics Model using TruckSim and Model Based Design of ABS and ESC Controllers in Simulink" [2] by Shreesha Rao.

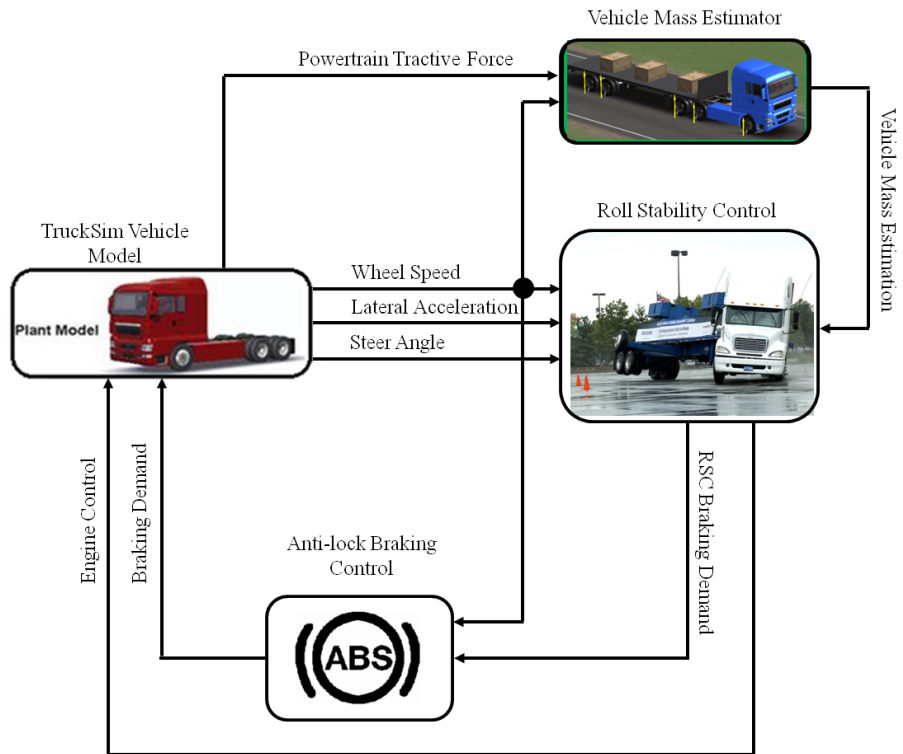


Figure 6.1: SIL Layout

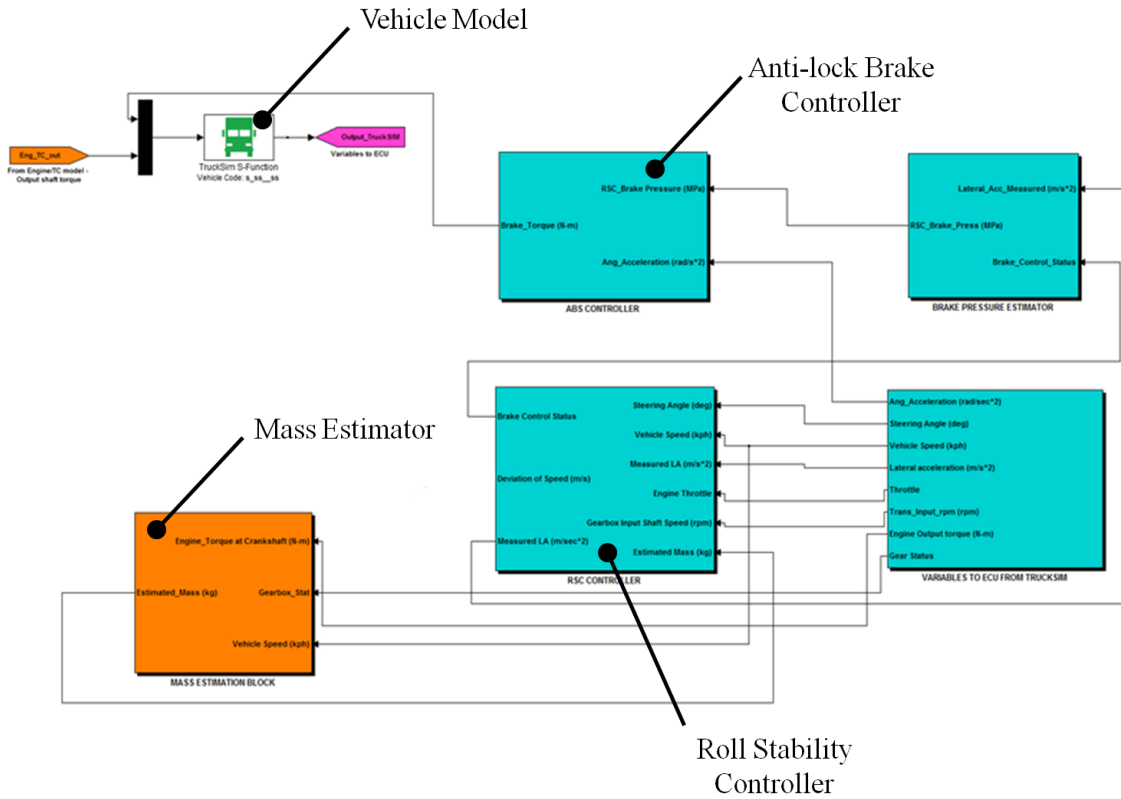


Figure 6.2: SIL Simulink Model Top Layer

6.2 Anti-lock Brake Controller

The first subsystem to be developed within the SIL simulation was the ABS controller. When operating in conjunction with the RSC controller, the ABS essentially refines the braking commands the RSC algorithm decides upon. The RSC controller never gives a direct braking command to the vehicle model since it does not take wheel lockup into account. Essentially, the ABS controller must import the RSC's braking commands and modify them in such a way that the vehicle will still decelerate and avoid

rollover while mitigating wheel lockup. The development of the ABS controller will be discussed in this section.

6.2.1 Anti-lock Brake Controller Design

Since the goal of the SIL simulation was to develop ABS and RSC algorithms comparable to the ones implemented by the vehicle manufacturer, it was decided that ABS data from the HIL simulation, which utilizes an ABS controller identical to the one on the production vehicle, would be used as a basis for the controller design. Data from a low μ braking test conducted with the HIL simulator is given in Figure 6.3. In the figure, the angular acceleration for the back left wheel, shown in green, is plotted with respect to time along with the brake chamber pressure modulations for that wheel, shown in blue. We can see from the figure that the wheel acceleration fluctuates with the chamber pressure. Whenever the chamber pressure rises, the wheel acceleration drops quickly and whenever the pressure drops, the acceleration rises. Upon examining this figure closely, it was determined there are three acceleration values, A1, A2 and A3, for which the ABS pressure modulator will respond to. Effectively, upon applying the brakes, the ABS modulators dump chamber pressure at A3, hold chamber pressure at A1, and then build pressure at A2. This relationship between wheel acceleration and ABS modulation was used as the basis for the ABS control in the SIL simulator. Table 6.1 defines the logic of this algorithm.

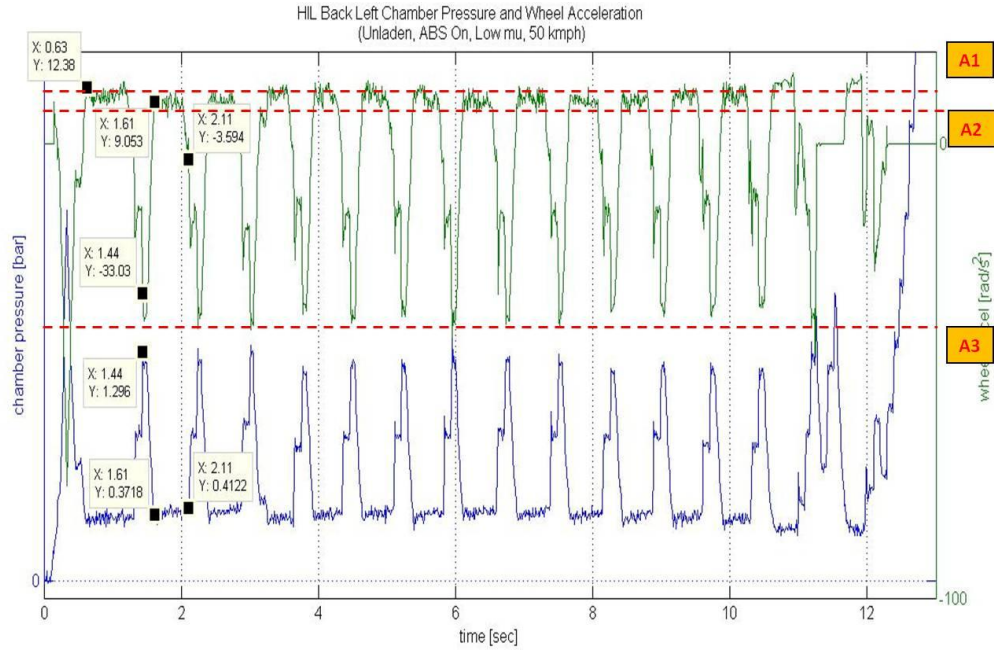


Figure 6.3: Analyzing ABS Control

Angular Acceleration $\leq A3$	Angular Acceleration $\geq A1$	Angular Acceleration $\leq A2$	Slope of Angular Acceleration	ABS Modulator Command
true	false	true	negative	dump
false	false	true	negative	build
false	true	false	negative	hold
false	false	false	negative	hold
true	false	true	positive	dump
false	false	true	positive	dump
false	true	false	positive	hold
false	false	false	positive	dump

Table 6.1: SIL ABS Logic

After the basic working principal for the ABS controller was developed, the control strategy could be implemented within the Simulink model. The contents of the ABS controller subsystem from Figure 6.2 are illustrated in Figure 6.4. As we can see from the figure, the wheel acceleration values are imported into the controller at input number one along with the braking pressure demand at input two. The blocks in this figure, which are labeled front left wheel system, front right wheel system, etc., house the ABS control algorithm, previously mention in Table 6.1, for each of the four modulated wheels. Upon passing the wheel accelerations and pressure demand through each of these algorithms, a dump, hold or build pressure command is decided upon and the resulting modulated pressures are exported through output one. It can be noted that each of the ABS control algorithm blocks take into account the pressure dynamics of an actual working modulator through the use of a first order transfer function which was developed experimentally.

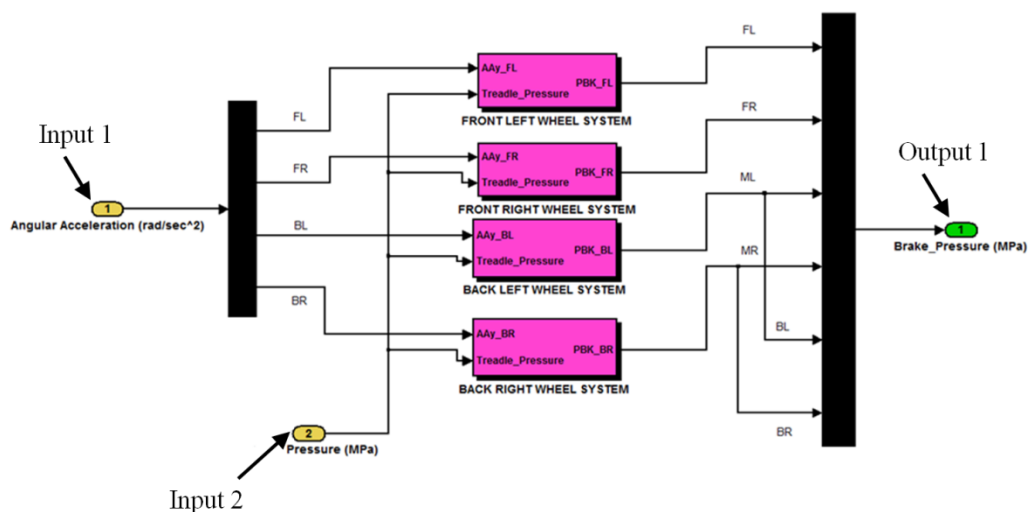


Figure 6.4: SIL Simulink Model for ABS

6.2.2 Validation of Anti-lock Brake Controller

In order to validate the performance of the SIL ABS control strategy, the simulation was placed through 16 different tests which mimic real world tests conducted by the manufacturer. These tests consisted of straight line braking maneuvers which are identical to the ones conducted for the HIL ABS validation in chapter five. The simulation was ran in a laden and unladen configuration as well as on low μ , high μ , jump μ and split μ test surfaces. The vehicle mass along with the test description, surface friction and vehicle braking speeds are all given in Table 6.2. In this section, we will discuss the results of test number one.

<u>Test No.</u>	<u>Vehicle Mass [kg]</u>	<u>Description</u>	<u>Brake Application Speed [kph]</u>
1	Unladen; 9320	Homogeneous low μ (0.16)	40
2	Unladen; 9320	Homogeneous low μ (0.16)	50
3	Unladen; 9320	Homogeneous low μ (0.16)	70
4	Unladen; 9320	Homogeneous high μ (0.91)	50
5	Unladen; 9320	Split μ , Left low (0.16) and Right high (0.91)	50
6	Unladen; 9320	Split μ , Left high (0.91) and Right low (0.16)	50
7	Unladen; 9320	Jump μ , High μ (0.91) to Low μ (0.16)	54
8	Unladen; 9320	Jump μ , Low μ (0.16) to High μ (0.75)	55
9	Laden; 18748	Homogeneous low μ (0.13)	40
10	Laden; 18748	Homogeneous low μ (0.13)	50
11	Laden; 18748	Homogeneous low μ (0.13)	70
12	Laden; 18748	Homogeneous high μ (0.75)	50
13	Laden; 18748	Split μ , Left low (0.13) and Right high (0.75)	50
14	Laden; 18748	Split μ , Left high (0.75) and Right low (0.13)	50
15	Laden; 18748	Jump μ , High μ (0.75) to Low μ (0.13)	50
16	Laden; 18748	Jump μ , Low μ (0.13) to High μ (0.75)	55

Table 6.2: Test Configuration for SIL ABS Validation

TEST 1: UNLADEN TRACTOR on LOW MU SURFACE

Figure 6.5 illustrates pressure versus time for the front left brake chamber and wheel speed versus time for the front left wheel of the HTM tractor and SIL simulation. The subplots in this figure as well as those in proceeding figures have been adjusted so that brake application occurs near time equals zero. This was done to make comparison between the HTM and SIL data easier.

As we can see from subplots a and b, there are similarities in the pressure curves for the HTM and SIL data. We can first notice that the pressures rise quickly upon initial brake application until a pressure of around two bar is reached. At this point, ABS modulation begins for both the HTM tractor and SIL simulation resulting in a rapid pressure dump. Similarly in subplots c and d, the wheel speeds quickly drop as this initial ABS modulation cycle takes place. The HTM braking system and SIL braking system both bring the front wheels to a stop in just over eight seconds.

Figure 6.6 illustrates pressure versus time for the back left brake chamber and wheel speed versus time for the back left wheel of the HTM tractor and SIL simulation. We can see from subplots a and b that the pressures rise quickly upon initial brake application until a pressure of around two bar is reached. We can also see from the figure that the HTM and SIL rear chambers fluctuate with similar pressure values.

In Figure 6.7, the wheel speed and vehicle speed versus time is plotted for the test vehicle and the simulation along with speed versus distance. We can see from the figure that the HTM vehicle stops nearly one second quicker and several meters shorter than the SIL simulation, however, overall the results are fairly similar.

Front Left Chamber Pressures and Wheel Velocities
(Unladen, ABS On, Low μ , 40 kmph)

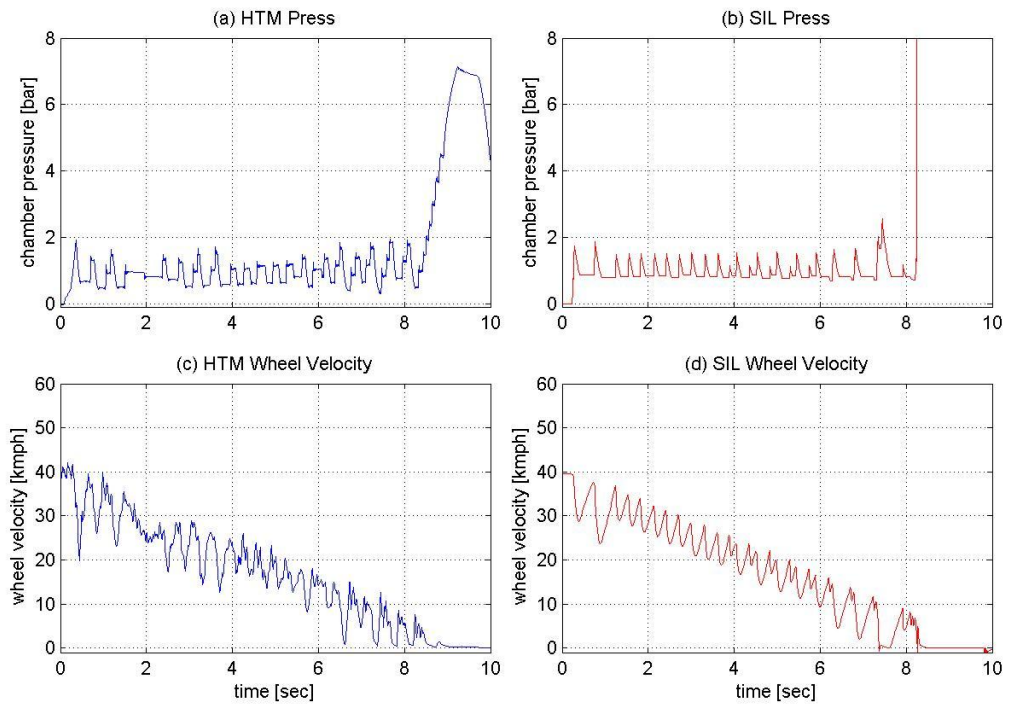


Figure 6.5: SIL ABS Test 1 Front Left Pressure and Wheel Speed

Back Left Chamber Pressures and Wheel Velocities
(Unladen, ABS On, Low μ , 40 kmph)

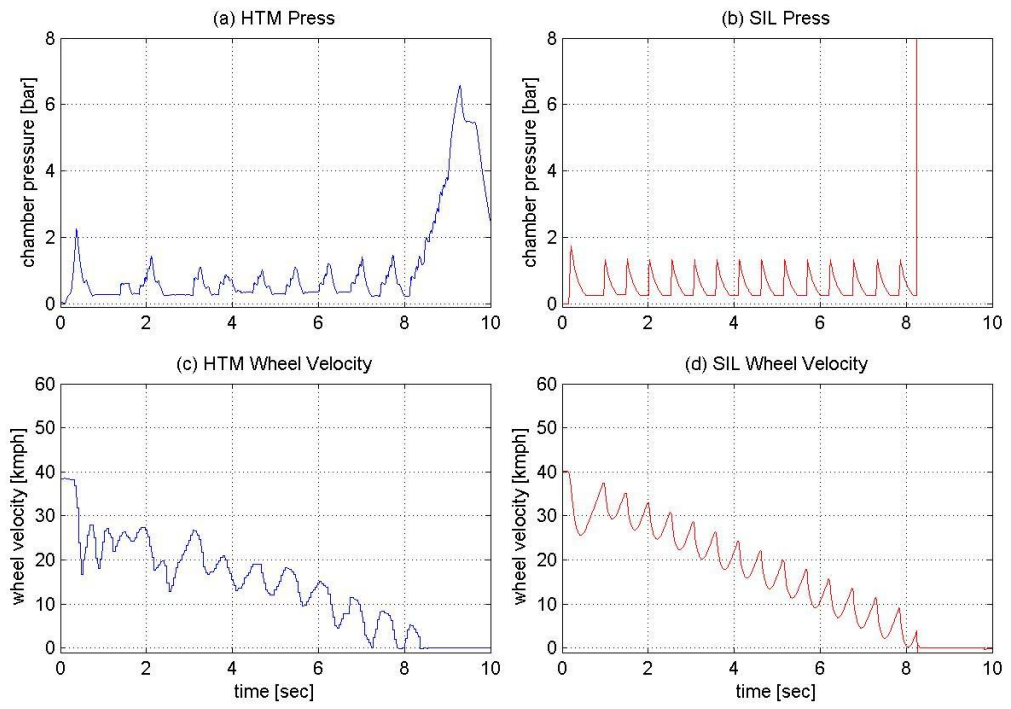


Figure 6.6: SIL ABS Test 1 Back Left Pressure and Wheel Speed

Velocity and Stopping Distance
(Unladen, ABS On, Low μ , 40 kmph)

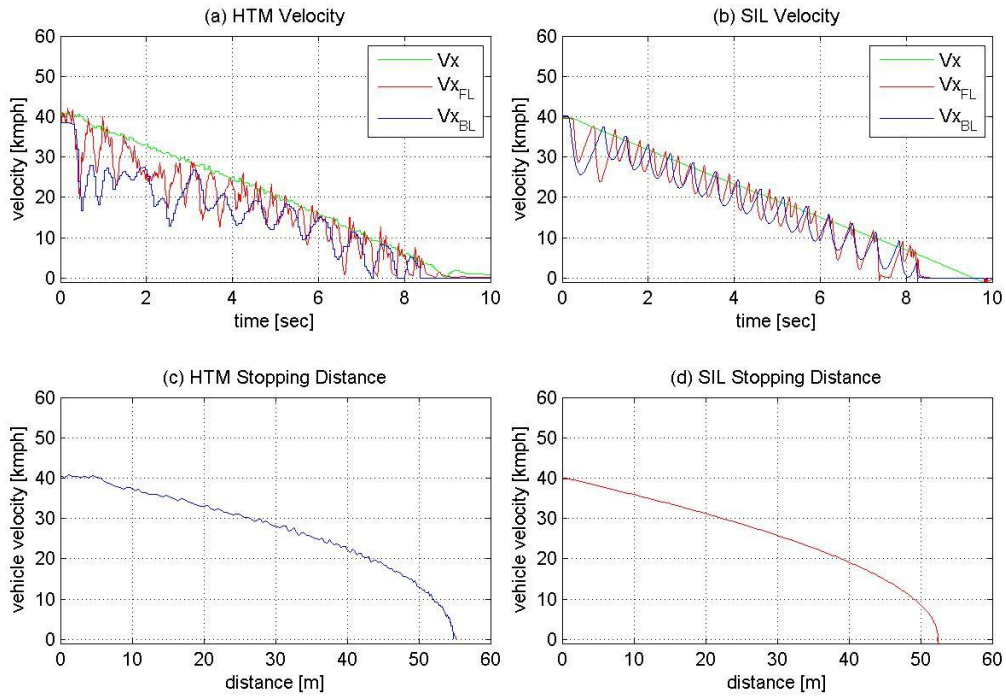


Figure 6.7: SIL ABS Test 1 Stopping Performance

6.3 Vehicle Mass Estimator

6.3.1 Mass Estimator Design

The vehicle mass estimator subsystem is designed to estimate the mass of the tractor-trailer rig so the RSC controller can decide upon an appropriate lateral acceleration rollover threshold. The mass estimator is able to accomplish this by calculating the vehicle's acceleration, determined from the wheel speeds, and power train tractive force and applying Newton's second law; given in Equation 6.1. The tractive force is the longitudinal driving force exerted on the vehicle by the power train.

Essentially, the total tractive force acting upon the vehicle must be equal to the vehicle's

total mass times the vehicle's acceleration; assuming no external forces such as gravity are accelerating the vehicle.

$$\sum F = ma \quad \text{Equation 6.1}$$

Within a real world RSC controller, the power train tractive force is determined through the use of the J1939 CAN bus. Essentially, the ECUs that control the power train broadcast information on the CAN bus regarding the current torque output of the engine as well as the current transmission gear selection. Based on this information, along with constant parameter data such as the tire rolling radius, the transmission gear ratio and the differential gear ratio, the RSC controller can determine the power train tractive force.

The mass estimator for the SIL simulation works off of this same principal, however, with the simulation there is no need to obtain power train data through a CAN bus. This data can be obtained directly from the TruckSim vehicle model. As we can see in Equation 6.2, the power train tractive force is equal to the engine torque exerted on the transmission input shaft (T_E) times the transmission gear ratio (N_g) times the differential gear ratio (N_d) times the power train torque transfer efficiency (η) divided by the tire rolling radius (R_r) of the drive wheels. It can be noted that this equation assumes the transmission and differential are the only gear systems between the engine and the drive wheels.

$$\sum F = \text{Power Train Tractive Force} = \frac{T_E N_g N_d \eta}{R_r} \quad \text{Equation 6.2}$$

6.3.2 Validation of Mass Estimator

In order to assess the performance of the mass estimator subsystem, three different vehicle configurations were tested with the SIL simulation. First, the solo tractor without any trailer was tested, followed by the tractor and low C.G. trailer and finally the tractor and high C.G. trailer. In each of these three tests, the vehicle was accelerated from a stop and the mass estimator algorithm was activated. As the vehicle was accelerated, the mass estimator analyzed power train and wheel speed data to determine the vehicle mass. The resulting mass estimations and percent errors are given in Table 6.3. We can see from the table that the maximum error was -9.5 percent which is comparable to the errors produced with the real world RSC ECU mass estimator.

<u>Test No.</u>	<u>Vehicle Configuration</u>	<u>Actual Vehicle Mass [kg]</u>	<u>Estimated Vehicle Mass [kg]</u>	<u>% Error</u>
1	Solo Tractor	9320	8438	-9.5
2	Tractor and Low C.G. Trailer	27300	28261	+3.5
3	Tractor and High C.G. Trailer	28200	30721	+8.9

Table 6.3: Test Results for SIL Mass Estimator

6.4 Roll Stability Controller

With the SIL ABS subsystem and mass estimator subsystem designed and tested, work began on the RSC controller. The design of this controller was influenced by data obtained from the vehicle manufacturer in which roll prevention strategies for a real world RSC ECU were disclosed. The overall design and validation of the RSC subsystem will be discussed in this section.

6.4.1 Roll Stability Controller Design

Figure 6.8 illustrates the working principal of the RSC controller designed for this simulation. The controller observes the vehicle's measured lateral acceleration and compares this value with a value for predicted lateral acceleration, i.e. preview lateral acceleration. These two acceleration values are then compared in the "MAX" box and whichever value is greatest is then designated as the monitored lateral acceleration. As this process is occurring, the vehicle's mass estimator determines the vehicles overall mass and corresponding rollover threshold. This is done in the box labeled "CRITICAL LATERAL ACCELERATION THRESHOLD". The lateral acceleration threshold is then subtracted from the monitored lateral acceleration in the "COMPARE" box. If this resulting value greater than zero, the RSC controller must take action and slow the vehicle to prevent rollover from occurring. This is done by activating the vehicles braking system and cutting throttle to the engine. The RSC controller will only release the brakes and relinquish throttle control when the deviation between the actual vehicle speed and the desired vehicle speed is equal to zero. In other words, the speed deviation must be equal to or less than zero for RSC to return to a non-active state. The methods

for determining the preview lateral acceleration, critical lateral acceleration threshold and speed deviation will be discussed in the following paragraphs.

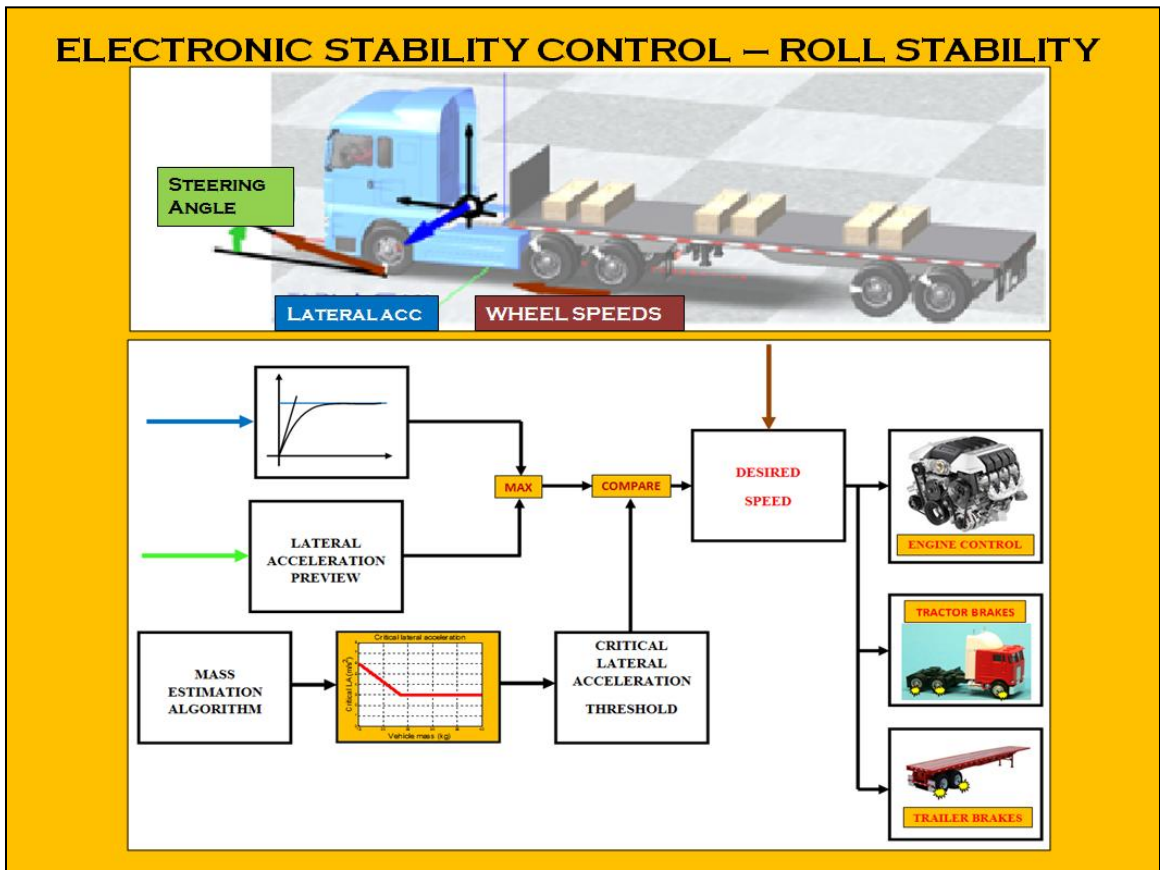


Figure 6.8: SIL RSC Working Principal

PREVIEW LATERAL ACCELERATION

In a real world RSC system, the controller is able to measure the lateral acceleration of the vehicle's sprung mass through the use of a lateral acceleration sensor which is mounted near the C.G. of the vehicle. During a cornering maneuver, the

vehicle's tires and axles, i.e. unsprung mass, generate a lateral force which is transferred to the sprung mass via the suspension. This lateral force exerted upon the sprung mass will ultimately result in a lateral acceleration of the sprung mass which can then be detected by the lateral acceleration sensor. Since the cornering force originates in the unsprung mass and is propagated to the sprung mass via the non-rigid suspension, there is some delay which exists between the time in which the vehicle begins the cornering maneuver and the time in which the sensor will actually detect lateral acceleration. When making a sharp turn, the tractor-trailer rig may experience the onset of an unrecoverable roll in mere fractions of a second. For this reason, the RSC system cannot afford to have any delays with lateral acceleration measurement.

The preview lateral acceleration subsystem, pictured in Figure 6.9, attempts to mitigate the problems brought on by lateral acceleration time delay by estimating a more effective acceleration value. This preview lateral acceleration is calculated using Equation 6.3 in which the road wheel steering angle (δ) given in radians, the vehicle speed (v_x) given in $\frac{m}{sec}$, the vehicle roll coefficient (R_δ) given in $\frac{rad}{m/sec^2}$, and vehicle wheelbase (L), given in m are taken into account. We can see from Figure 6.9 that values for the steering angle and vehicle speed are imported to the preview lateral acceleration subsystem via inputs one and two respectively. It can be noted that the vehicle roll coefficient in Equation 6.3 defines the relationship between the roll angle of the vehicle and lateral acceleration. This coefficient was determined experimentally by performing a slowly increasing steer (SIS) maneuver and calculating the slope of the plot for roll angle versus lateral acceleration.

$$a_{y_preview} = \frac{\delta v_x^2}{R_\delta v_x^2 + L} \quad \text{Equation 6.3}$$

CRITICAL LATERAL ACCELERATION THRESHOLD

As mentioned previously in Section 6.3, the mass estimator subsystem is able to determine the overall mass of the tractor-trailer rig based on the power train tractive force and vehicle acceleration. The RSC controller utilizes this mass estimation in order to determine the critical lateral acceleration threshold. This threshold represents the maximum lateral acceleration the vehicle should be allowed to achieve before the RSC system recognizes rollover is imminent and slows the vehicle. As mentioned previously in chapter two, the rollover threshold is determined experimentally for a given vehicle by adding various payloads and recording the lateral acceleration at which the vehicle rolls over. Typically, the acceleration at which the vehicle rolls over will decrease as the payload mass increases. Based on this experimental data, the critical lateral acceleration threshold subsystem can determine an appropriate rollover threshold for the current vehicle mass. In Figure 6.9, the critical lateral acceleration threshold subsystem is given and as we can see, the estimated mass is the main input to the subsystem and is labeled here as input six.

SPEED DEVIATION

After preventing a rollover from occurring, the RSC controller will only relinquish braking and engine control when the speed deviation is equal to or less than zero. This deviation is equal to the measured vehicle speed minus the desired vehicle speed; refer to Equation 6.4. The desired vehicle speed is determined from the critical lateral acceleration threshold ($a_{y_critical}$) given in $\frac{m}{sec^2}$, the vehicle wheelbase (L) given in m and the road wheel steer angle (δ) given in radians. The formula for calculating

desired speed is given in Equation 6.5 and is essentially an adaptation of the lateral acceleration preview equation. The only difference here is that the vehicle roll stiffness has not been included, the lateral acceleration is set to the critical threshold value and the velocity is the variable being solved for.

$$v_{x_deviation} = v_x - v_{x_desired} \quad \text{Equation 6.4}$$

$$v_{x_desired}^2 = \frac{a_{y_critical}L}{\delta} \Rightarrow v_{x_desired} = \sqrt{\frac{a_{y_critical}L}{\delta}} \quad \text{Equation 6.5}$$

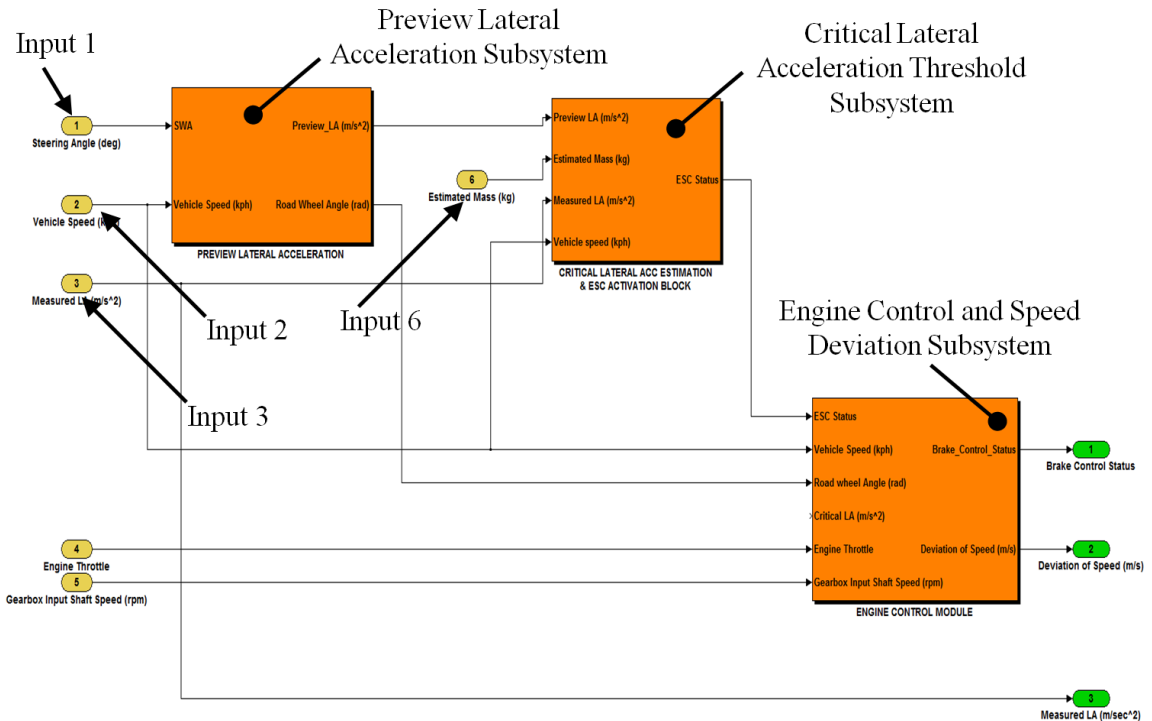


Figure 6.9: SIL Simulink Model for RSC Inner Layer

6.4.2 Validation of Roll Stability Controller

In order to validate the performance of the SIL RSC control strategy, the simulation was placed through 17 different tests which mimic real world tests conducted by the manufacturer. These tests consisted of a follow the cone path test, in which a cone course was laid out in TruckSim identical to the course used for real world testing, a high dynamic steer test, a lane change test, and a J-turn test. The simulation was tested with both the low C.G. and high C.G. trailers developed in chapter three. The trailer configuration, cornering maneuver, road surface and vehicle speed speeds for each test are given in Table 6.4. It can be noted that the term c.l.a.t., given in tests eight through 17 in Table 6.4, refers to the critical lateral acceleration threshold. In these tests, the mass estimator subsystem was not utilized and the rollover threshold was set manually. In the remainder of this section, the results for test number one will be discussed.

<u>Test No.</u>	<u>Trailer Configuration</u>	<u>Maneuver</u>	<u>Road Surface</u>	<u>Speed [kph]</u>
1	Low C.G.	Follow cone path	Dry asphalt	50
2	Low C.G.	High dynamic steer input	Dry asphalt	48
3	Low C.G.	Follow cone path	Dry asphalt	49
4	Low C.G.	Follow cone path	Dry asphalt	50
5	Low C.G.	High dynamic steer input	Moist asphalt	55
6	High C.G.	Lane change	Wet to Dry asphalt	50
7	High C.G.	J-Turn	Wet to Dry asphalt	50
8	High C.G.	Follow cone path (c.l.a.t - 3.2 m/s ²)	Dry asphalt	48
9	High C.G.	Follow cone path (c.l.a.t - 3.2 m/s ²)	Dry asphalt	52
10	High C.G.	Follow cone path (c.l.a.t - 3.2 m/s ²)	Dry asphalt	57
11	High C.G.	Follow cone path (c.l.a.t - 3.2 m/s ²)	Dry asphalt	58
12	High C.G.	Follow cone path (c.l.a.t - 3.4 m/s ²)	Dry asphalt	53
13	High C.G.	Follow cone path (c.l.a.t - 3.4 m/s ²)	Dry asphalt	60
14	High C.G.	Follow cone path (c.l.a.t - 3.6 m/s ²)	Dry asphalt	48
15	High C.G.	Follow cone path (c.l.a.t - 3.6 m/s ²)	Dry asphalt	53
16	High C.G.	Follow cone path (c.l.a.t - 4.0 m/s ²)	Dry asphalt	57
17	High C.G.	Follow cone path (c.l.a.t - 4.0 m/s ²)	Dry asphalt	60

Table 6.4: Test Configuration for SIL RSC Validation

TEST 1: LOW C.G. TRAILER - FOLLOW CONE on DRY ASPHALT

For test one, the low C.G. trailer was coupled to the tractor and a predefined cornering maneuver, specified by the HTM test engineers, was followed. The test surface was dry asphalt and the maneuver was conducted at 50 kilometers per hour. In Figure 6.10, the brake chamber pressure data for the HTM test, represented as experimental in the legend, and the simulation test is given. We can see the SIL RSC controller actuates the front left, front right, back left and back right brakes at the same instance as the actual test vehicle's RSC system does.

In Figure 6.11, lateral acceleration, yaw rate, road wheel angle and vehicle speed of the test vehicle, given in red, and the simulation, given in blue, are plotted. As we can see from the road wheel angle subplot, the simulation vehicle precisely follows the road wheel angle of the test vehicle throughout the maneuver. In addition to this, we can see in the vehicle speed subplot how the real world RSC controller and simulated RSC controller both decelerate to mitigate rollover. As a result of accurate RSC modeling, the lateral acceleration and yaw rate curves match as well. Finally, in Figure 6.12 we can see the manner in which the RSC controllers cut power to the engine and apply the brakes. Both controllers activate and deactivate at nearly the same instance.

Follow Cone Path on Dry asphalt
(Tractor + Low CG trailer, ESC ON, 50 kmph)

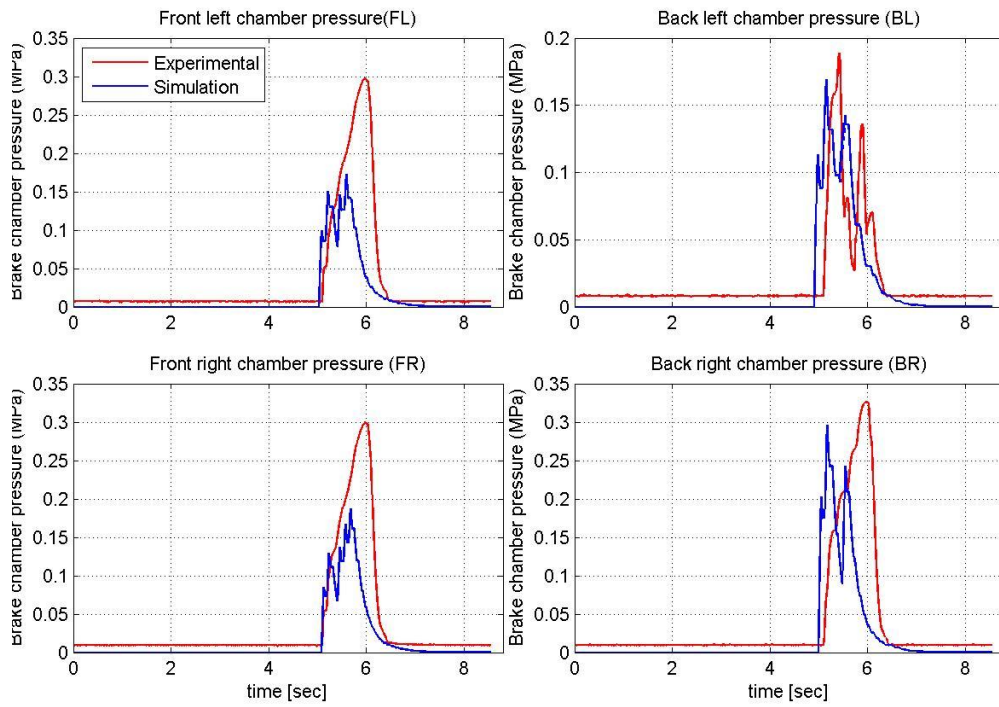


Figure 6.10: SIL RSC Test 1 Pressure

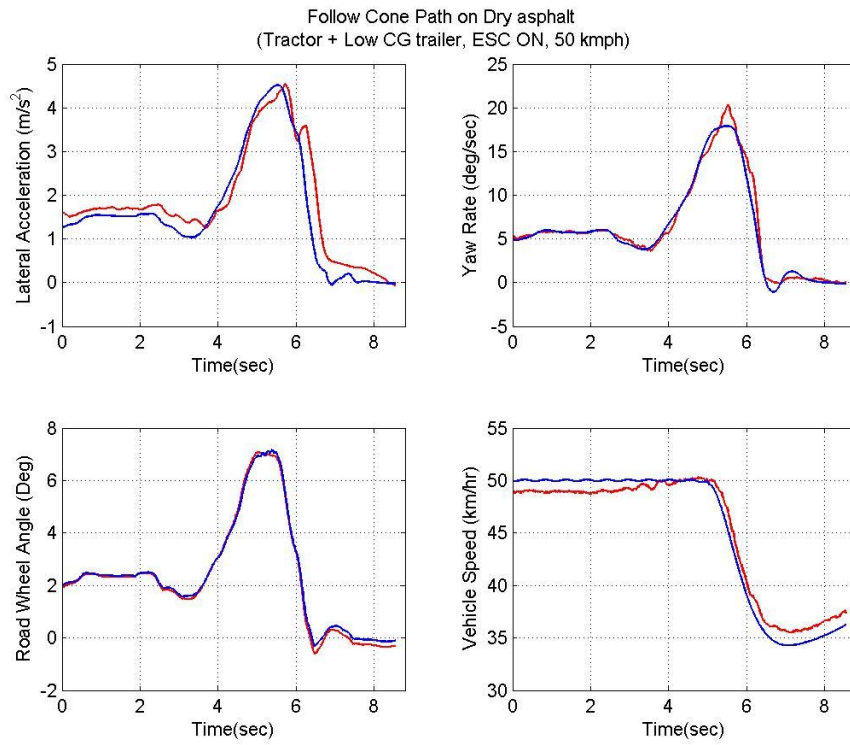


Figure 6.11: SIL RSC Test 1 Vehicle Behavior

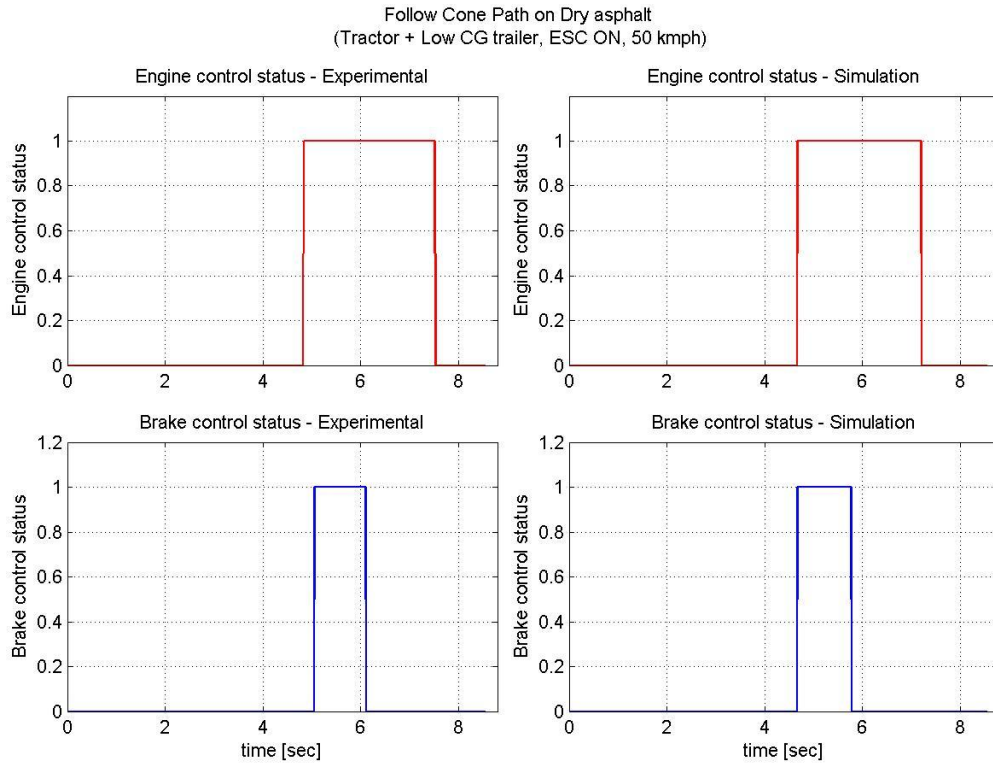


Figure 6.12: SIL RSC Test 1 Engine and Brake Control

Figure 6.13 illustrates the TruckSim simulation animator for the tractor-trailer rig as it undergoes a severe left hand turn. The yellow vertical arrows at the base of each wheel represent the magnitude of the vertical tire loading. These arrows increase in height as loading increases. We can see from the figure that the inner wheels, left hand side, have relatively small loading compared to the outer wheels. This is due to the lateral load transfer from the cornering maneuver. In this particular simulation, the tractor-trailer rig would have rolled over had the RSC controller not intervened and decelerated the vehicle.

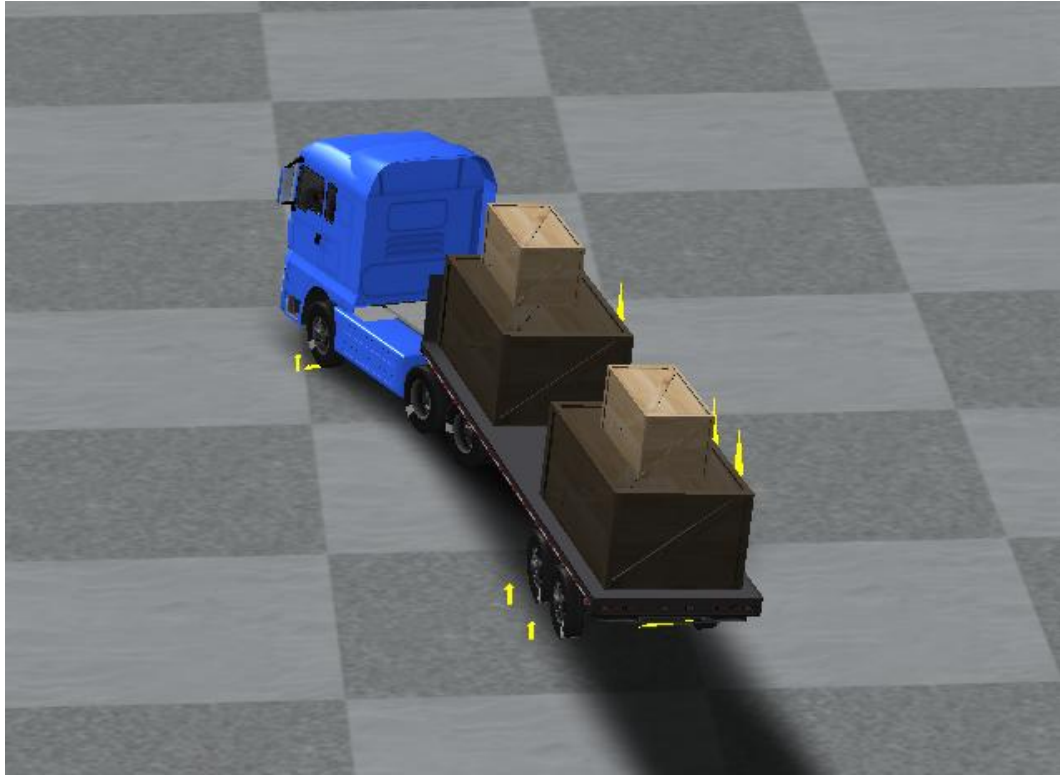


Figure 6.13: SIL RSC TruckSim Animation During Severe Turn

Chapter 7: Summary and Recommendations

7.1 Summary

Parameters for a production 6x4 tractor were obtained from a heavy truck manufacturer. These parameters included sprung mass specifications such as center of gravity location, roll inertia, yaw inertia and pitch inertia as well as suspension specifications such as spring stiffness and shock absorber damping coefficients and much more. These parameters were entered into the vehicle dynamics modeling software, TruckSim, and a working tractor model was developed.

Along with the 6x4 tractor, two trailer models were developed in TruckSim using real world parameters. One trailer model was configured with a low center of gravity and the other with a high center of gravity. Each trailer was coupled to the tractor model and various tests were conducted to validate the overall performance of TruckSim model.

After the modeling and validation of the vehicle was complete, work began on developing a hardware in the loop simulation in which the TruckSim model interacts with a 4s4m ABS brake system provided by the manufacturer. The brake system consisted of an ABS ECU capable of measuring four independent wheel speeds, four brake chamber pressure modulators, six brake chambers, two air reservoirs, a brake treadle and pneumatic tubing with appropriate fittings.

The ABS ECU works by monitoring the vehicle's wheel speeds and accelerations. In the event of large wheel deceleration, the ECU gives an electrical command to the

modulators to either dump, hold or build brake chamber pressure. By modulating the brake chamber pressures in this fashion, wheel lockup is avoided and the vehicle stops in a rapid and controlled manner.

When developing the hardware in the loop simulation, an overall simulation layout was created first. The layout consisted of a software based plant model, in this case the TruckSim vehicle model, which interacts with real hardware, in this case the ABS braking system. In order to facilitate this software/ hardware interaction, a dSPACE Midsize simulator was utilized. The dSPACE simulator is able to run the vehicle model in real time via a real time processor. In order to accomplish this, the TruckSim vehicle model must first be converted to a Simulink S-Function and inserted into a Simulink model. The resulting Simulink model is then converted to C-code and uploaded to the dSPACE real time processor.

The dSPACE simulator facilitates interaction between the vehicle model and ABS brake system through the use of a signal input/output board. This board takes wheel speed values from the TruckSim/ Simulink vehicle model and converts them to sinusoidal voltages in which each sine wave frequency is proportional to the corresponding wheel speed. These sine wave voltages are then fed into the ABS ECU so it can determine the speed of each wheel.

As the hardware in the loop simulation is ran, the simulator operator can depress the brake treadle to fill the chambers with pressure. The pressure of all six brake chambers is measured with the use of pressure transducers which produce DC voltages proportional to chamber pressure. These transducer voltages are imported to the Simulink/TruckSim vehicle model via the dSPACE analogue to digital converts located

in the input/output board. The Simulink model is able to convert these voltages back to chamber pressure and ultimately to brake torque with the use of a drum brake model developed from data provided by the manufacturer. The resulting torque values are imported to the TruckSim S-Function and effectively decelerate the vehicle model.

In addition to simulating ABS braking functionality, a controller area network was simulated using dSPACE. Essentially, a controller area network (CAN) consists of a network of ECUs which transmit and receive variables and parameters with one another using the CAN communication protocol. For this simulation, messages were transmitted and received with the ABS ECU using the SAE J1939 protocol.

After the hardware in the loop simulator was created, its ability to emulate the actual 6x4 tractor was put to the test. In total, eight tests were conducted to validate the simulator. These tests consisted of straight line braking maneuvers which were conducted at 50 kilometers per hour on four different test surfaces; low μ , high μ , jump μ and split μ . In addition to this, two loading configurations were tested; an unladen configuration which consisted of the solo tractor with no additional loading and a laden configuration in which a 9,428 kilogram load was added atop the rear axles of the tractor.

The overall performance of the hardware in the loop simulator was good with stopping times and stopping distances deviating from -3.5 percent to +12.3 percent with respect to the actual vehicle. In addition to this, the ABS pressure modulations for the simulator's brake chambers were nearly identical to the actual test vehicle's brake chambers in most cases.

The simulator demonstrated some deviations from the test vehicle data during high power braking maneuvers conducted on high μ surfaces. Specifically, the front

wheels of the simulator produced greater wheel slip during braking than the actual vehicle. These deviations may have been the result of inaccuracies in the HIL brake torque model for high power, high pressure braking scenarios. In addition to this, self-energizing braking effects were observed in the front brakes of the test vehicle during high power braking. This behavior was characterized by instances of large wheel deceleration even after brake chamber pressure was dumped.

Along with the hardware in the loop simulation, a software in the loop simulation was developed in which ABS and RSC control algorithms were created. The concept of software in the loop simulation is that a software based plant model, in this case the TruckSim vehicle model, interacts with peripheral software subsystems, in this case the ABS and RSC controllers. The software in the loop simulation was developed using Simulink in which the TruckSim vehicle model was represented with an S-Function.

The first step in developing the software in the loop simulation was to analyze ABS performance data from the hardware in the loop simulation. From this data, a 4s4m ABS control algorithm was developed. This algorithm works by monitoring the vehicle wheel deceleration values, provided by the TruckSim S-Function. During severe wheel deceleration, the algorithm is designed to dump, hold or build pressure to the simulated brake chambers in order to prevent wheel lockup. This algorithm was then validated using test data provided by the manufacturer and in most cases, the ABS controller was able to accurately emulate the actual vehicle.

With the ABS algorithm validated, work began on developing an RSC controller. The RSC controller prevents the vehicle from rolling over during severe cornering maneuvers. It works by first calculating the vehicle's lateral acceleration and preview

lateral acceleration to determine the severity of the current cornering maneuver. Next, a mass estimator determines the mass of the current vehicle configuration so a lateral acceleration threshold can be determined. If the severity of the current cornering maneuver surpasses the rollover threshold, the RSC controller will automatically cut the engine and apply brakes to decelerate the vehicle to avoid rollover.

The RSC controller was then validated with test data provided by the manufacturer. In these tests, the tractor-trailer rig was equipped with a production RSC ECU. Several maneuvers were conducted including a double lane change, J-turn, follow cone path, high dynamic steer input and constant radius test with increasing speed on various friction surfaces. The lateral acceleration, yaw rate, road wheel angle, vehicle speed, brake chamber pressures, engine control and brake control activation signals were used as validation metrics for making comparisons. Overall, the simulation RSC controller functioned similar to the production RSC ECU. The initiation of engine and brake control occurred during similar time frames and the brake chamber modulators behaved similarly as well.

7.2 Recommendations

The hardware in the loop and software in the loop simulation techniques proved effective for the development and evaluation of vehicle controls. In most cases, the simulations were able to accurately emulate the behavior of the actual test vehicle. One exception is in the case of high power braking for the straight line ABS testing. During the first one or two seconds of these tests, large spikes occurred with the front brake chamber pressures and wheel speeds of the HTM tractor. As these tests proceeded, the

slip ratio magnitudes for the front wheels diminished and the ability of the drum brakes to generate torque seemingly declined. In order to better understand this behavior and produce better simulation results, it is recommended that further efforts be made to refine the brake torque generator model for the HIL drum brakes. The model should be modified so dynamic brake torque behavior such as brake torque delay and self-energizing effects are taken into account.

In addition to refining the drum brake model, it is recommended that a yaw stability control algorithm be developed and integrated into the software in the loop simulation. This algorithm should be designed to work in parallel with the current roll stability control and anti-lock brake subsystems. With the addition of yaw stability control, the software in the loop simulation will feature all the main components of a modern day electronic stability control system.

References

1. American Road and Transportation Builders Association
<http://www.artba.org/about/faqs-transportation-general-public/faqs/#9>
2. Rao, Shreeshha. *"Development of a Heavy Truck Vehicle Dynamics Model using TruckSim and Model Based Design of ABS and ESC Controllers in Simulink."*
The Ohio State University: MS Thesis, 2013
3. Gillespie, Thomas. D., *Fundamental of Vehicle Dynamics*. SAE, Warrendale, PA, 1992.
4. <http://topalwaysdown.com/2011/04/15/snap-oversteer-making-the-bear-dance/>
5. Rao, Sughosh. *"Vehicle Modeling and Adams-Simulink Co-Simulation with Integrated Continuously Controlled Electronic Suspension (CES) and Electronic Stability Control (ESC) Models "*. The Ohio State University : MS Thesis, 2009.
6. Sontheim Industrie Elektronik
<http://www.sontheim-industrie-elektronik.de/en/service-support/knowhow/sae-j1939.html>
7. *"SAE J1939-71 Vehicle Application Layer"*. SAE Surface Vehicle Recommended Practice, 2011.
8. *"SAE J1939-14 Physical Layer, 500 Kbps"*. SAE Surface Vehicle Recommended Practice, 2011.
9. *"SAE J1939-21 Data Link Layer"*. SAE Surface Vehicle Recommended Practice, 2006.

10. "SAE J1939-73 Application Layer - Diagnostics". SAE Surface Vehicle Recommended Practice, 2010.
11. Chandrasekharan, Santhosh. "*Development of a Tractor-Semitrailer Roll Stability Control Model*". The Ohio State University : MS Thesis, 2007.
12. Hardware Installation and Configuration Guide For DS1006 Processor Boards and I/O Boards
13. ASE Study Guides
<http://www.freeasestudyguides.com/wheel-speed-sensor.html>
14. ControlDesk Experiment Guide For ControlDesk 3.7